ML-TDR-64-125
Volume I

5 6 7 0 1

# IMPROVED GRAPHITE MATERIALS FOR

# HIGH-TEMPERATURE AEROSPACE USE

# VOLUME I. RESEARCH AND DEVELOPMENT

# FOR IMPROVED GRAPHITE MATERIALS

May 1964

WARNING

Air Force Materials Laboratory
Research and Technology Division
Air Force Systems Command
Wright-Patterson Air Force Base, Ohio

Project No. 7350, Task No. 735002

AMPTIAC

20011221 157

NOTICES

When U. S. Government drawings, specifications, or other data are used for any purpose other than a definitely related Government procurement operation, the Government thereby incurs no responsibility nor any obligation whatsoever; and the fact that the Government may have formulated, furnished, or in any way supplied the said drawings, specifications, or other data, is not to be regarded by implication or otherwise as in any manner licensing the holder or any other person or corporation, or conveying any rights or permission to manufacture, use, or sell any patented invention that may in any way be related thereto.

Qualified requesters may obtain copies of this report from the Defense Documentation Center (DDC), (formerly ASTIA), Cameron Station, Bldg. 5, 5010 Duke Street, Alexandria, Virginia, 22314.

This report has been released to the Office of Technical Services, U. S. Department of Commerce, Washington 25, D. C., in stock quantities for sale to the general public.

Copies of this report should not be returned to the Research and Technology Division, Wright-Patterson Air Force Base, Ohio, unless return is required by security considerations, contractual obligations, or notice on a specific document.

IMPROVED GRAPHITE MATERIALS FOR
HIGH-TEMPERATURE AEROSPACE USE

VOLUME I.  RESEARCH AND DEVELOPMENT
FOR IMPROVED GRAPHITE MATERIALS

May 1964

Air Force Materials Laboratory
Research and Technology Division
Air Force Systems Command
Wright-Patterson Air Force Base, Ohio
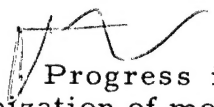
Project No. 7350, Task No. 735002

## FOREWORD

This report was prepared by the Union Carbide Corporation, Carbon Products Division, under Contract No. AF 33(657)-11171. The contract was initiated under Project No. 7350, "Refractory Inorganic Nonmetallic Materials", Task No. 735002, "Refractory Nonmetallic Materials: Graphitic". The research and development program was accomplished at the Carbon Products Division, Advanced Materials Laboratory, Lawrenceburg, Tennessee, and the Carbon Products Research Laboratory, Parma, Ohio. The work was administered under the direction of the Air Force Materials Laboratory, Research and Technology Division; Major R. H. Wilson and C. A. Pratt, Jr., were the project engineers.

Volume I of this report covers work conducted from 1 May 1963 to 31 March 1964 on Task 1, "Research and Development for Improved Graphite Materials". Volume II covers work conducted from 1 May 1963 to 30 April 1964 on Task 2, "Development of Graphite-Refractory Composites".

The program has been under the direction of Mr. R. M. Bushong. Work at the Carbon Products Research Laboratory was under the supervision of Mr. J. C. Bowman, with Dr. W. W. Lozier serving as Project Coordinator. Scientists at the Research Laboratory were Messrs. M. Janes, I. C. Lewis, T. Edstrom, C. V. Mitchell, L. S. Singer, M. Haun, A. R. Cherry, C. E. Lowell, and Mrs. S. B. Wallon. Work at the Advanced Materials Laboratory was under the supervision of Mr. R. C. Stroup, with Mr. M. B. Carter serving as Project Coordinator. "Task 1" experimentalists were Messrs. C. F. Stout (Group Leader), G. C. Tolley, E. R. McHenry, and J. H. Turner. "Task 2" experimentalists were Messrs. K. J. Zeitsch (Group Leader), W. C. Beasley, W. E. Biles, and J. D. Cannon, with testing, processing and applications support by Dr. R. B. Dull and Messrs. C. W. Waters and D. C. Hiler.

# ABSTRACT

Progress is reported on the basic studies of mechanisms of carbonization of model aromatic compounds. The survey of the thermal reactivity of model compounds has been continued with the examination by differential thermal analysis of 63 additional substituted aromatics and heterocyclics. The pyrolysis behavior of two different pitches has been examined in a thermogravimetric apparatus. Electron spin resonance (ESR) spectra have been obtained under conditions of high resolution for solutions of acenaphthylene in m-quinquephenyl. Nuclear magnetic resonance (NMR) measurements are reported for some aromatic ions, aromatic pyrolysis products, and complex raw materials for graphite. The thermal decomposition of organic diazocompounds has been investigated as an example of a pyrolysis reaction involving radical intermediates but yielding stable diamagnetic products. X-ray data have been obtained for the [002] semilattice spacing in graphite prepared from pure aromatic hydrocarbons and from complex raw materials. Molecular structure is seen to influence graphite properties, through both steric and reactivity effects. Generalized reaction sequences have been prepared for the formation of graphite from the model compounds acenaphthylene and 9, 9'-bifluorenyl. The carbonization of two aromatic hydrocarbons, fluoranthene and p-terphenyl, both of which yield disordered graphite, has been investigated.

The addition of carbon blacks to coking charge stocks prior to the coking operation results in cokes which have isotropic high thermal expansion characteristics. Laboratory air-blown asphalts were found to be source stocks for producing isotropic high thermal expansion graphites. Experiments in the pilot coker on thermal expansion reduction of a virgin residuum-based coke have produced low thermal expansion coke of good uniformity. High and low thermal expansion cokes from vacuum residuum and slurry oil charge stocks have been processed into graphite. Testing shows that the original coke properties affect the final graphite properties.

This technical documentary report has been reviewed and is approved.

W. G. RAMKE
Chief, Ceramics and Graphite Branch
Metals and Ceramics Division
Air Force Materials Laboratory

iii

TABLE OF CONTENTS

TABLE OF CONTENTS (CONT'D)

ILLUSTRATIONS

ILLUSTRATIONS (CONT'D)

ILLUSTRATIONS (CONT'D)

ILLUSTRATIONS (CONT'D)

TABLES

# 1. INTRODUCTION

This volume covers the first year's work on Task 1, "Research and Development for Improved Graphitic Materials", of a program to provide graphite materials for high-temperature aerospace use. This research and development effort is a continuation of selected portions of the program for studies leading to the understanding required for development of uniform reproducible carbon-based materials capable of being tailored to meet high-temperature materials requirements in advanced aerospace systems conducted under Contract AF 33(616)-6915. This work included scale-up, characterization, and evaluation of graphites to permit their successful use as engineering materials. Major emphasis was placed on acquiring a better understanding of the specific chemistry and pyrolysis reactions of raw materials; the limiting properties of single crystals; the relationship between the basic chemical and physical processes and processing techniques; and improved testing methods. The work conducted under Contract AF 33(616)-6915 is covered in the various volumes of WADD TR 61-72.

The objective of the present program is to obtain a more detailed understanding of the relation between the chemical characterization of the raw materials and the properties of the final graphite. This has been continued in a two-phase concurrent program. The first phase has been concerned primarily with the chemical mechanisms of pyrolysis, carbonization and graphitization of model compounds and the development of specific chemical and physical techniques to follow the reactions. The second phase has been directed to the examination of the commercially available charge stocks and their modification to produce graphites with a broad spectrum of physical properties. The next step is then to attempt to use the methods and information developed in phase one to correlate the results of phase two. The continuation of these two lines of work plus this correlation is planned for the second year's work.

The approach in the first phase of the prior and current program has been to follow the carbonization of pure, model organic compounds and then mixtures by specialized physical and chemical techniques. Considerable progress has been made in the development of differential thermal analysis, nuclear magnetic resonance, electron spin resonance, polarographic, X-ray and spectral techniques for the detailed characterization and mechanism studies.

The applied research effort under the previous contract served as a basis for much of the present phase one effort and was concerned primarily with a survey of the carbonization behavior of various raw materials. These data formed the basis for choosing representative model compounds for the study of the relation between chemical structure and thermal reactivity.

---

1

The work relating thermal reactivity to chemical structure, emphasizing the effect of substituent groups on the thermal reactivity, has been continued.

Detailed studies have been made on the pyrolytic reaction mechanisms of several selected model compounds. Several of the intermediate radicals have been identified. The electron distribution and hence the reactivity of a number of aromatic radicals have been determined. Combining these various types of experimental information, we have clarified the mechanisms of carbonization and graphitization.

The parallel effort has been directed toward evaluating some of the commercially available raw materials, which are complex mixtures, as charge stocks to produce binder and filler materials for graphite. Bench-scale batch experimentation has demonstrated that the characteristics of coke can be varied over a wide range not only by varying the initial compositions of the material processed, but also by varying the time, temperature and pressure during the coking process.

Properties of the finished graphites are influenced by the characteristic of the raw materials, particularly the filler component. The major effort has been the investigation of reproducible raw materials with desirable combinations of thermal and physical properties.

During the period of this report, contact with Air Force Contractors and Subcontractors was maintained to expedite the awareness of improved materials developed under this program and to coordinate the evaluation of the materials from this program in the different locations.

# 2. SUMMARY

The survey of the thermal reactivity of model compounds has been continued with the examination by differential thermal analysis of 63 additional substituted aromatics and heterocyclics. The results substantiate previous conclusions that thermal reactivity depends on several factors, including molecular size and configuration; and type, number, and position of substituent groups.

The development of the thermogravimetric apparatus to simultaneously determine the change in weight and in volume of noncondensable gases evolved from a sample during pyrolysis is described. The pyrolysis behavior of two different pitches, one a highly aromatic coal tar pitch, the second a predominantly aliphatic coal tar pitch, has been examined in this apparatus. The highly aromatic pitch produces much larger quantities of hydrogen and less methane, ethane, and ethylene on pyrolysis to 750°C than the more aliphatic low-temperature coal tar pitch.

X-ray data have been obtained for the [002] semilattice spacing in graphite prepared from pure aromatic hydrocarbons and from complex raw materials. Molecular structure is seen to influence graphite properties, through both steric and reactivity effects.

Generalized reaction sequences have been proposed for the formation of graphite from the model compounds acenaphthylene and 9, 9'-bifluorenyl. The carbonization of two aromatic hydrocarbons, fluoranthene and p-terphenyl, both of which yield disordered graphite, has been investigated.

Substituted diazocompounds and some fluorene derivatives have been prepared in order to study the free radical intermediates formed by their thermal decomposition. Several suggested reaction products of pyrolysis have been synthesized.

Electron spin resonance (ESR) spectra have been obtained under conditions of high resolution for solutions of acenaphthylene in m-quinquephenyl. The initial spectrum observed has been attributed to the perinaphthenyl radical. This radical has been observed during the pyrolysis of a number of other organic compounds containing mobile side chains. The spectrum for the second, more stable radical entity from acenaphthylene has tentatively been reduced to coupling constants and indicates a 13-proton-containing aromatic radical. ESR measurements of acenaphthylene and deuterated acenaphthylene cokes show that the ESR linewidth of the low-temperature cokes and carbons can be attributed to proton hyperfine structure of stable aromatic free radicals.

The thermal decomposition of organic diazocompounds has been investigated as an example of a pyrolysis reaction involving radical intermediates but yielding stable diamagnetic products. High-resolution ESR spectra have been obtained for the pyrolysis intermediates from diazodiphenylmethane, diazodiphenylmethane-$D_{10}$, diazofluorene, and diazobenzil. Tentative structural assignments have been made where possible.

3

The ESR of the methylated aromatic, hexamethylbenzene, has been investigated in $H_2SO_4$, $SbCl_5$ and $I_2$ solvents. These results indicate the formation of a stable pentamethylbenzyl radical in these acceptor solvents.

Proton magnetic resonance measurements have been obtained for a variety of aromatic and substituted aromatic hydrocarbons. Hydrogens associated with aromatic structures have been classified according to chemical type. The position of the methyl peak in polynuclear aromatic systems has been found to be diagnostic of aromatic structure. NMR measurements are reported for some aromatic ions, aromatic pyrolysis products, and complex raw materials for graphite.

Ultraviolet and visible absorption spectra have been measured for a variety of aromatic ions and aromatic radical ions, which are believed to be related to the reaction intermediates of pyrolysis. The results are discussed in terms of chemical structure and the reaction mechanisms involved.

In the parallel effort, examination of controlled commercial charge stocks has continued.

The addition of carbon blacks to coking charge stocks prior to the coking operation results in cokes which have isotropic high thermal expansion characteristics. The physical properties of graphite materials produced from these cokes depends upon the characteristics and origin of the carbon blacks which are used as the "seed" materials.

Laboratory air-blown asphalts were found to be source stocks for producing isotropic high thermal expansion graphites. By varying the air-blowing conditions, the final graphite properties were affected. Different commercial asphalts are also being investigated as possible raw materials for pilot coker experiments.

Experiments in the pilot coker on thermal expansion reduction of a virgin residuum-based coke have produced low thermal expansion coke of good uniformity and have shown the limits that can be achieved by changing the operating conditions during the coking cycle.

High and low thermal expansion cokes from vacuum residuum and slurry oil charge stocks have been formed into graphite. Testing shows that the original coke properties affect the final graphite properties. Variability of bulk density and compressive strength has been reduced by using these controlled sources of raw materials.

4

# 3. TASK 1. RESEARCH AND DEVELOPMENT FOR IMPROVED GRAPHITE MATERIALS

## 3.1. Pyrolysis Mechanisms

### 3.1.1. Differential Thermal Analysis (DTA)

Differential thermal analysis provides a continuous thermal record of phase changes and chemical reactions occurring in a sample while it is heated at a uniform rate. By comparing the temperature of a sample with the temperature of an inert reference material such as anhydrous aluminum oxide as both are heated together, temperature regions where heat is absorbed (endothermic reactions) or where heat is evolved (exothermic reactions) can be observed. The resulting thermogram gives information both as to the type of reaction occurring and the temperature where the reaction takes place.

DTA has been used to determine the thermal reactivity of a large number of model compounds of interest as chemical precursors to graphite. It permits classification of compounds into thermally stable and thermally reactive categories in an atmospheric pressure system. It provides a simple method of determining melting and boiling temperatures for the thermally unreactive compounds and melting and reaction temperatures for the thermally reactive species. The collection and evaluation of volatile products and reaction residues provide clues to the pyrolytic sequences.

This report is a continuation of the study of thermal reactivity of aromatic and heterocyclic compounds. Compounds have been arbitrarily designated as thermally "unreactive" if they produce no carbonaceous residue at 750°C in the DTA experiment and as thermally "reactive" if they undergo a condensation sequence and yield a measurable amount of carbonaceous residue.

### 3.1.1.1. Model Aromatic Compounds

### 3.1.1.1.1. Unreactive Substituted Aromatics and Heterocyclics

The DTA thermograms of fifteen substituted aromatic or heterocyclic compounds which produced no carbon residue on heating at 10°C per minute to 750°C in an argon atmosphere are given in Figure 1. The properties of these compounds as determined by DTA are given in Table 1. The thermograms are typical of unreactive species, exhibiting only the melting and vaporization endotherms; however, several of the compounds gave small amounts of new products in the volatile condensates trapped out in the KBr condensers. 1,5-Naphthalenediamine exhibited a change in relative intensities of the -NH bands indicating deamination probably occurred to a small extent and retene (1-methyl-7-isopropylphenanthrene) exhibited quite a number of relatively weak new IR bands, particularly in the skeletal region of the spectrum. This is probably the result of some

dealkylation reactions which are likely with an isopropyl substituent. 1-Methylfluorene gave a carbon yield of 0.6 per cent but the infrared spectrum of the condensate showed only starting material in the volatile fraction. The DTA thermogram gives only the melting and boiling endotherms.
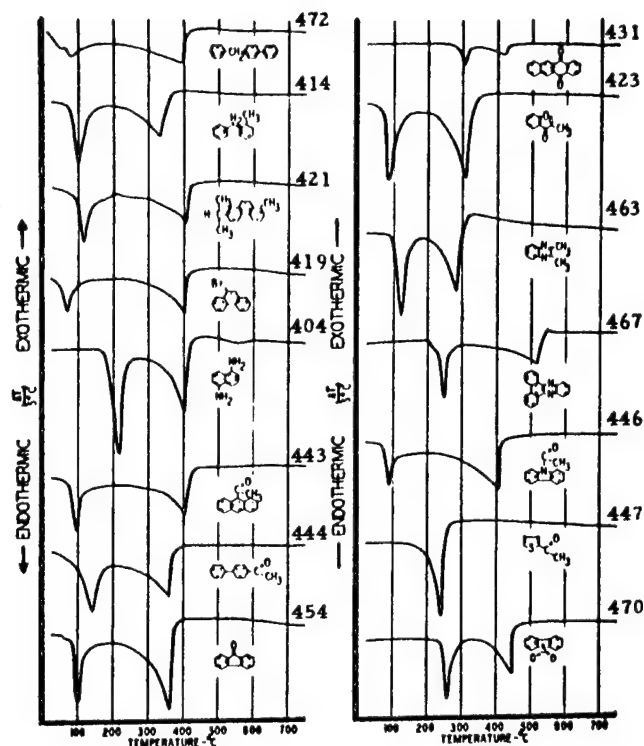


Figure 1.  DTA Thermograms of Thermally Unreactive Substituted Aromatic and Heterocyclic Compounds

Blocking the pyrazine ring with a benzo group apparently reduces the reactivity substantially as indicated by the DTA results on dibenzo-(a, c)-phenazine. A carbon yield of 0.5 per cent was obtained. The thermogram shows typical endotherms for melting and volatilization. The initial slope of the melting endotherm indicates the presence of a small amount of a lower melting impurity, but the spectral analysis does not indicate its identity. The condensate collected during the DTA run was only starting material. No new products were found.

2-Acetylthiophene gave no carbon residue and the DTA thermogram exhibits only a single endotherm caused by distillation but no starting material was found in the condensate trap. 2-Acetylthiophene apparently decomposed to thiophene or a substituted thiophene derivative.

6

Table 1. Thermally Unreactive Compounds

| Compound | Structure | DTA No. | M.p.-°C Lit. | M.p.-°C DTA | B.p.-°C DTA | Remarks* |
|---|---|---|---|---|---|---|
| 4-Benzylbiphenyl | | 472 | 85 | 50 Imp. 82 Major | 395 | SM only in condensate. |
| 1-Methylfluorene | | 414 | 87 | 82 | 335 | 0.6 per cent resid. |
| Retene | | 421 | 98.5 | 97 | 405 | Dealkylation indicated; 0.4 per cent resid. |
| 9-Bromophenanthrene | | 419 | 63 | ~ 50 | 402 | S. M. only. |
| 1,5-Naphthalenediamine | | 404 | 189.5 | 185 | 402 | Deamination indicated. |
| 9-Acetylanthracene | | 443 | 76 | 76 | 401 | S. M. only. |
| 4-Acetylbiphenyl | | 444 | 121 | 105 | 358 | S. M. only. |
| 9-Fluorenone | | 454 | 84 | 89 | 360 | S. M. only. |
| 5,12-Naphthacenequinone | | 431 | 294 | 290 | 418 | S. M. only. |
| 3-Methylchromone | | 423 | 73 | 75 | 310 | --- |
| 2,3-Dimethylquinoxaline | | 463 | 106 | 100 | 283 | S. M. only. |
| Dibenzo(a,c)phenazine | | 467 | --- | 203 230-Major | 520 | 0.5 per cent residue; S. M. only. |
| N-Acetylcarbazole | | 446 | 69 | 72 | 407 | S. M. only. |
| 2-Acetylthiophene | | 447 | 10.5 | -- | 237 | No S. M.; entirely new products; no C = O; possible thiophene or substituted thiophene. |
| Dibenzothiophene Sulfone | | 470 | 230 | 240 | 445 | S. M. only. |

*S. M.-Starting Material.

A comparison of the thermal behavior of 4-benzylbiphenyl with that of biphenyl and p-terphenyl is of interest particularly regarding the stability of the methylene bridge. The DTA thermogram of this compound indicates that the sample contained some lower melting impurity, in addition to the fact that the compound is thermally unreactive. Only melting and boiling endotherms are exhibited. The boiling endotherm covers a long temperature interval indicating gradual evaporation of the sample to about 400°C. No residue was obtained and only the starting material was found in the KBr condensate trap.

The thermal reactivity of naphthacenequinone is also of interest as a possible oxidation product of the hydrocarbon raw materials used to make carbon. The sample used in this experiment was synthesized by the air oxidation of naphthacene on activated alumina followed by chromatographic separation of the product. 5,12-Naphthacenequinone proved to be thermally unreactive, showing only the melting and boiling endotherms (see DTA curve 431 in Figure 1). The distillate contained only the pure starting material.

2,3-Dimethylquinoxaline was completely unreactive in the DTA run. The thermogram shows the typical melting and boiling endotherms of an unreactive volatile material. No carbon residue was obtained and only the starting material was found in the condensate trap. It can be concluded that quinoxaline, like quinoline and naphthalene is too volatile and too unreactive to carbonize at atmospheric pressure.

Dibenzothiophene sulfone, the oxidation product of dibenzothiophene proved to be as unreactive as dibenzothiophene itself. The DTA thermogram shows only the melting and boiling endotherms of typical unreactive materials. No carbon residue was obtained and the condensate consisted of the starting compound only.

### 3.1.1.1.2. Thermally Reactive Substituted Aromatic Compounds

The thermograms for 19 reactive organic compounds are shown in Figure 2, together with the structural formulae. Associated data on melting, boiling and reaction temperatures, and on resultant products are given in Table 2. These compounds have been grouped by structural type for discussion insofar as possible.

#### a. 9-Ethylanthracene

This rather low-melting compound undergoes an exothermic reaction starting around 125°C and reaching a maximum at 170°C. The reaction products are essentially all volatile, however, as a carbon residue of only 1.4 per cent was obtained. Neither anthracene, 9-phenylanthracene, or 9-methylanthracene gave carbon residues on heating under similar conditions,[1] however, 9-methylanthracene showed slight exothermic reactivity around 200°C indicating that the formation of benzyl-type radicals by hydrogen dissociation and subsequent cleavage of the alkylaryl bonds followed by polymerization may be responsible. The formation

8
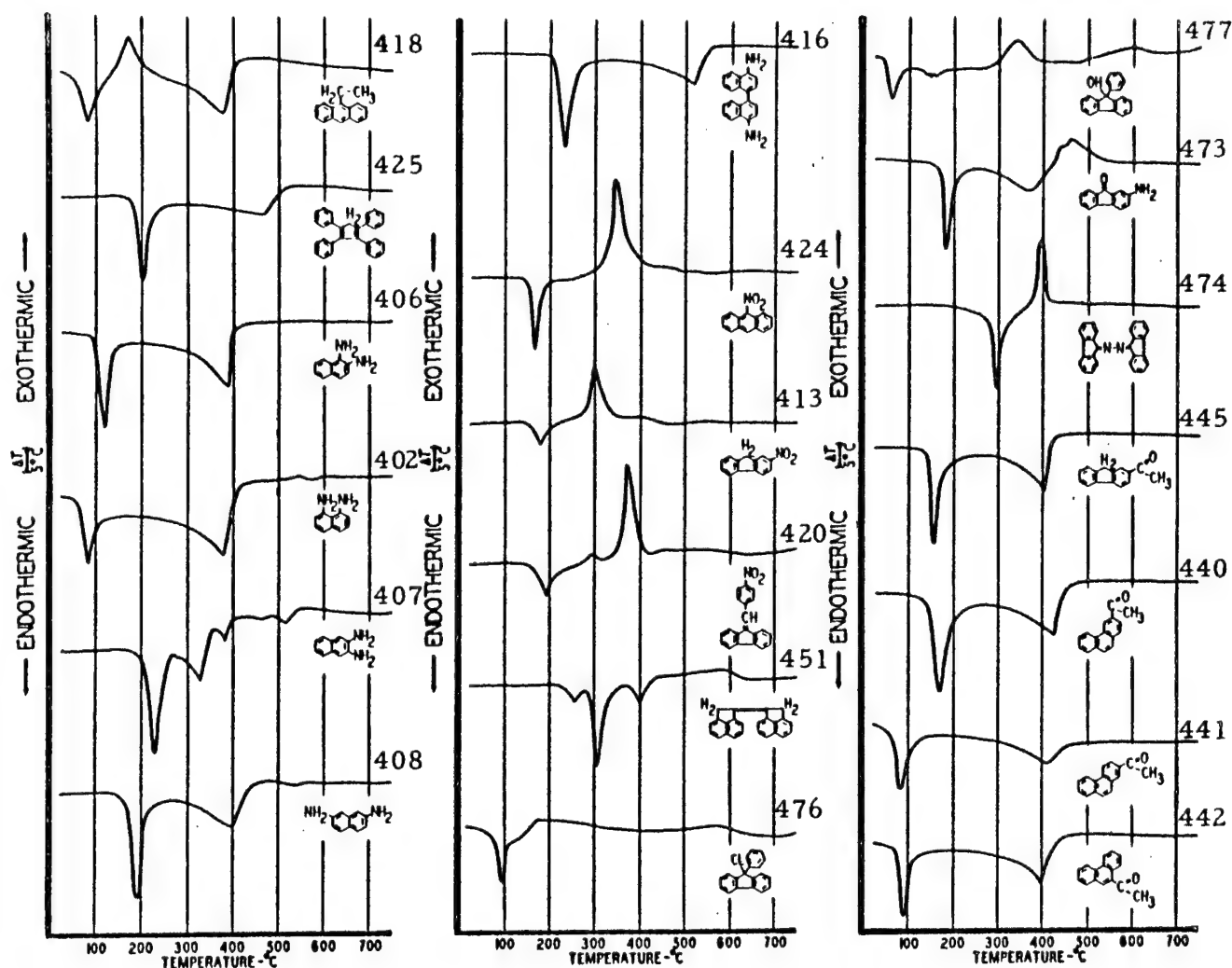
Figure 2. DTA Thermograms of Thermally
Reactive Substituted Aromatics

N-5203

of alkyl bridges would account for the low carbon yields in these cases.

b.   1, 2, 3, 4-Tetraphenyl-1, 3-Cyclopentadiene

Cyclopentadiene is devoid of aromatic character and its double bonds are available for addition reactions in some instances.  The phenyl substituents greatly increase the molecular size and the melting and boiling points, but may adversely affect the reactivity through steric hindrance. The DTA thermogram shows only the melting endotherm at 180°C and the long, low intensity vaporization endotherm somewhat typical of many slightly reactive materials.  A carbon residue of 1. 8 per cent was obtained in the DTA experiment.  Examination by IR absorption of the condensate

9

Table 2.  Thermally Reactive Substituted Aromatics

| Compound | Structure | DTA No. | M.p.-°C Lit. | M.p.-°C DTA | B.p.-°C DTA | Rx.T °C | % C Residue | Remarks |
|---|---|---|---|---|---|---|---|---|
| 9-Ethylanthracene | | 418 | 59 | 55 | 378 | 172 | 1.4 | S.M. but relative intensities of many bands have changed. No new IR bands |
| 1,2,3,4-Tetraphenyl-1,3-cyclopentadiene | | 425 | 178 | 180 | 465 | --- | 1.8 | S.M. plus a large number of new IR bands. New products could not be identified. |
| 1,2-Diaminonaphthalene | | 406 | 96 | 98 | 390 | --- | 3.1 | S.M. only. |
| 1,8-Diaminonaphthalene | | 402 | 67 | 63 | 377 | --- | 4.4 | S.M. only. |
| 2,3-Diaminonaphthalene | | 407 | 191 | 195 | ? | 525-515 | 2.8 | S.M. plus major changes and many new IR bands of unidentified origin. |
| 2,7-Diaminonaphthalene | | 408 | 166 | 167 | 400 | --- | 10.3 | S.M. plus a few minor changes in IR bands. A new weak N-H band at 2.90 microns. |
| Naphthidine | | 416 | 198 | 210 | 518 | --- | 3.0 | Mostly S.M. plus two new weak IR bands at 8.56 and 9.67 microns. |
| 9-Nitroanthracene | | 424 | 146 | 153 | none | 348 | 24.1 | Some S.M. but mostly new products unidentified. |
| 2-Nitrofluorene | | 413 | 157 | 156 | none | 303 | 67.4 | Some S.M. but mostly new products with both -OH and C=O groups. |
| 9-p-Nitrobenzylidenefluorene | | 420 | 167 | 163 | ? | 295,375 | 45.9 | No S.M.; completely new products; strong C=O band. |
| Acenaphthylidene | | 451 | 277 | 240 Imp. 290 Major | 403 | 585 broad | 39.2 | Some S.M. plus mostly acenaphthene. |
| 9-Chloro-9-phenylfluorene | | 476 | 78 | 78 | none | 172 broad | 51.7 | No new IR bands but several bands are missing in condensates |
| 9-Phenyl-9-fluorenol | | 477 | 107 | 45 103 | ~150 | 340 Exo. | 43.4 | (A major impurity in S.M.) No S.M. in condensate -OH bands gone, several new bands. |
| 2-Amino-9-fluorenone | | 473 | 163 | 166 | ? | 410 Exo 430 " 460 " | 63.0 | SM only in condensate. |
| 9-Fluorenone azine | | 474 | 259 | 275 | none | 360 Exo | 42.7 | S.M. plus many new IR bands in condensate. |
| 2-Acetylfluorene | | 445 | 129 | 140 | 403 | --- | 1.4 | S.M. only. |
| 2-Acetylphenanthrene | | 440 | 143 | 140 | 428 | --- | 1.3 | S.M. only. |
| 3-Acetylphenanthrene | | 441 | 72 | 70 | 415 | -- | 4.5 | S.M. plus new bands at 9.81, 11.37 and 12.75 μ (1 band at 11.15 missing). |
| 9-Acetylphenanthrene | | 442 | 74 | 72 | 395 | --- | 3.4 | S.M. only. |

10

trapped in the exit KBr condenser indicated that new products were formed during pyrolysis. These products could not be identified from the IR spectra.

### c. Diaminonaphthalenes

DTA measurements have been made on a series of diamino-naphthalenes. These results are shown in Figure 2 as well as in Figure 1 and indicate the usual dependence of thermal behavior on structure. Unfortunately, with the exception of 2,3-diaminonaphthalene, the thermograms show only melting and boiling endotherms revealing little information about the reactions occurring at elevated temperatures. The DTA curve of 2,3-diaminonaphthalene is quite complex with four additional endotherms following melting. The condensate also indicates new products were formed. In spite of this indicated reactivity, a carbon yield of only 2.8 per cent was obtained. The 2,7-isomer produced the most stable thermal products which resulted in an ultimate yield of 10.3 per cent carbon residue. Further studies on these interesting compounds are indicated.

### d. Naphthidine

This compound, a diaminobinaphthyl, is structurally related to the previous class of compounds and may represent a possible reaction product of aminonaphthalenes. Its high molecular weight lowers its volatility and the amine substituents are expected to increase its reactivity. Unsubstituted binaphthyl has been found to be thermally unreactive under the conditions of these experiments. The DTA thermogram of naphthidine does not reveal any specific reaction information as only the melting and boiling endotherms are obtained. A carbon yield of only 3 per cent was obtained and mostly starting material was found in the condensate with only two new weak IR bands indicating some new compound in the volatile products.

### e. Nitro-Substituted Aromatics

The nitro group strongly enhances thermal reactivity of polynuclear aromatic compounds. The mechanism of these reactions is not yet known. Possible reaction routes include complex formation, thermal elimination of the substituent group, activation of other ring positions by the $-NO_2$ group, and an oxidizing action of the nitro compound. The DTA thermograms of almost all of the nitro compounds examined to date show strong exothermic reactions occurring between 300 and 400°C. The three thermograms shown in Figure 2 are all similar in this respect.

9-Nitroanthracene gives a strong, sharp exotherm which peaks at 350°C and a carbon yield of 24.1 per cent was obtained. The condensate was found to contain new products in addition to starting compound and there is evidence of quinonoid oxygen, indicating oxidation.

2-Nitrofluorene produced a very similar thermogram with the exothermic reaction peaking at 300°C. This compound gave a very high 67.4

11

per cent carbon yield and also indicated oxidation products in the condensates. It is interesting that the di-substituted compound, 2, 7-dinitrofluorene, did not react exothermally even though it produced a 26 per cent carbon yield on pyrolysis in the DTA apparatus.

9-p-Nitrobenzylidenefluorene also reacted exothermally to produce a high carbon yield of 45.9 per cent. The condensate contained no starting material and again gave evidence of oxidation products. The activating effect of the nitro group is illustrated if one recalls that 1, 2-di-9-fluorenylethane gives only a small carbon residue of about 5 per cent, and 9-cinnamylidene fluorene which possesses a reactive double bond yields 9 per cent carbon in the DTA experiment.

### f. Miscellaneous Substituted Aromatics

The DTA thermograms were obtained on a number of substituted aromatic compounds which are of interest in other areas of the raw materials program. Acenaphthylidene is suspected to be one of the intermediates formed during the carbonization of acenaphthylene. The substituted fluorene and fluorenone compounds are intermediates made in our attempts to synthesize 9, 9'-biphenyl-9, 9'-bifluorenyl for the reaction studies and for ESR studies.

The DTA thermograms are given in Figure 2 and a summary of the thermal properties determined by DTA is given in Table 2. A brief discussion of each compound follows.

### Acenaphthylidene

This compound is believed to be one of the important reactive intermediates formed in the thermal conversion of acenaphthylene to pitch and to carbon. The DTA thermogram indicates the presence of two compounds in our samples. These are believed to be the cis and trans isomers. Three different authentic samples of this material have been examined. One was purchased from a chemical supply house, Aldrich Chemicals, one was synthesized at the ERA laboratory in Brussels, and the third sample was synthesized in our laboratory. All three samples gave identical DTA thermograms and identical IR spectra. Attempts are now in progress to separate these isomers chromatographically. The DTA thermogram shows three consecutive endotherms and a broad low-intensity exotherm peaking at 585°C. A carbon residue of 39.2 per cent was obtained. The condensate contained starting material but was mostly acenaphthene.

### 9-Chloro-9-phenylfluorene

This compound was synthesized for ESR studies. The thermal behavior on pyrolysis is shown in the DTA thermogram in Figure 2. This compound has a relatively low melting point of

12

78°C. Upon melting it appears to exhibit a slow continuous exothermic activity up to nearly 350°C where the DTA curve returns to the baseline. Again at higher temperatures, a second broad low exotherm extends from about 475 to 650°C. No volatilization endotherm appears although volatiles appear in the condensate trap. A carbon yield of 51.7 per cent was obtained. The condensate spectrum is similar to that of the starting material except that a few bands are missing.

### 9-Phenyl-9-fluorenol

This compound is an intermediate in the synthesis of 9-chloro-9-phenylfluorene from 9-fluorenone. The DTA thermogram indicates the presence of a low-melting or low-boiling impurity. Independent melting point determinations with the hot-stage microscope indicated melting occurred between 41 and 65°C and that evaporation of some component occurred between 120 and 160°C. Analysis of the infrared spectrum did not identify the impurity although it is believed to be another aromatic alcohol. An exothermic reaction between 300 and 350°C is shown in the thermogram followed by a second broad exotherm between 500 and 625°C. A carbon residue of 43.4 per cent is obtained. No starting material was found in the condensate. The reaction products did not contain the hydroxyl group.

### 9-Fluorenone

9-Fluorenone is the starting compound used in the synthesis of the two previously discussed compounds. The DTA thermogram is typical of a thermally unreactive compound which undergoes simple melting and distillation leaving no residue. The condensate proved to be only the pure starting material.

### 2-Amino-9-fluorenone

The introduction of an amino substituent on an aromatic system has been found to greatly enhance the thermal reactivity. In the case of 9-fluorenone, substitution with an amino group in the 2-position raises the melting point from approximately 80 to 166°C. After melting, the compound vaporizes gradually as the temperature increases. A typical boiling endotherm develops until the temperature reaches about 370°C. At this temperature, a series of exothermic reactions take place up to about 460°C where these reactions begin to taper off. A carbon residue of 63 per cent was obtained. Only the starting material was found in the condensate indicating that the volatile reaction products were mostly noncondensable.

### 9-Fluorenone Azine

This compound has been of interest in ESR studies of pyrolysis. The DTA thermogram of 9-fluorenone azine offers a beautiful example of sharply defined thermal behavior. The com-

13

pound exhibits a sharp endothermic spike on melting at about 275 °C. This is followed by an equally sharp exotherm peaking at 396°C and returning to the baseline. The thermogram indicates the possibility that a single and perhaps a simple reaction mechanism is involved which is initiated abruptly, proceeds rapidly, and is concluded just as abruptly. The reaction is favorable to carbonization producing a residue of 42.7 per cent in the DTA experiment. The condensate volatiles contained both starting compound and new products.

### g. Acetyl-Substituted Aromatic Compounds

The DTA thermograms of four aromatic compounds substituted with an acetyl group are shown in Figure 2 and the physical properties and analytical results are summarized in Table 2.

The compounds were obtained for coking studies on the theory that the acetyl group might undergo a thermal conversion to a vinyl group which would subsequently polymerize to carbonizable materials. The DTA results are disappointing in that none of the compounds exhibit a marked reactivity and the thermograms are devoid of reactivity information. In all cases the DTA thermograms show only the melting and boiling endotherms. In addition, six of the eight compounds examined produced no volatile reaction products, only 3-acetylphenanthrene and 2-acetylthiophene gave condensates containing new compounds. The product from 3-acetylphenanthrene was not identified.

### 3.1.1.1.3. Thermally Reactive Polycyclic Quinonoid Compounds

The differential thermal analysis thermograms of 12 polycyclic quinonoid compounds, the majority of which produced large carbon yields on heating to 750°C, are shown in Figure 3. Pertinent data derived from the DTA experiments as melting and boiling temperatures, reaction temperatures, carbon yield, and volatile reaction products are given in Table 3. The thermal behavior of each compound examined is discussed briefly.

### a. 2,6-Dichloroquinone-chloroimide

This very low molecular weight chlorinated compound is highly reactive at a low enough temperature to prevent significant volatilization. The DTA thermogram indicates that melting occurs around 70°C. The molten material begins to react at 150°C and peaks at 170°C followed by a rapid return to equilibrium furnace temperature. Following the exothermic spike, the DTA curve lies flat on the baseline all the way to 750°C. A carbon yield of 39.4 per cent was obtained. The condensate did not contain any of the starting compound. Only new reaction products collected in the KBr condensate trap.
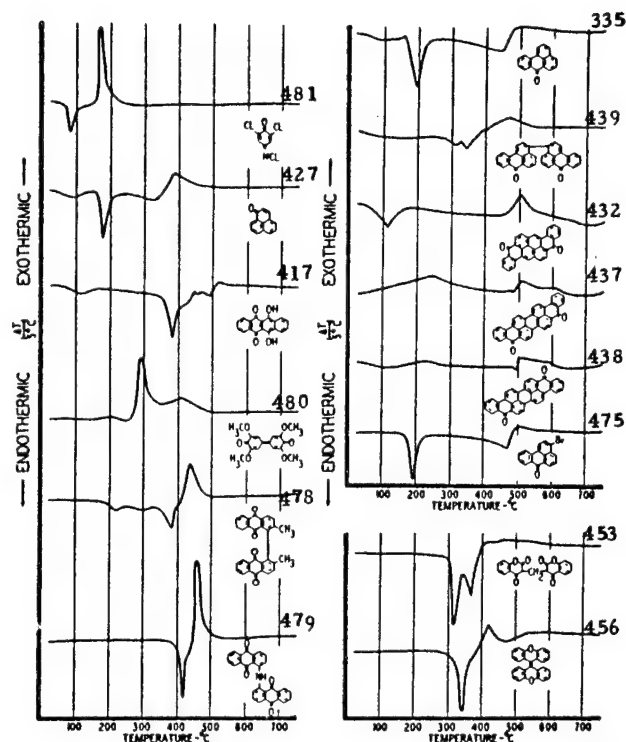
14

Figure 3. DTA Thermograms of Thermally
Reactive Quinonoid and Heterocyclic
Oxygen Compounds

N-5204

### b. 1H-Benzonaphthen-1-one (Perinaphthenone)

This is an interesting aromatic ketone in that it represents a
very compact structural configuration with a somewhat reactive
double bond in addition to the quinone group. It is quite reactive, yield-
ing a 25.6 per cent carbon residue in the DTA experiment. The thermo-
gram in Figure 3 exhibits a pronounced exotherm starting at 325°C and
peaking at 380°C. The condensate was found to contain new species in ad-
dition to the starting material.

### c. 6,11-Dihydroxynaphthacenequinone

The thermal reactivity of hydroxyquinones has previously been
shown to be very dependent on structure or position of the substit-
uents. The parent aromatic compound, naphthacene, has been found to be
quite reactive undergoing an exothermic reaction around 480°C to produce
a 14 per cent carbon yield. Extensive substitution in this case further en-
hanced reactivity to give a 20.6 per cent yield at 750°C. The DTA therm-
ogram shows a rather complex pattern of thermal reactions above the
melting point of 350 to 360°C. The condensate contained no starting mate-
rial. The IR spectrum indicated new products only containing both -OH
and C=O structures.

15

Table 3. Thermally Reactive Polycyclic Quinonoid Compounds

| Compound | Structure | DTA No. | M.p.-°C Lit. | M.p.-°C DTA | B.p.-°C DTA | Rx.T °C | % Residue | Remarks |
|---|---|---|---|---|---|---|---|---|
| 2,6-Dichloroquinone-chloroimide |  | 481 | --- | 70 | none | 170- Exo. | 39.4 | No S.M; entirely new products in condensate. |
| 1H-Benzonaphthen-1-one | | 427 | 142 | 163 | none | 380 | 25.6 | S.M. plus 5 new IR bands at 5.93, 6.83, 7.44, 9.25, and 9.83 μ. |
| 6,11-Dihydroxynaphthacenequinone | | 417 | 350-360 | 360 | 490 | 425-490 | 20.6 | No S.M. in condensate-completely new products containing both -OH and C=O structures. |
| Coerulignone | | 480 | --- | none | none | 295°- Exo. 400° Exo. | 25.8 | No S.M.; entirely new products in condensate; sharp ~OH band. Many bands in 6 to 9μ region. |
| 2,2'-Dimethyl-1,1'-dianthraquinone | | 478 | 366 | 357 | none | 435 Exo. | 53.5 | Impurity - mp ~175°C.- IR shows condensate is almost identical to S.M. |
| 1,1'-Dianthrimide | | 479 | --- | 395 | none | 460- Exo. | 70.8 | SM only in condensate. |
| 7H-Benz(de)anthracen-7-ene | | 335 | 170 | 175 | 445 | none | 15.9 | --- |
| (3,3'-Bi-7H-benz(de)anthracene)-7,7'-dione | | 439 | 315(d) | 290 320 | --- | Exo 465° | 77.2 | S.M. plus some benzanthrone plus sl.violanthrene plus new bands. |
| Pyranthrone | | 432 | Chars. w/o melting | broad -60°C | --- | Exo 500° | 79.8 | Low temp. endotherm; no S.M.; completely new cmpds; (has C=O). |
| Violanthrone | | 437 | --- | none | ~480 sl | Exo 240 Exo 510 Exo 600 | 84.3 | Mostly new material; v. sl. S.M. and sl.benzanthrone. |
| Isoviolanthrone | | 438 | --- | none | 495 | Exo 220 Exo 508 Exo 575 | 85.6 | No S.M.; some benzanthrone plus many new bands, including new C=O at 5.95. |
| 3-Bromobenzanthrone | | 475 | 170 | 172 | 470 | 490 Exo | 14.9 | S.M. only in condensate. |

16

### d. Coerulignone

This tetramethoxy-substituted diphenoquinone does not exhibit any melting endotherm prior to its strong exothermic reaction at 295 °C which produces a variety of volatile products as well as an appreciable carbonizable residue. A carbon yield of 25.8 per cent was obtained. The second exotherm at 400°C may be a true exotherm or may result from a slowing down of volatilization rate. No starting material was found in the condensate collected in the KBr trap. The condensate gave a rich spectrum containing a strong OH band and aliphatic CH bands with no C=O indicated.

### e. 2,2'-Dimethyl-1,1'-Dianthraquinone

The DTA thermogram obtained for this material indicates the presence of a small amount of impurity with a melting point around 200°C. The dianthraquinone reacts exothermally at 435°C soon after melting to produce a carbon yield of 53 per cent. Although there is no boiling endotherm, the condensate contained only the starting compound. Apparently no condensable reaction products were formed.

### f. 1,1'-Dianthrimide

The coupling of two anthraquinone molecules with an imino bridge produced a very thermally reactive compound which yielded 70.8 per cent carbon in the DTA experiment. The thermogram in Figure 3 shows a strong, sharp exotherm immediately following the melting of this material. Some volatilization occurs during the course of this exothermic reaction as the condensate collected in the KBr trap proved to be only the starting compound. No condensable reaction products were found. Anthraquinone does not undergo thermal reaction under the conditions of these DTA experiments. 1-Aminoanthraquinone is more reactive, yielding about 13 per cent carbon in the DTA run.

### g. 7H-Benz(de)anthracen-7-one(Benzanthrone) Derivatives

Four compounds which are structurally related to benzanthrone have been examined in the DTA apparatus to 750°C. Benzanthrone was examined some time ago[2] and found to be moderately reactive, giving a carbon yield of about 16 per cent in the DTA experiment.

### h. 3,3'-Bi-7H-benz(de)anthracene-7,7'-dione

This compound is a dimeric product of two benzanthrone molecules bridged by a single C-C bond across the 3,3' positions. Dimerization is seen to greatly increase the thermal stability, as shown by the melting point rise from 170°C for the monomer to 315°C. The double endotherm seen in Figure 3 is probably due to an isomeric impurity. Exothermic reactivity begins around 400°C and exhibits a maximum at 465°C. Apparently the C-C bridge is thermally stable to this temperature, at which point

17

bond scission with radical formation initiates molecular growth and rearrangement to produce carbonizable products. An ultimate carbon yield of 77.2 per cent is obtained at 750°C. The infrared analysis of the condensable distillates indicates some of the starting material as well as benzanthrone and a small amount of violanthrone plus other unidentified products.

### i. Pyranthrone

Pyranthrone is a fusion product in which two benzanthrone moieties share four carbon atoms. The cross-hatched section in the structural diagram of Table 3 indicates one benzanthrone entity and the plain section the second. This material undergoes a low temperature endothermic phase transition beginning near 60°C which does not entail melting. This is followed by an exothermic reaction that starts around 450°C and reaches a maximum at 505°C. A carbon yield of almost 80 per cent is obtained at 750°C. The condensable distillates collected in the KBr trap proved to be entirely new compounds. The only identifiable feature was the carbonyl band at 5.95 microns. No pyranthrone distilled over as such.

### j. Violanthrone

Violanthrone is a dimer of benzanthrone in which two carbon-carbon bridges join the two molecules together and in so doing form an additional aromatic ring. This large molecule is seen to be very reactive, undergoing a number of exothermic reactions with essentially no evidence of either melting or vaporization. A very high carbon yield of 84.3 per cent was obtained. The distillate condensed in the KBr trap consisted mostly of new products with only a trace of starting material and a small amount of benzanthrone.

### k. Isoviolanthrone

Isoviolanthrone is an isomer of violanthrone. This material appears to undergo essentially identical thermal reactions as violanthrone. The DTA thermograms of both compounds are very similar with only small temperature shifts for the exothermic bands. The carbon yield of 85.6 per cent was also approximately the same as obtained on violanthrone. The IR spectrum of the condensable distillates indicated all new volatile products including some benzanthrone as well as a new carbonyl-containing compound with a C=O band at 5.95 microns.

### l. 3-Bromobenzanthrone

This bromine substituted compound is seen to behave thermally very much like the parent benzanthrone. The melting and boiling temperatures are similar and both gave carbon yields of approximately 15 per cent in the DTA experiments.

### 3.1.1.4. Thermally Reactive Heterocyclic Oxygen Compounds

The DTA thermograms of two polycyclic aromatics with oxygen substituents or heterocyclic oxygen are given in Figure 3. These compounds

were all thermally reactive and produced high carbon yields. Pertinent properties derived from the DTA thermograms such as melting and boiling temperatures, reaction temperatures, and volatile reaction products are given in Table 4. The thermal behavior of each compound is discussed briefly.

### a. Dicoumarin

This compound is thermally stable to its melting point of about 300°C, above which it decomposes producing both volatile fragments and carbonizable residues. A carbon yield of 27.3 per cent was obtained at 750°C. The condensate collected in the KBr trap contained no starting material, indicating that all of the volatiles were reaction products. The IR spectrum of the condensate was very complex with a large number of strong, sharp bands in the 6-9 micron region. C=O, -OH, and aromatic C-H bands were identified in this spectrum.

### b. 9,9'-Bixanthylene
($\Delta^{9,9'}$-Bixanthene)
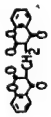
The DTA thermogram of 9,9'-bixanthylene indicates that it reacts exothermally soon after melting. The exothermic reaction peaks at 420°C and the compound produces a 35.0 per cent carbon yield in this experiment. The starting compound apparently does not volatilize as the condensates contained only new products. Two distinct carbonyl oxygen bands are found in the spectrum of the condensable products. This compound, along with $\Delta^{10,10'}$-bianthrone and $\Delta^{9,9'}$-bifluorene, might be looked upon as bridged homologues of tetraphenylethylene. These compounds all have been found to be very reactive and to produce large carbon yields. Tetraphenylethylene did not give any carbon residue although it did exhibit an exothermic reaction at about 435°C.

### 3.1.1.1.5. Thermally Reactive Heterocyclic Nitrogen Compounds

The thermal reactivity of a series of heterocyclic nitrogen compounds consisting of substituted quinoxalines and phenazines has been determined. The heterocyclic compounds in general have been found to be relatively thermally unreactive; however, these compounds contain a pyrazine ring with two nitrogens in the 1 and 4 positions which might possibly enhance the thermal reactivity. Pyrazine is a weak base and is decomposed by some electrophilic reagents. Benzopyrazine is usually called quinoxaline and dibenzopyrazine is called phenazine.

The DTA thermograms of eight pyrazine derivatives are given in Figure 4. All produced a carbon residue in these experiments. The thermal properties derived from DTA are given in Table 5. In addition, a number of other heterocyclic nitrogen compounds have been examined and are discussed below.

19

Table 4. Thermally Reactive Heterocyclic Oxygen Compounds

| Compound | Structure | DTA No. | M.p.-°C Lit. | M.p.-°C DTA | B.p.-°C DTA | Rx T °C | % C Residue | Remarks |
|---|---|---|---|---|---|---|---|---|
| Dicoumarin |  | 453 | 289 | 300 | 363 | 455 minor | 27.3 | No S.M. Entirely new products in condensate; complex spectrum containing C=O, OH groups. |
| 9,9'-Bixanthylene |  | 456 | 315 | 323 | none | 420 Exo | 35.0 | No S.M.; new products containing carbonyl oxygen. |

20
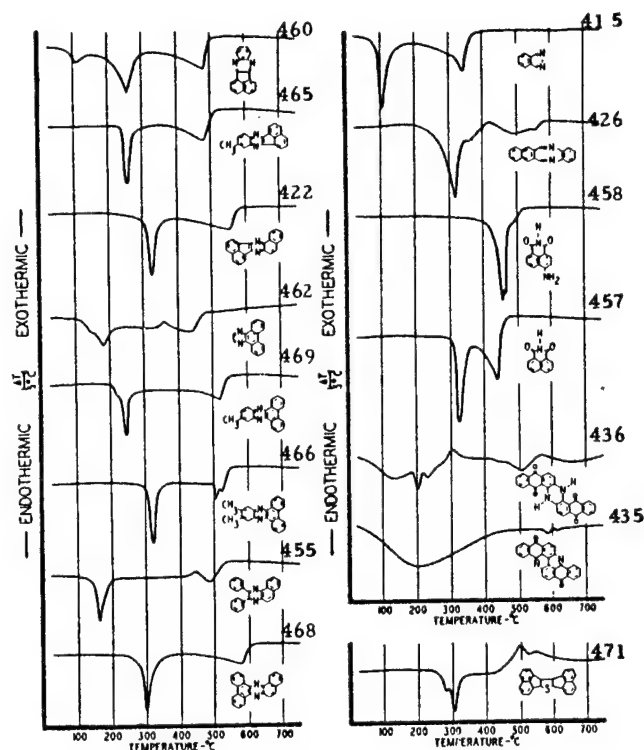
Figure 4.  DTA Thermograms of Thermally Reactive
Heterocyclic Nitrogen and Sulfur Compounds

N-5205
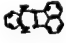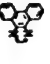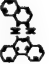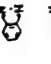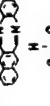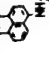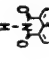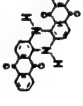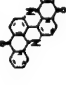
### a.  Acenaphtho(1, 2-b)quinoxaline

The DTA thermogram of this sample indicates the presence of an
impurity and the IR spectrum of the sample has a weak band at
2.98μ indicating an amine group.   Quinoxalines are readily synthesized
from 1,2-dicarbonyl compounds and aromatic 1,2-diamines so this im-
purity is likely 1,2-diaminobenzene, which has a melting point of 102°C
and a boiling point of 252°C.   The thermogram indicates melting and boil-
ing endotherms in agreement with these properties.   The 250° endotherm
also includes the melting of the quinoxaline compound .   The volatilization
endotherm peaking at 480°C has the typical attenuated shape of the reac-
tive compound which does not exhibit an exotherm.   A relatively low car-
bon yield of 2.9 per cent was obtained.   A very surprising result was
obtained on examining the condensate in the KBr trap.   No starting mate-
rial was found.   The condensate was all new products and exhibited very
strong -NH₂ bands in the IR.   The material appears to be a complex mix-
ture.   No specific compounds could be identified.

### b.  9-Methylacenaphtho(1, 2-b)quinoxaline

The 9-methyl derivative of the previously discussed compound
was also examined in the DTA apparatus.   The thermogram ob-
tained is shown in Figure 4.   It is a typical thermogram for a slightly

21

Table 5. Thermally Reactive Heterocyclic Nitrogen Compounds

| Compound | Structure | DTA No. | M.p.-°C Lit. | M.p.-°C DTA | B.p.°C DTA | Rx.T °C | % Residue | Remarks |
|---|---|---|---|---|---|---|---|---|
| Acenaphtho(1,2-b)quinoxaline | | 460 | --- | 216 (85-impur.) | 480 | none | 2.9 | No S.M.; all new product in condensate; IR spectrum very different. |
| 9-Methylacenaphtho(1,2-b)quinoxaline | | 465 | 232 | 240 | 480 | none | 3.2 | S.M. only in condensate. |
| 8,9-Benzoacenaphtho(1,2-b)quinoxaline | | 422 | 295 | 305 | 555 | none | 3.1 | S.M. mostly plus one new weak IR band at 5.80 μ. |
| 5,6,7,8-Dibenzoquinoxaline | | 462 | 180.5 | 177 195 major | 435 | 357 Exo | 10.5 | S.M. plus one new IR band at 5.90 μ. |
| 7-Methyl-1,2,3,4-dibenzo(a,c)phenazine | | 469 | --- | 205 221 major | 520 | none | 7.7 | S.M. plus six IR bands either new or very much stronger. |
| 11,12-Dimethyldibenzo(a,c)-phenazine | | 466 | 292 | 298 | 504 524 | Exo 513 | 9.7 | S.M. plus two new IR bands at 12.22 and 12.52 μ. |
| 2,3-Diphenyl-5,6-benzoquinoxaline | | 455 | 147 | 146 | 485 | 440 Exo | 7.9 | S.M. mostly, plus several rather weak new bands--a weak -NH band at 3.00 μ. |
| 1,2,3,4,6,7-Tribenzophenazine | | 468 | --- | 280 | 578 | none | 3.3 | S.M. only. |
| Phthalazine | | 415 | 90 | 90 | 344 | -- | 2.3 | S.M. only. |
| 2,3-Benzo-1,4-diaza-(2',3',6,7-naphtho)-cyclooctatetraene | | 426 | 285-8 | 275 | ? | 365-555 | 32.6 | No S.M.; all new products. |
| 4-Amino-1,8-naphthalimide | | 458 | --- | 420 | 460 | ? | 15.2 | S.M. only in condensate. |
| 1,8-Naphthalimide | | 457 | 300 | 309 | 440 | --- | 1.0 | Some S.M. plus several new IR bands. |
| Indanthrone | | 436 | 470-500 (decomp.) | ? 3 Low T Endo. | ?505°C | Exo 305 Exo 565 | 53.9 | This cmpd. undergoes much thermal reactivity; poorly resolved spectrum; complex products but no S.M. |
| Flavanthrone | | 435 | --- | Large broad Endo. Rm. Temp to 400°C | ? | Endo 585 Endo 605 | 55.1 | Looks like much purer sample of the S.M. The S.M. (22056) has a strong N-H band at 3 μ; DTA trap material does not. |

reactive material, with a sharp, well-defined melting isotherm and the broad attenuated vaporization endotherm indicating some thermal reactivity during the volatilization stage. This compound gave a carbon yield of 3.2 per cent at 750°C, only slightly greater than the unsubstituted homologue. Surprisingly, however, the condensate in the KBr trap proved to be only starting material.

### c. 8,9-Benzoacenaphtho(1,2-b)quinoxaline

The thermal reactivity of this benzo derivative is similar to that observed with the 9-methyl derivative discussed above. The thermogram shows the melting and reduced boiling endotherms only. A carbon yield of 3.1 per cent was obtained. The condensate was mostly starting compound although the IR spectrum indicated a small amount of a carbonyl-containing product.

### d. 5,6,7,8-Dibenzoquinoxaline

This compound may be considered as the pyrazine analog of benzo(l)phenanthrene which was found to be thermally unreactive in our examinations.[1] The pyrazine ring appears to induce thermal reactivity, since a carbon yield shows an exothermic reaction in the temperature region around 350°C. A small shoulder on the melting endotherm indicates an impurity in the starting material but the spectroscopic analysis does not identify it. The infrared spectrum of the condensate collected in the KBr condenser indicates that a small amount of a carbonyl compound is produced during the thermal analysis. The major fraction in the condensate was starting material, however.

### e. 7-Methyl-1,2,3,4-dibenzo(a,c)phenazine

The introduction of a methyl group results in considerably greater thermal reactivity producing a carbon residue of 7.7 per cent in this instance. The DTA thermogram does not furnish much definitive information about the temperatures of reaction. The thermogram consists of a melting and boiling endotherm. The melting endotherm has a shape similar to that described for dibenzo(a,c)phenazine indicating the possible presence of a contaminant. The boiling endotherm is considerably more attenuated than in the case of the unsubstituted dibenzophenazine. The IR spectrum of the condensate indicates new reaction products as well as starting material volatilized from the heated sample during the run.

### f. 11,12-Dimethyldibenzo(a,c)phenazine

This dimethyl derivative exhibits a large increase in melting point and an expected increase in thermal reactivity to give a carbon residue of 9.7 per cent. The thermogram shows a peculiar double endotherm in the boiling region which might result from exothermic reactivity superimposed on the vaporization curve. The condensed volatile products were found to contain new compounds as well as the starting material.

23

### g.  2,3,-Diphenyl-5,6-benzoquinoxaline

Substitution on the pyrazine ring with two phenyl groups appears to produce a more reactive material than substitution of the same two positions with a naphthyl moiety as in 8,9-benzoacenaphtho(1,2-b)-quinoxaline. The diphenyl derivative has a much lower melting point but retains a high boiling point. The DTA thermogram indicates that an exothermic reaction occurs between 400 and 450°C followed by the boiling endotherm. A carbon yield of 7.9 per cent resulted. Examination of the condensate by IR spectroscopy indicated some amino compound formation occurred as a result of the thermal reactions.

### h.  1,2,3,4,6,7-Tribenzophenazine

This compound differs from the previous one only in the joining of the two phenyl groups to produce another 6-carbon ring adjacent to the pyrazine ring. Although this increases the rigidity and compact configuration of the molecule from a steric point of view, it appears to reduce the thermal reactivity by a factor of two. A carbon residue of 3.3 per cent was obtained in the DTA run. The thermogram consists of the melting endotherm and usual reduced boiling endotherm associated with a slightly reactive material. Only starting compound was found in the condensate from the DTA experiment.

In general, it is concluded that polycyclic aromatics containing the pyrazine ring are somewhat more thermally reactive than the analogous polynuclear aromatic hydrocarbons. This does not appear to result from ring scission but rather from an enhancement of reactivity of specific positions perhaps on adjacent aromatic rings. From the DTA results alone, however, no conjecture as to where or how this activation occurs can legitimately be made.

Two compounds which fall in a miscellaneous category of compounds containing rings with two hetero atoms have been examined by DTA. The first of these contains the 2,3-diazine moiety and the second contains a 1,4-diazocyclooctatetraene ring. The diazine compound is only slightly reactive yielding from 2 to 3 per cent carbon but the 2,3-benzo-1,4-diazo-(2',3',6,7-naphtho)-cyclooctatetraene produced a 32.6 per cent carbon yield.

Phthalazine is more reactive than naphthalene since the two adjacent nitrogen atoms in the six-membered ring reduces the resonance stabilization appreciably. The DTA thermogram shows only the melting and boiling endotherms with very little indication of reactivity and the condensate contained only starting material. Notwithstanding, a carbon residue of 2.3 per cent was obtained in this DTA run.

2,3-Benzo-1,4-diazo-(2',3',6,7-naphtho)-cyclooctatetraene gave a rather complex thermogram with a rather unusual melting endotherm which indicates a gradual melting occurred. Following melting are several endotherms undoubtedly related to chemical reactivity and volatiliza-

24

tion of new products since no starting material was found in the conden-
sates. In addition, the large carbon yield is indicative of high reactivity.

### i. 4-Amino-1,8-Naphthalimide

This rather interesting naphthalene derivative shows an excep-
tional thermal stability to 400°C. The DTA thermogram in
Figure 4 indicates that melting and boiling occur very close together and
the examination of the condensable volatiles showed only the starting ma-
terial in the KBr trap. Although a carbon yield of 15.2 per cent was ob-
tained, no volatile reaction products were found.

### j. 1,8-Naphthalimide

The 4-amino substituent increases the melting temperature as
well as the eventual reactivity of the naphthalimide molecule.
The DTA thermogram of the unsubstituted compound shows that melting
occurs around 300°C and that the sample has volatilized out of the system
when the temperature has reached 450°C. A carbon yield of 1.0 per cent
was obtained and the condensate contained both the original sample and
some new unidentified reaction products.

### k. Anthraquinonoid Dimers Having Nitrogen Bridges

Two interesting dimeric compounds obtained by the alkali fusion
of β-aminoanthraquinone are indanthrone and flavanthrone.

### Indanthrone

Indanthrone is essentially an anthraquinone dimer joined by
two nitrogen bridges. This compound proved to be very re-
active thermally, undergoing several endothermic and exothermic
reactions and producing a complex volatile product as well as an
appreciable carbon yield of 53.9 per cent at 750°C. No starting
compound was found in the distillate. Previous examination of
1-aminoanthraquinone[2] showed that the monomer reacted exo-
thermally at temperatures around 450°C to produce a 13 per cent
carbon yield.

### Flavanthrone
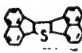
When the fusion of β-aminoanthraquinone is carried out at
temperatures above 270°C, the product is not indanthrone
but flavanthrone, the more condensed heterocyclic quinonoid com-
pound shown in Table 5. The DTA thermogram indicates that this
particular sample, obtained from a chemical supplier, is quite
impure. Attempts will be made to purify it by chromatographic
fractionation. The thermogram of this as-received sample shows
a very large and broad endotherm over the entire low-temperature
region to 400°C followed by a very small endotherm and exotherm

25

585 and 605°C, respectively. A carbon residue of 55.1 per cent was obtained.

### 3.1.1.1.6. Thermally Reactive Heterocyclic Sulfur Compounds

Only one heterocyclic sulfur compound was found to be reactive on examination by DTA. The thermogram obtained is shown in Figure 4 and the related thermal properties are given in Table 6. A brief discussion of the thermal behavior of this compound follows.

Table 6. Thermally Reactive Heterocyclic Sulfur Compounds

| Compound | Structure | DTA No. | M.p.-°C Lit. | M.p.-°C DTA | B.p.-°C DTA | $R_x$.T °C | %C Residue | |
|---|---|---|---|---|---|---|---|---|
| Dinaphthylene thiophene | | 471 | --- | 257 Imp. 283 Major | none | 495 Exo 540 Exo | 68.2 | Mostly S. M. in condensate plus several new weak bands. |

#### a. Dinaphthylene Thiophene

The DTA thermogram indicates the presence of an impurity in this sample with a double melting point of 257°C and 283°C. The molten sample begins to react exothermally around 450°C and exhibits two exothermic maxima, at 495°C, and a smaller peak at 540°C. From the shape of the exotherms, however, it is believed that an endothermic volatilization is superimposed and produced the dip which gives the appearance of two exothermic reactions. The condensate collected in the KBr condenser contained mostly starting material with a small amount of new reaction products which could not be identified from the IR spectra.

### 3.1.1.2. Gilsonite Pitches

Three samples of gilsonite pitches were received for DTA examination. The development group, during an investigation of the possible use of these materials for coke stocks, experienced a difficulty with excessive foaming during the coking operation, suspected to be due to exothermic reactions; the DTA thermograms shown in Figure 5 were obtained to check this possibility. The properties of these three samples are shown in Table 7.

The DTA behavior of all three of these pitches was very similar. No exothermic regions were evident. The major endothermic activity appeared to be due to volatilization which occurred over a broad temperature region. The endotherm curves all have a sharp minimum between 425 and 445°C above which the curve rises to a new baseline. This resulted from the hardening and shrinkage of the carbonizing mass and changed the thermal properties and thermal contact with the detecting thermocouples. All three of these samples foamed during the DTA examination. The foaming
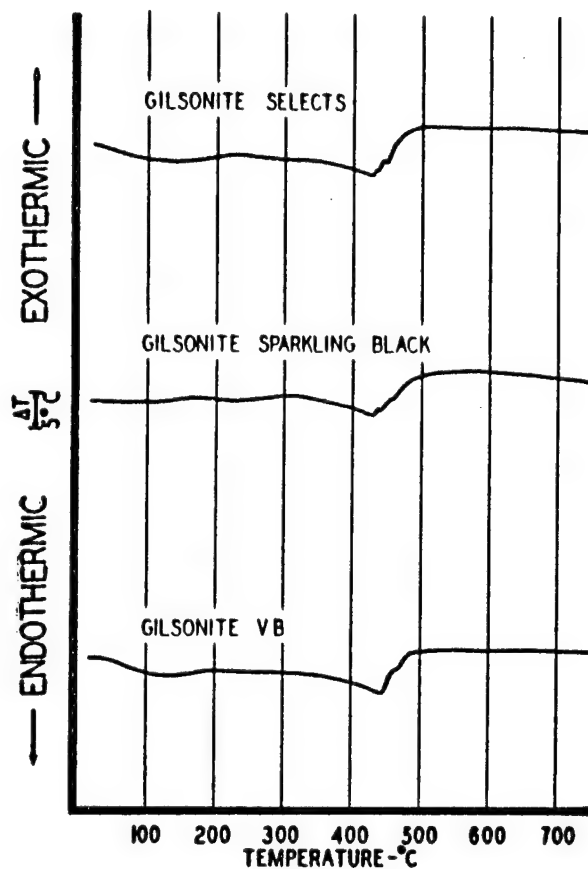
Figure 5.  DTA Thermograms of Gilsonite Pitches

N-5206

Table 7.  Properties of Gilsonite Pitches

| Name of Pitch | Ring Ball Soft. Pt. °C | Spec. Grav. | Fixed Carbon Per Cent |
|---|---|---|---|
| Gilsonite Selects | 133 | 1.035 | 13.5 |
| Gilsonite Sparkling Black | 177 | 1.052 | 19.5 |
| Gilsonite VB | 166 | 1.060 | 18.0 |

appears to be related to the rapid evolution of gases in a material of increasing viscosity.  The situation is similar to that experienced with coal tar pitch.

27

## 3.1.2. Thermogravimetric and Gas Evolution Analysis of Coal Tar Pitches

Thermogravimetric Analysis (TGA) is the simple technique of continuously measuring the weight of a material while it is being heated at a uniform rate. The simultaneous measurement of the weight change an and the evolution of noncondensable gases in a hydrocarbon system during pyrolysis provides additional information important to an understanding of the carbonization mechanisms.

Effort has been expended in developing an apparatus in which materials can be pyrolyzed under precisely controlled conditions while the sample weight and volume of fixed gases evolved are monitored and recorded continuously and the condensable volatiles are collected and prevented from undergoing secondary reactions. By suitable analysis of the results of such pyrolysis experiments, the rate and extent of distillation of unreactive components as well as considerable information about the thermally reactive components can be obtained. In addition, analysis of the products permits some judgments as to reaction mechanisms.

### 3.1.2.1. Description of TGA-GE Apparatus

The thermogravimetric balance consists of a differential transformer head on which a pedestal is mounted to hold the sample in the center of a 1-inch diameter vertical tube furnace. The milled sample is held in a stainless steel cup having dimensions approximately $\frac{7}{8}$ inch in diameter by $\frac{3}{4}$ inch in depth. The cup may or may not be covered. Control and monitoring thermocouples are set in wells located just below the sample. The furnace atmosphere is controlled by a gas inlet at the bottom of the furnace tube. The gas flow is upward over the sample and out of the furnace through a condenser and into a gas collection burette. The system operates at constant pressure through a differential pressure manometer which responds to a pressure change of 0.2 mm Hg by adjusting the volume of the gas collector. Both the weight of the sample and the volume of the system are automatically recorded.

The initial performance tests of the combined TGA-GE apparatus have been made using two experimental coal tar pitches which were obtained by the Lawrenceburg laboratory for development studies. The principal purpose of these runs was to evaluate the performance characteristics of the apparatus with two quite different but difficult materials rather than to examine the thermal behavior of the pitches. After each experiment, modifications in the apparatus were made, so a strict comparison of results between runs is not possible.

In addition to changes in the gas evolution measuring and recording systems to improve their reliability, the major modification involved the problem of completely removing the condensable tarry distillates from the reaction tube to prevent their recirculating to the hot zone at higher temperatures and undergoing secondary flash pyrolysis.

28

The original design employed a water-cooled side-arm condenser coming off the combustion tube just above the top of the furnace. This did not work, no matter how effectively the top of the combustion tube was cooled. The high boiling distillates always condensed on the tube walls well below the water-cooled area, and when the furnace temperature increased would melt and flow back down into the hot zone where it would carbonize on the walls of the tube. Run 39, discussed later, was the final experiment performed with an external condenser.

The next modification was an internal cold-finger type condenser made of quartz tubing extending into the furnace about two inches and centered in the combustion tube. This cold finger proved to be inadequate in Runs 40 and 41 because some of the condensate still collected on the tube walls and, in addition, at temperatures above 600°C the condensate on the cold finger dripped off the tip back onto the sample on the balance. Obviously, a condenser with a larger surface area capable of holding more liquid was required.

Several condensers were made up of small-diameter stainless-steel tubing and tested. The condenser which proved to be completely effective in removing all of the condensable tars produced in Run 44 was made of eight feet of 0.040-inch ID stainless-steel tubing wound into a double coil 2 inches in length with a $\frac{1}{2}$-inch OD and a $\frac{1}{4}$-inch ID as shown in Figure 6. With cold water passing through this coil at 85 cc per minute the temperature of the water did not increase measurably with the furnace temperature at 750°C. The effectiveness of these internal condensers was increased by the use of a covered sample container with a $\frac{1}{8}$-inch diameter chimney inserted into the cover. This is placed directly under the coil and directs the volatiles into the center of the condenser thereby eliminating any opportunity of by-passing the condenser. In addition, the larger sample cup prevents overflowing of the sample and permits covering of the sample with filler coke or other inert material if desired.

### 3.1.2.2. Experimental Results

Four TGA-GE runs have been analyzed on two experimental coal tar pitches produced at the Lawrenceburg laboratory: one, a low-temperature coal tar pitch (M-176), and the other a high-temperature coal tar pitch (M-177). Notwithstanding the experimental variations introduced into the data presented here, they are of interest in illustrating the pyrolytic behavior of two chemically dissimilar coal tar pitches.

A comparison of the physical properties and the elemental analysis as well as the ash analysis of the two pitches is given in Table 8.

As a product of a low-temperature coal carbonization process, pitch M-176 would be expected to be less aromatic than the usual high-temperature coal tar pitch, such as the medium hard pitches used in carbon production and pitch M-177. The analysis summarized in Table 8 verifies this expectation. The lower specific gravity of M-176 shows a lower degree of aromaticity as does the lower carbon-to-hydrogen ratio. An inter-
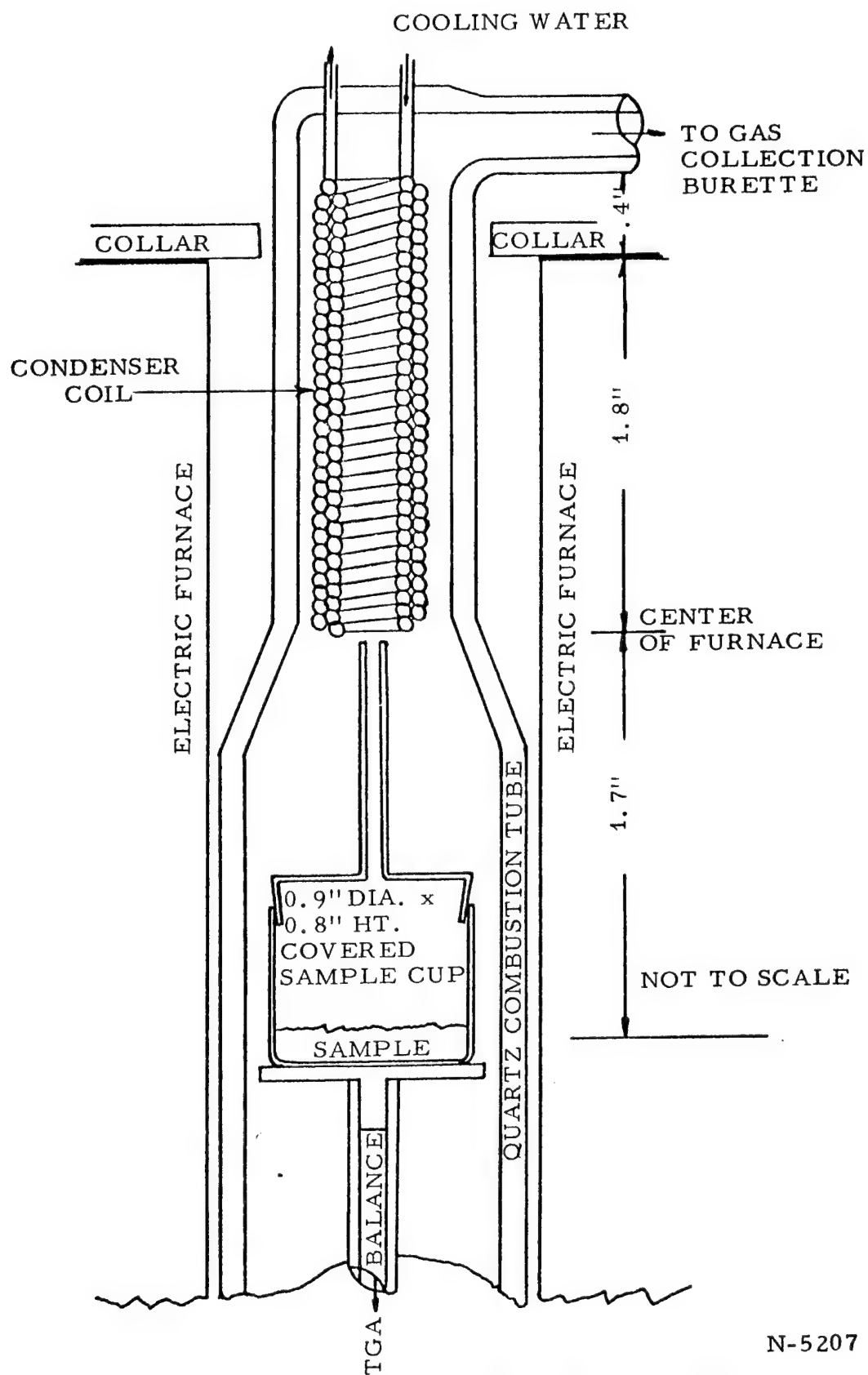
Figure 6.   Gas Evolution System of TGA-GE Apparatus

30

Table 8. Analysis of Experimental Coal Tar Pitches

| Analysis | | Low-Temperature Coal Tar Pitch M-176 | High-Temperature Coal Tar Pitch M-177 |
|---|---|---|---|
| Specific Gravity - 25°C (He Pycnometer) | | 1.2590 | 1.2898 |
| Softening Point (CIA) - °C | | 102.5 | 96.4 |
| Ash Content - % | | 4.05 | 0.14 |
| Benzene Insolubles -% | | 40.14 | 24.70 |
| Quinoline Insolubles -% | | 23.74 | 2.69 |
| Volatile Content -% | | 55.5 | 51.2 |
| Elemental Analysis: | | | |
| % Carbon | | 81.29 | 92.27 |
| % Hydrogen | | 5.49 | 4.73 |
| % Sulfur | | 1.04 | 0.51 |
| % Nitrogen | | 1.06 | 0.79 |
| % Oxygen | | 6.06 | 1.37 |
| Ash Analysis: (Emission Spect. on Whole Pitch) - % | Fe | 0.20 | 0.03 |
| | Mg | .03 | .002 |
| | Mn | .002 | <.002 |
| | Pb | .002 | .01 |
| | Si | .90 | .03 |
| | Al | .50 | .03 |
| | Ti | .03 | <.002 |
| | Ni | -- | <.002 |
| | V | -- | -- |
| | Ca | .06 | .007 |
| | Cu | .02 | .002 |
| | Ag | <.002 | <.002 |
| | Na | Pres. | -- |

esting point is the high oxygen content in M-176. The infrared absorption spectrum contains only an -OH band with no indication of carbonyl or ether oxygen. In addition, the ash content of the M-176 is very high resulting from high levels of iron, silicon, and aluminum, possibly from contamination from poor refractory brickwork in the coal tar furnace. The high oxygen level may therefore be associated with the high ash content. The high BI and QI values obtained on the M-176 pitch suggest either a high fixed carbon content, high inorganic contamination, or a

31

relatively high average molecular weight as compared to M-177 or a normal binder pitch. Nuclear magnetic resonance (NMR) examination of these two pitches is discussed in Section 3.1.7.

The results of two separate pyrolysis experiments on pitch M-176 (low-temperature coal tar pitch) are shown in Figures 7 and 8. The thermogravimetric and gas evolution curves in Figure 7 show the cumulative fixed gas evolution as the temperature of the sample is increased. The derivative curves in Figure 8 show the weight loss rates and gas evolution rates as a function of the temperature of the sample.
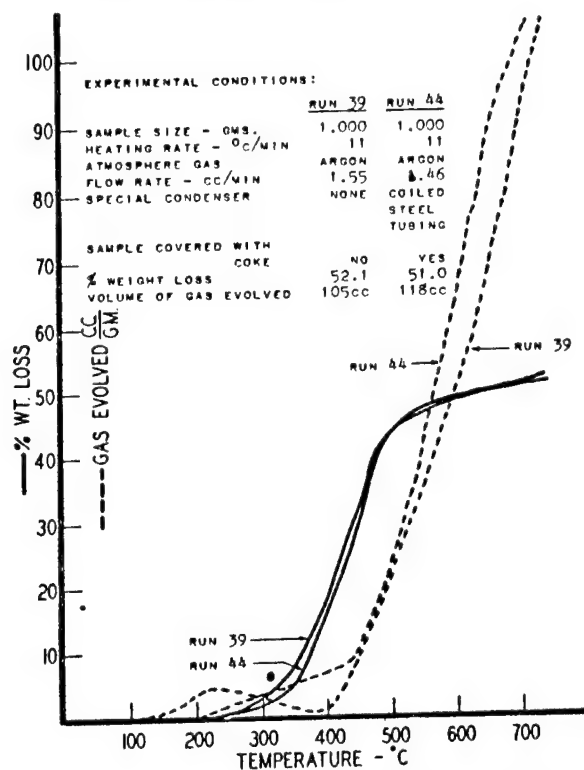


Figure 7. TGA-GE Curves for the Pyrolysis of a Low-Temperature Coal Tar Pitch M-176

N-5208

The experimental conditions of the two runs are tabulated in Figure 7 showing that the sample size, heating rates, and argon flow rates were essentially the same in both experiments. The experimental parameters differed in two important respects. Run 39 did not have the internal condenser to prevent the condensable distillates from returning to the pyrolysis tube and Run 44 had the most efficient coil condenser that removed all the condensate as it was distilled out of the pitch. Also, in Run 44 the pitch sample was covered with a 2-gram layer of petroleum coke flour. This was done to reduce foaming which proved to be a real problem with pitch M-176. The pitch would foam and extrude up the chimney and into the condenser coil and disrupt the TGA record. The coke layer served to minimize the foaming problem.

32
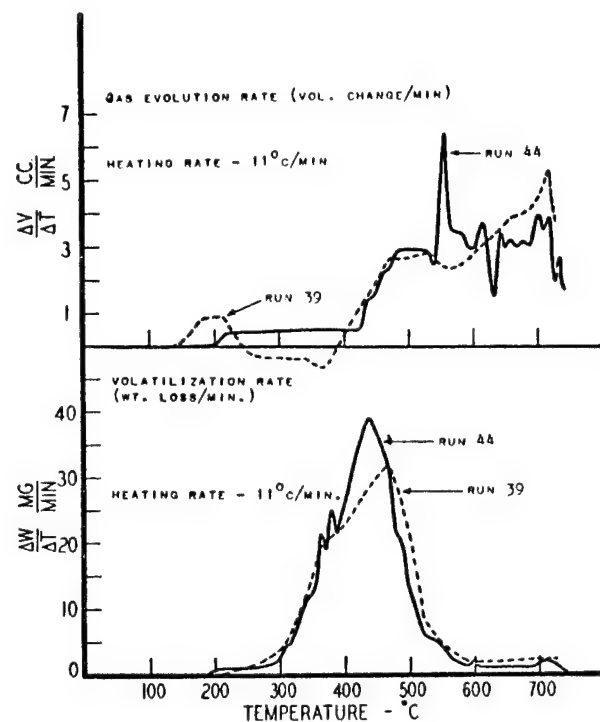
N-5209

Figure 8. Derivative TGA-GE Curves for Pyrolysis
of Low-Temperature Coal Tar Pitch M-176

The TGA curves in Figure 7 agree quite closely despite the experimental variations. M-176 pitch begins to lose weight around 200°C. The volatilization rate increases to about 450 to 475°C at which point the rate decreases steadily as the temperature continues to rise to around 600°C. Above 600°C, the volatilization rate becomes fairly constant at a low level. The change in rate is shown graphically in Figure 8. The gas evolution curves show a somewhat greater divergence than the weight loss curves. This observation might be predicted as the presence of coke flour is known to increase the carbon yield from a pitch. The noncondensable gases can only result from such chemical reactions as dehydrogenation, dealkylation, oxidation, or ring rupture which also lead to molecular growth of the residual molecular fragments. Thus, the progress of the coking reaction is charted by the gas evolution curve.

The gas evolution appears to begin at relatively low temperatures between 150 and 200°C. Since relatively small fluctuations in the argon flow rates might account for this low-temperature portion of the GE curve, it is not considered to be positively established. The apparent readsorption effect shown by Run 39 between 225 and 390°C is also very suspicious. It has not been observed since more effective internal condensers have been used in the combustion tube and may be associated with the condensable vapors. In the earlier versions of the TGA apparatus, yellowish

33

vapors could be seen circulating in the hot zone of the combustion tube below temperatures of 400 to 450°C. About 10 per cent more gas was produced in Run 44 than in Run 39.

A comparison of the derivative curves in Figure 8 shows that the volatilization rates in the two runs are fairly similar. In Run 44 the maximum rate was reached about 25° lower than in Run 39, probably because the coke flour improved the heat transfer into the pitch. The greater detail in the derivative curves is the result of much better sensitivity of the detector and recording systems. In the case of the gas evolution curves, this improved sensitivity showed that our temperature controller was not adequate. Most of the hash in the gas evolution rate curves are due to fluctuations in the heating rate. A new proportioning temperature controller has been ordered to eliminate this problem.

Two TGA-GE runs made on high-temperature coal tar pitch M-177 are shown in Figure 9 and the derivative curves are compared in Figure 10.
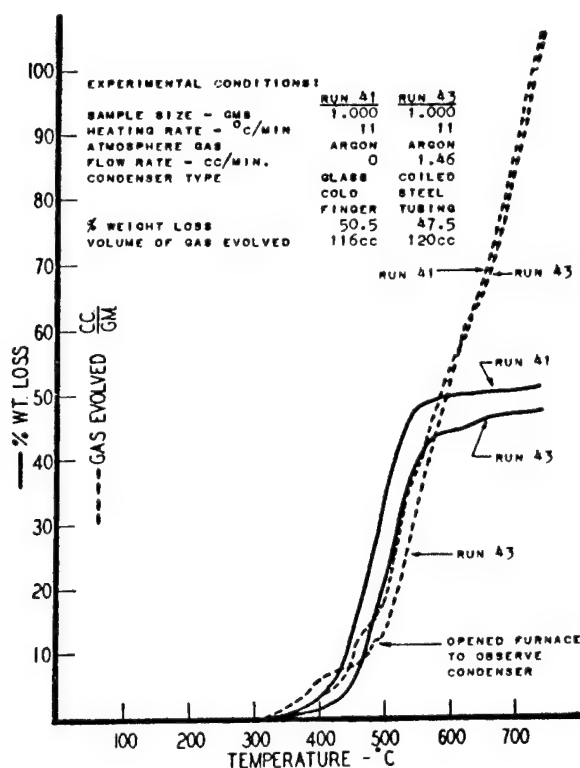


N-5210

Figure 9. TGA-GE Curves for the Pyrolysis of a
High-Temperature Coal Tar Pitch M-177

34
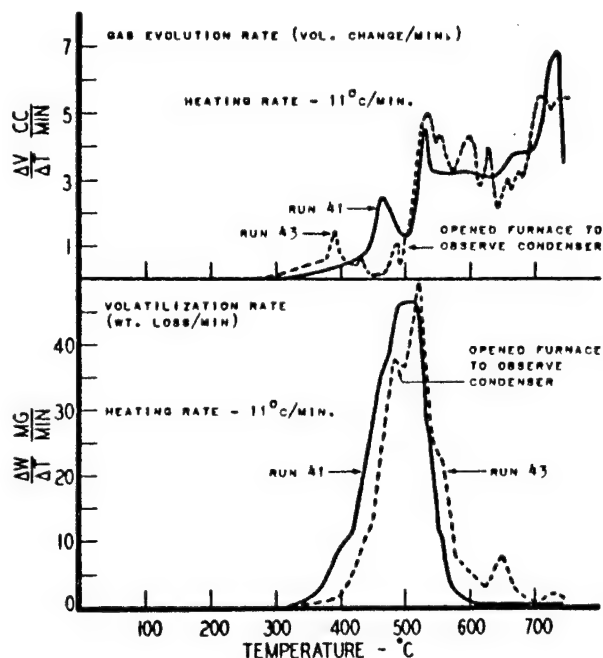
Figure 10. Derivative TGA-GE Curves for Pyrolysis
of High-Temperature Coal Tar Pitch M-177

N-5211

Although pitches M-176 and M-177 give approximately the same
carbon yields, M-177 begins to lose weight at a much higher temperature
than M-176, exhibiting no measurable weight loss below 300°C. No ready
explanation of the rather wide difference between the TGA curves obtained
during Runs 41 and 42 is evident. The experimental differences tabulated
on Figure 9, namely, a stagnant argon atmosphere versus a 1.5 cc/minute
argon flow or the differences in condenser design, would not be expected
to produce this large difference in pyrolysis behavior. The difference of
3 per cent in carbon yield is much greater than normally experienced with
pitches in this apparatus.

The cumulative gas evolution curves in Figure 9 are similar and
in relatively good agreement. The major dissimilarities in either curve
can be explained by the observed experimental difficulties. These abrupt
changes in rate are more evident in the derivative curves in Figure 10.
In Run 41 an internal quartz glass cold-finger type condenser was used to
remove the condensable vapors from the furnace atmosphere. This cold
finger was about $\frac{3}{8}$ inch in diameter and long enough to extend about $1\frac{1}{2}$
inches below the top of the furnace. The cold finger had smooth side walls
and a rounded tip which was located about $\frac{1}{2}$ inch above the outlet of the
chimney on the sample container (see Figure 6). By the time the tempera-
ture reached 450°C, a sufficiently thick layer of condensate had accumu-
lated on the tip of the condenser to prevent solidification at the outer surface
and some condensate dripped back into the hot furnace. This occurred
periodically as the weight of the accumulating liquid exceeded the surface
tension holding it to the condenser tip. Although this is hardly evident in

35

the TGA curves because the weight data is recorded digitally at 30-second intervals, the gas volume curves show it very well. The condensate flash evaporates and produces a significant bump in the gas evolution rate. Four of these occurred during Run 41, easily seen in the gas evolution rate curve, at 465, 530, 590, and 670°C. No dripping of the condensate occurred in Run 43. However, in Run 43, one rather large rate change was brought about because the furnace was opened momentarily to observe the operation of the coiled tubing condenser. This operation produced a rather severe drop in temperature and resulted in the minima in both the TGA rate curve and the GE rate curve seen at about 480°C. Most of the other variations in gas evolution rate in Run 43 are the result of the variations in heating rate described previously.

A comparison of the pyrolytic behavior of pitches M-176 and M-177 is more readily seen in Figures 11 and 12. The results of the last and best two runs (from the experimental point of view) on these pitches are plotted together. Pitch M-176 is seen to undergo its initial and major volatilization losses at temperatures from 75 to 100°C lower than pitch M-177. The gas evolution curves, however, except initially, are only about 25 to 30°C apart and the total volume of gas evolved from both pitches is similar although the composition and therefore the weight is not. The gas composition at the end of the runs as determined by gas chromatographic analysis is given in Table 9. The results are the averages from several runs corrected for argon, oxygen, and nitrogen. For this correction, it was assumed that the oxygen and nitrogen evolved from the sample were negligible.
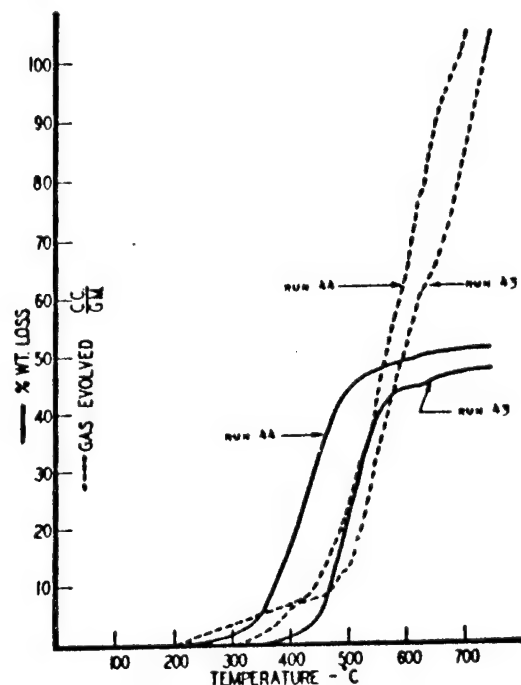


N-5212

Figure 11.  Comparison of TGA and GE Curves for the Pyrolysis of a Low-Temperature Coal Tar Pitch M-176 (Run 44) and a High-Temperature Coal Tar Pitch M-177 (Run 43)

36
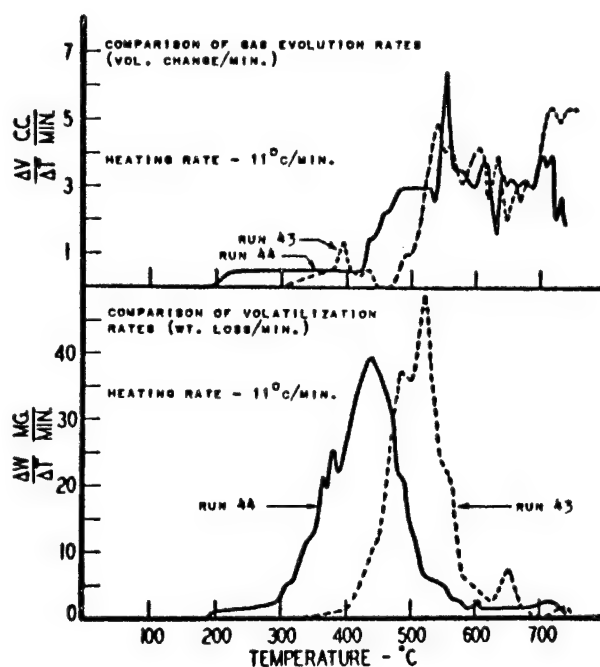
N-5213

Figure 12.   Derivative TGA-GE Curves for Pyrolysis of Low-
Temperature Coal Tar Pitch M-176 (Run 44) and
High-Temperature Coal Tar Pitch M-177 (Run 43)

Table 9.   Comparison of the Composition of the Fixed Gases
Evolved During the Pyrolysis of Pitches M-176 and
M-177

| Gas | Low-Temperature Coal Tar Pitch M-176 | | High-Temperature Coal Tar Pitch M-177 | |
|---|---|---|---|---|
| | Mol % | Wt., grams | Mol % | Wt., grams |
| Hydrogen | 45 ± 5 | .005 | 73 ± 10 | .008 |
| Methane | 31 ± 3 | .026 | 15 ± 2 | .013 |
| Ethane | 3 ± .5 | .004 | 1.7 ± .5 | .003 |
| Ethylene | 2.5 ± .5 | .003 | 0.8 ± .5 | .001 |
| Carbon Monoxide | 8 ± 1 | .012 | none | - - - |
| Carbon Dioxide | 10.5 ± 2 | .025 | 9.5 ± 2 | .021 |
| Totals | 118 cc | .075 g | 120 cc | .046 g |

The gas analysis results agree with the chemical composition of
the starting materials as indicated in Table 8.   The more aromatic pitch
M-177 produces significantly more hydrogen and less methane, ethane,
and ethylene.   The carbon monoxide results are surprising and require
further investigation.

37

The problem of baking carbon articles is greatly complicated by the necessity of removing the volatile products as they are formed without seriously damaging the internal structure of the bonded aggregate. For this reason, most baking rates through the critical low-temperature range are very slow to permit the volatile products to diffuse to the surface of the carbon mass without forming cracks, pores, bubbles, or blisters. The TGA and GE data may be useful in establishing guidelines for determining critical temperatures and evaluating materials.

If the solubility of the condensable vapors in the liquid pitch is assumed to be negligible, the maximum volume of the vapors as well as the volume of the fixed gases evolved at any given temperature can be calculated. The results of such calculations on the TGA data of Runs 43 and 44 are plotted in Figure 13. It is evident that both the condensable vapors
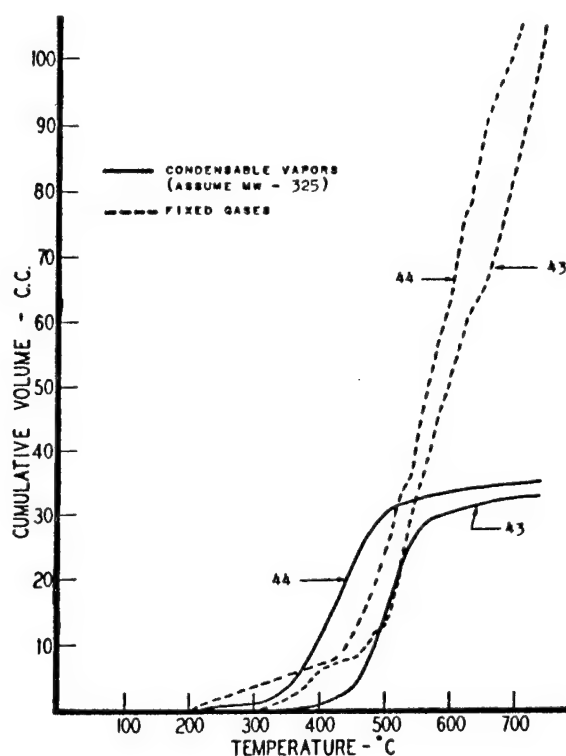


N-5214

Figure 13. Comparison of Volumes (STP) of Condensable Vapors and Fixed Gases Evolved on Pyrolysis of Pitches M-176 (Run 44) and M-177 (Run 43)

and the fixed gases contribute about equally to the volume of gaseous products emitting from the pitch at temperatures below about 500 to 540°C. Above this temperature the fixed gases become the major contributors and the condensable hydrocarbons cease evolving almost entirely.

Since a pitch-bonded carbon article consists of solid particles in a fluid matrix at temperatures between the softening point of the pitch and the resolidification temperature around 525°C, the critical temperature range lies between 300 and 540°C with a high-temperature coal tar pitch binder. The condensable volatile fraction contributes significantly to the problem of maintaining structure and anything that can be done to reduce the volatility of the lighter hydrocarbons without producing additional quantities of fixed gases would contribute to improved bakeability.

## 3.1.3. Chemical Structure and Graphitization

## 3.1.3.1. Introduction

The previous sections have been concerned with the relation between chemical structure and thermal reactivity. The DTA method has been employed primarily as a survey method for comparing the reactivity of model compounds to carbonization under a fixed set of conditions. By definition, the reactive compounds yield carbon residues at 700°C, the amount of which has been used to assess thermal reactivity.

A question of at least equal importance is the relation between chemical structure and the course of thermal reaction. The properties of the final carbon and graphite depend to a large extent on the chemical constitution of the organic precursors. For this purpose, we have begun a systematic investigation of the effects of chemical structure on the degree of graphitization in synthetic graphites. The X-ray technique has been employed as a diagnostic method for classifying various graphites. This survey is designed not only to help answer the questions already raised but to serve as a basis for selecting individual compounds for detailed reaction mechanism studies.

An earlier report[3] gave some values for the lattice spacing measured from the position of the 002 peak for a limited number of synthetic graphites. A wide variation in 002 parameters was observed among the different starting materials; however, the X-ray procedure employed seemed to have severe experimental limitations. We have now refined the X-ray method in order to obtain lattice spacing parameters of relatively high precision. It is eventually anticipated that all of the thermally reactive model compounds included in our studies will be subjected to this method. The present report summarizes the X-ray data for some 35 aromatic hydrocarbons as well as for several commercial raw materials. The data are discussed in relation to chemical structure.

## 3.1.3.2. Experimental

## 3.1.3.2.1. Preparation of Synthetic Graphites

In the course of the DTA examination of model compounds, carbon residues are obtained at 700°C for all reactive materials. The residues from approximately 100 of these compounds have been converted to

39

graphite at 3000°C in a conventional graphitization furnace. Additional residues of compounds currently under investigation are being collected and will subsequently be graphitized for inclusion in this survey.

A number of organic compounds which are of interest do not possess any reactivity in the DTA method. These compounds have been carbonized to 450°C in a closed pressure system. The synthetic cokes obtained in this manner were then graphitized in a conventional manner.

### 3.1.3.2.2. X-Ray Measurements

The graphite samples were all ground through 100 mesh. They were mounted on a 5-mil thick tantalum fiber which had first been dipped in Apiezon grease. The function of the grease was to permit the graphite particles to adhere to the tantalum fiber. The use of tantalum permitted the accurate measurement of the 002, 004, 006, and 008 reflections in the synthetic graphites. The interference effects that had previously been found for tungsten were thus obviated. Tantalum additionally provides distinct lines in the back-reflection for film shrinkage corrections.

The X-ray patterns were measured on films with the use of a Norelco diffractometer and a Debye-Scherer powder camera, 114.6 mm diameter. Copper radiation and a nickel filter were employed and the films were exposed for a period of 20 hours. Each film was measured and corrected for shrinkage a total of four times. After each measurement, the film was removed from the film measuring device and then reinserted. An average of the four measurements was then obtained for all values.
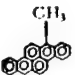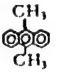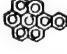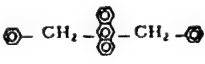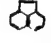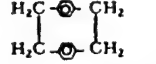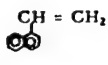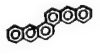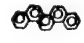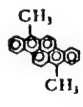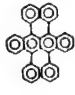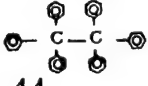
### 3.1.3.3. Results

The 002 and 004 lines were observed in all the synthetic graphites. The 006 lines could be observed in nearly all of the materials, while the 008 lines were discernible in approximately one-half of the films. The accuracy of the line measurement increased significantly in the higher order peaks, with the 002 lines showing the largest discrepancy. The 006 line positions were, therefore, utilized as the most accurate measure of the semilattice spacing in the graphite. When no 006 line could be observed, use was made of the 004 peak. These values were then converted directly to 002 spacing by employing the proper factor, 2(004) and 3(006). The 002 spacings thus determined are listed in Table 10 for 35 synthetic graphites. Table 11 contains the values for some graphites obtained from commercial raw materials.

### 3.1.3.4. Discussion

The aromatic hydrocarbons are listed in Table 10 in order of increasing 002 values for their derived graphites. It seems evident from the data in Table 10 that even for the pure aromatic hydrocarbons, the nature of the final graphite is highly dependent on the starting chemical

# Table 10. 002 Lattice Spacings for Graphites Derived from Aromatic Hydrocarbons

| Aromatic Hydrocarbons | Structure | 002 Lattice Spacing, Å |
|---|---|---|
| (1) 7-Methylbenzo(a,h)pyrene | | 3.347 |
| (2) 9,10-Dimethylanthracene | | 3.348 |
| (3) Benzo(e)pyrene | | 3.350 |
| (4) Benzo(a)coronene | | 3.350 |
| (5) 9,10-Dibenzylanthracene | | 3.350 |
| (6) Acenaphthylene | | 3.351 |
| (7) 9,9'-Bianthryl | | 3.351 |
| (8) Naphthacene | | 3.351 |
| (9) Di-p-xylylene | | 3.351 |
| (10) Dibenzo(a,i)pyrene | | 3.352 |
| (11) 1-Vinylnaphthalene | | 3.353 |
| (12) Dibenzo(a,l)pentacene | | 3.353 |
| (13) Dibenzo(b,k)chrysene | | 3.353 |
| (14) Picene | | 3.354 |
| (15) 7,14-Dimethyldibenzo-(a,h)pyrene | | 3.354 |
| (16) 5,6,11,12-Tetraphenyl-naphthacene | | 3.354 |
| (17) Dibenzo(h,rst)pentaphene | | 3.355 |
| (18) Pentacene | | 3.356 |
| (19) Hexaphenylethane | | 3.356 |

Continued

Table 10.   Continued

| Aromatic Hydrocarbons | Structure | 002 Lattice Spacing, Å |
|---|---|---|
| (20)  Decacyclene | | 3.358 |
| (21)  Rubicene | | 3.359 |
| (22)  2-Vinylnaphthalene | CH=CH₂ | 3.359 |
| (23)  Di-9-fluorenylethane | H H CH₂ CH₂ | 3.360 |
| (24)  Pyranthrene | | 3.361 |
| (25)  14 H-acenaph(1, 2-j)indeno-(1, 2-1)fluoranthene | H H | 3.361 |
| (26)  Quarterrylene | | 3.364 |
| (27)  Coronene | | 3.366 |
| (28)  Fluoranthene | | 3.367 |
| (29)  Dibenzo(a, c)triphenylene | | 3.369 |
| (30)  9, 9'-Bifluorene | H H | 3.370 |
| (31)  14, 15-Dihydro-9H-diindeno-(1, 2-1)fluoranthene | H₂ H₂ H₂ | 3.376 |
| (32)  9, 10-Di-1-naphthylanthracene | | 3.389 |
| (33)  Diphenylacetylene | C≡C | 3.421 |
| (34)  p-Terphenyl | | 3.437 |
| (35)  Δ⁹, ⁹'-Bifluorene | | 3.470 |

Concluded

42

Table 11.　002 Lattice Spacings in Å for
Graphitized Raw Materials

| Material | 002 Lattice Spacing, Å |
|---|---|
| (1)　Canadian Natural Graphite | 3.350 |
| (2)　30-Medium Pitch | 3.350 |
| (3)　AX Coke | 3.351 |
| (4)　15-Vacuum Pitch | 3.353 |
| (5)　Acenaphthylene Pitch | 3.354 |
| (6)　DK Coke | 3.355 |

structure.　The connection is not obvious in all cases; however, it appears that two major factors are involved:

    1.　The planarity and steric overcrowding in the original molecule;

    2.　The chemical reaction sequence and the nature of the thermally formed intermediates.

Nearly all of the compounds in Table 10 are common constituents of the usual raw materials for carbon and graphite; i.e., coal tar pitch and petroleum residues.　The majority of these compounds yield highly oriented graphite, low 002 spacings.　About half of the compounds fall in the same range of well-ordered graphites as that represented by the raw materials in Table 11.

Expecially interesting are the compounds listed at the end of Table 10.　All but one of the compounds with lattice spacing greater than 3.366 are either nonplanar or sterically overcrowded molecules.[4]　The thermal reactions of these entities would most likely yield nonplanar reactive intermediates.　The course of graphitization for fluoranthene is likely a result of the nonplanarity of thermally formed reaction intermediates (see the following section).

For the compounds with low 002 values, reactivity seems to be of major importance.　Alkyl-substituents and side-chain groups appear to enhance the degree of graphitization.　Such compounds can readily form aromatic radicals.　The side-chain groups offer a mobile means of rearrangement to planar conjugated systems through radical intermediates.

3.1.4.　Carbonization Studies of Model Compounds

The previous sections of this report have shown how the thermal reactivity to graphite formation as well as the graphite properties can be influenced by chemical structure.　These relationships are intimately connected to the thermal reaction mechanisms.　An important phase of

43

this program, therefore, is to study the carbonization mechanisms for selected model compounds and attempt to establish general relationships between chemical structure, thermal mechanisms, and graphite properties.

The initial results of chemical investigations on the pyrolysis of two model aromatic hydrocarbons, acenaphthylene and bifluorenyl, have already been reported.[3] Supplemental low-angle X-ray studies have since provided a generalized sequence for the formation of graphite from these materials. The reaction sequences are outlined in Figures 14 and 15.
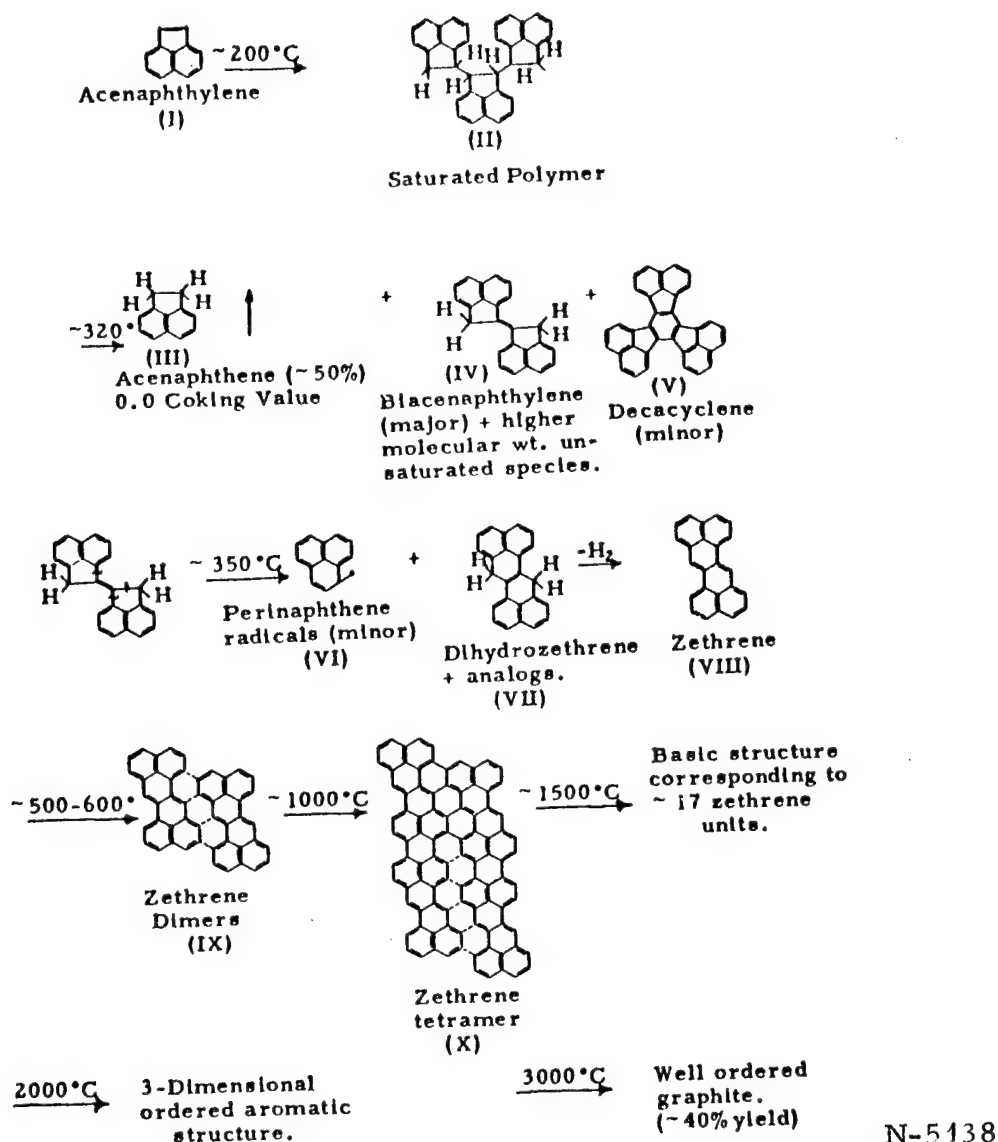


Figure 14. Formation of Graphite from Acenaphthylene

44

9,9'-Bifluorenyl    Fluorene    $\Delta^{9,9'}$-Bifluorene
(XI)    0.0 Coking Value    (XIII)
(XII)

~ 400°C    +

450°C    ~ 500°C    800°C

Biphenylmethylene    (Nonplanar) Tetrabenzo-
fluorene radicals    naphthalene
(XIV)    + analogous small
nonplanar radicals, etc.
(XV)

1000°C    Aromatics about
4-Tetrabenzonaphtha-
lene units, not planar.

Tetrabenzonaphthalene
dimers (XVI)

1500°C    Aromatic about same size    2000°C    No 3-dimensional
as acenaphthylene system    order. Layers about
~ 17 basic units.    as large as ace-
naphthylene system
3000°C    Graphitic carbon with    but there are im-
imperfect 3-dimensional    perfections in hex-
order.    agonal structure

N-5137

Figure 15.    Formation of Graphite from 9,9'-Bifluorenyl

### 3.1.4.1.  Acenaphthylene

The polymer (II) formed thermally from acenaphthylene has been characterized by X-ray.  The polymer possesses a coiled helical structure with three to five monomer units per turn.  The CH-CH sequence is in a trans-orientation and the bulky naphthalene units point outward.  The orientation of this polymer favors the reactions which proceed subsequently.  Thermal degradation of the polymer units results in reactive acenaphthene radicals which can abstract hydrogen to form the volatile acenaphthene or cyclize to decacyclene (V).  The important step for further reaction is the formation of dimeric unsaturated units (IV).  These units undergo carbon-carbon bond cleavages within the strained 5-membered ring.  Among the products formed are perinaphthene (VI) and zethrene analogs (VII) and (VIII).  Further growth appears to proceed via zethrene-like structures. At 500 to 600°C an infusible solid coke structure is developed.  The average chemical structural units correspond to species of the size of (IX).  At

45

1000°C, the average chemical structure corresponds to the size of (X). At 1500°C, the growth proceeds rapidly to the size of about 17 zethrene units while 3-dimensional ordering begins at 2000°C. A highly graphitic product built up through planar condensation is thus achieved at 3000°C.

### 3.1.4.2. 9,9'-Bifluorenyl

The general thermal reaction sequence of 9,9'-bifluorenyl is shown in Figure 15. Bifluorenyl initially disproportionates to yield reactive fluorene radicals which can abstract hydrogen atoms to form volatile fluorene or dimerize to $\Delta^{9,9'}$-bifluorene (XIII). Disproportionation of (XIII) results in the formation of nonplanar aromatic radicals such as (XIV). The major products are nonplanar aromatic structures of the tetrabenzonaphthalene type (XV). The further growth of the basic aromatic system is quite slow as expected for a nonplanar structure. Actually at 800°C, the average aromatic size in the solid coke corresponds only to that of a dimer of tetrabenzonaphthalene. At 1000°C and 1500°C, however, the growth increases to achieve the same proportions as the acenaphthylene system. The overall layer stacking is much more imperfect than for acenaphthylene. At 2000°C, 3-dimensional order has not yet progressed. Although the molecular size is about as large as the acenaphthylene, there are imperfections in the hexagonal structure. At 3000°C, a graphitic carbon with an imperfect 3-dimensional order is formed.

### 3.1.4.3. Fluoranthene

The hydrocarbon fluoranthene (XVII) yields a poorly oriented graphite structure. The carbonization of this compound is being studied



(XVII)
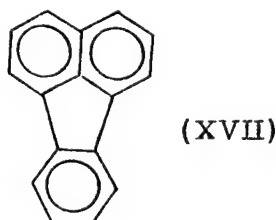
in the same manner as that employed for acenaphthylene and bifluorenyl. Due to the inertness of this material, the preparation of carbonized samples had to be performed in a closed pressure system. This compound possesses a zero coking value at atmospheric pressure.

Fluoranthene (Terra Chemical Company) was initially purified by recrystallization. Samples were then placed in thick-walled glass tubes and sealed in argon. Under these conditions the fluoranthene remained completely unreactive below a temperature of 450°C, where a red solid product was obtained. Continued reaction was observable at temperatures of 475 and 500°C. Reaction in this temperature region was accompanied

46

by the formation of light noncondensable gases. Considerable gas pressure was thus encountered upon opening the tubes.

For the higher temperature products, a "fluoranthene pitch," prepared in a large batch pressure operation at about 525°C was employed. Samples of "fluoranthene pitch" were carbonized in standard sagger furnaces under argon up to 1000°C. The 1000°C material was then heat-treated in standard tube furnaces at temperatures up to 3000 °C.

The preparation temperature, yield, and softening points of all the products are given in Table 12. The fluoranthene, like bifluorenyl and unlike acenaphthylene, possesses a very narrow "thermoplastic-pitch" range. Both of the aforementioned "poorly graphitizing" compounds appear close to thermosetting materials in their thermal behavior.

In addition to the data in Table 12, elementary analysis data are being obtained for all samples possible.

Table 12. Properties of Carbonized Fluoranthene

| Preparation Temperature °C | % Yield* | Mol. Wt. in $C_6H_6$ | Color | M.P. °C |
|---|---|---|---|---|
| 450 | ~ 100 | -- | Red | 90 |
| 475 | ~ 100 | 228 | Red | 101 |
| 500 | ~ 100 | 273 | Red | 96 |
| 525** | ~ 100 | 314 | Black | > 350 |
| 550 | 86.4 | Insol. | Black | Infusible |
| 600 | 75.2 | Insol. | Black | Infusible |
| 700 | 74.2 | Insol. | Black | Infusible |
| 800 | 73.0 | Insol. | Black | Infusible |
| 900 | 73.0 | Insol. | Black | Infusible |
| 1000 | 72.0 | Insol. | Black | Infusible |
| 1250 | 72.0 | Insol. | Black | Infusible |
| 1500 | 72.0 | Insol. | Black | Infusible |
| 2000 | 72.0 | Insol. | Black | Infusible |
| 3000 | 72.0 | Insol. | Black | Infusible |

*Yield based on 525°C material (fluoranthene pitch).
**Fluoranthene pitch (M. Janes–54-8-83) employed as the 525°C sample.

Infrared and UV absorption spectra of the low-temperature products are shown in Figure 16. The infrared spectra show only minor changes to 500°C, these being concentrated in the aromatic substitution range 12 to 14μ. The UV spectra show the continued development of three major bands in the UV-visible region at 459, 492, and 527 mμ. The UV portion of the spectrum is identical to that of the starting compound. This spectrum has been tentatively attributed to the red fluoranthene dimeric

compound periflanthene. The UV-visible spectrum of this latter structure is shown at the bottom of Figure 16.[5]
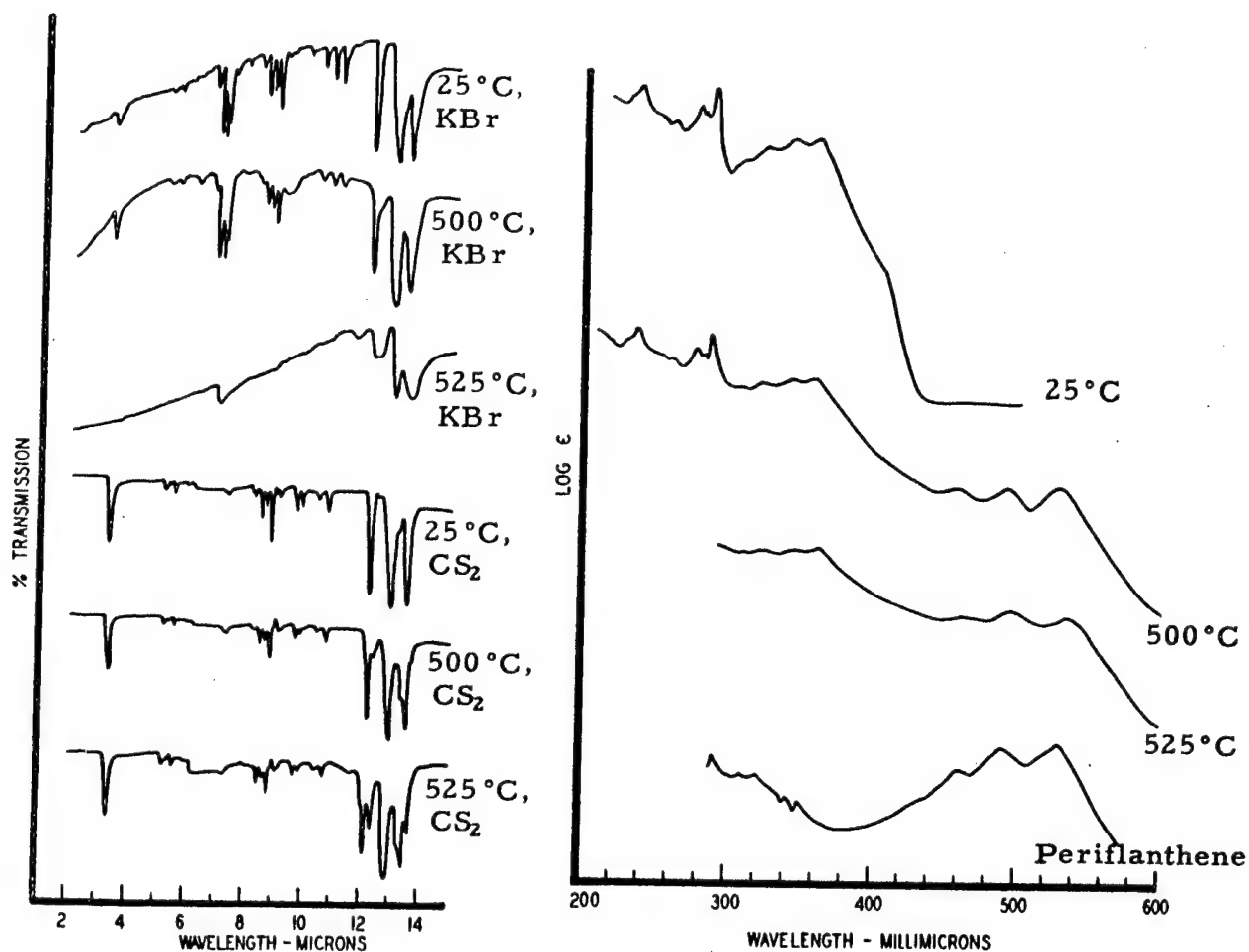


Figure 16. IR and UV Spectra of Fluoranthene and Pyrolysis Products

These results indicate that the first thermal reaction of fluoranthene is a dehydrogenation and dimerization at the reactive ring sites to form periflanthene:



Periflanthene

48
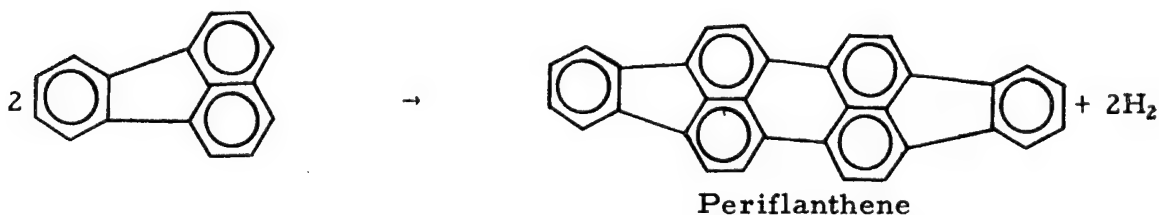
It is not yet clear whether dehydrogenation involves the direct loss of hydrogen gas or whether internal hydrogen transfer is involved. Preliminary chromatographic extraction studies indicate the possibility of aliphatic containing species. It is possible that the next reaction of a periflanthene species could be random combination of nonplanar phenylperylene radicals:
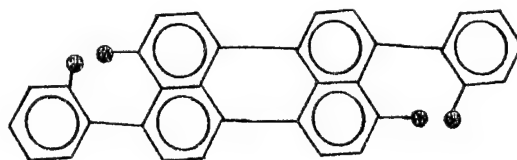


X-ray studies are expected to amplify on these hypotheses.


### 3.1.4.4. p-Terphenyl
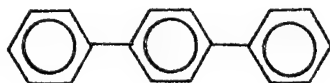


The polyphenyls are the most thermally stable aromatics encountered in our studies to date. This stability has been advantageously exploited in our ESR studies of pyrolysis. The polyphenyl hydrocarbon, p-terphenyl, has been found to yield a poorly oriented graphite (refer to Section 3.1.3.). We have therefore selected this compound as another model compound for pyrolysis studies.

Samples of p-terphenyl in sealed tubes showed complete inertness through temperatures of 500°C with hold times as long as 16 hours. Only after 4-hour heat-treatment at 525°C did some reaction become apparent. After 10 hours at 525°C, a brown residue was formed. After 20 hours at 525°C, a major reaction had occurred, resulting in the formation of a black pitch-like product and about 20 per cent of a liquid material.

The latter proved to be predominantly benzene with some dissolved biphenyl and an additional unidentified solid material. These products indicate the importance of thermal cleavage of polyphenyl bond linkage to yield reactive phenyl radicals. These can undergo hydrogen abstraction to produce benzene and biphenyl and lead to the formation of condensable radical species.

At 550°C, p-terphenyl is already an infusible coke. In order to obtain the higher temperature p-terphenyl cokes, a large batch of p-terphenyl coke was prepared at 550°C in a closed pressure system. This 550°C coke was employed as a starting material for the subsequent heat-treated products, which were prepared in the same manner as described previously. The heat-treatment temperatures, yields, and some proper-

→ Condensable
polynuclear
aromatic species
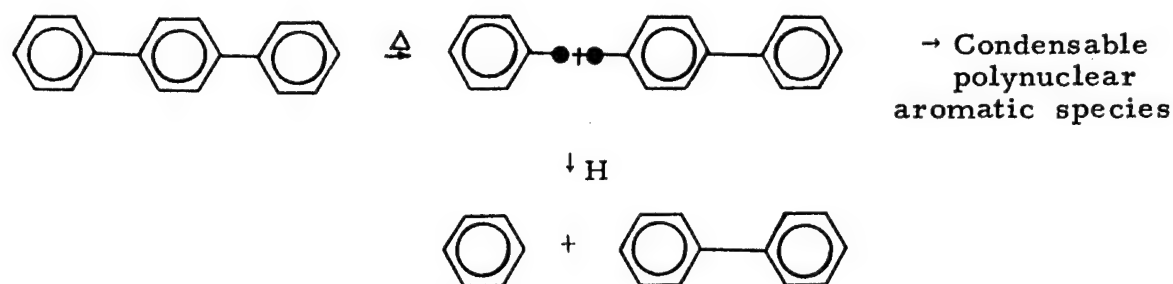
ties of the p-terphenyl carbonized residues are given in Table 13.

Table 13.   Properties of p-Terphenyl Residues

| Temp. °C | Mol. Wt. in $C_6H_6$ | Color | M.P. °C | Yield % |
|---|---|---|---|---|
| 525-4 hours | 371 | Light Brown | 103 | ~90 |
| 525-10 hours | 286 | Brown | 149 | ~85 |
| 525-20 hours | 295 | Black | >350 | ~80 |
| 550 | --- | Black | Infusible | 98.8 |
| 600 | --- | " | " | 98.6 |
| 700 | --- | " | " | 95.3 |
| 800 | --- | " | " | 94.3 |
| 900 | --- | " | " | 93.1 |
| 1000 | --- | " | " | 93.5 |
| 1500 | --- | " | " | 92.8 |
| 2000 | --- | " | " | 91.9 |
| 2500 | --- | " | " | 91.9 |
| 3000 | --- | " | " | 91.9 |

The infrared and UV absorption spectra for the 525°C p-terphenyl residues are shown in Figure 17.   The infrared spectra show considerable change with time at 525°C, especially in the aromatic substitution region along with hydrogen abstraction.   The lack of any visible spectrum in the black "pitch-like" material is surprising and indicates that the condensation reactions have produced extremely large insoluble aromatic species. Only a small portion of the material was soluble.

These results indicate that the p-terphenyl pyrolysis proceeds with the formation of extremely reactive radicals which undergo rapid condensation to large infusible products.   Since standard chemical methods cannot be applied to such materials, X-ray methods will be employed to characterize the thermal products.

50

IR Spectra                        UV Spectra
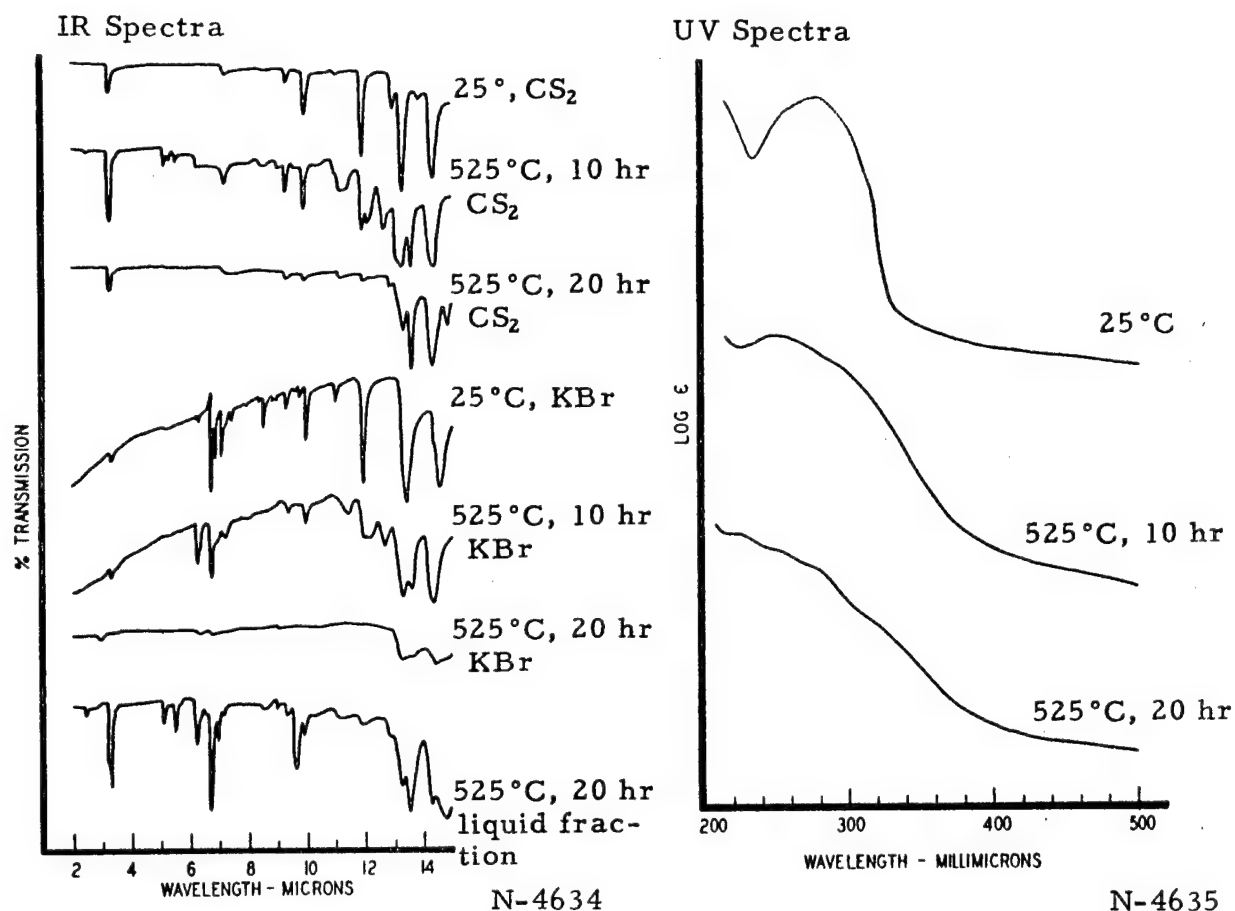


Figure 17.   IR and UV Spectra of p-Terphenyl
             Residues at 525°C

## 3.1.5.   Organic Synthesis

## 3.1.5.1.   Synthesis of Aromatic Compounds for Pyrolysis Studies

A number of aromatic compounds have been synthesized for thermal reaction studies.

## 3.1.5.1.1.   Aromatic Diazo Compounds

A series of substituted aromatic diazo compounds has been synthesized for electron spin resonance (ESR) studies.  Compounds of this type readily undergo thermal decomposition to form radicals.  By investigation of structurally different diazo compounds, an insight can be gained into the nature and behavior of aromatic radicals formed through thermal decomposition or pyrolysis reactions.

The compounds were prepared employing the following standard organic reaction procedures.

51

## a. Aromatic Hydrazones

The aromatic substituted diazo compounds are most conveniently prepared by the oxidation of the corresponding hydrazones. The hydrazones were therefore prepared initially from the aromatic ketones by the method of Grummitt and Jenkins.[6]

$$
\begin{array}{ccc}
\text{R-C-R'} & \xrightarrow[\text{Isopropanol, 150°C, 7 hrs.}]{H_2N \cdot NH_2 \cdot H_2O} & \text{R-C-R'} \\
\overset{\|}{\underset{O}{}} & & \overset{\|}{\underset{\overset{|}{NH_2}}{N}}
\end{array}
$$
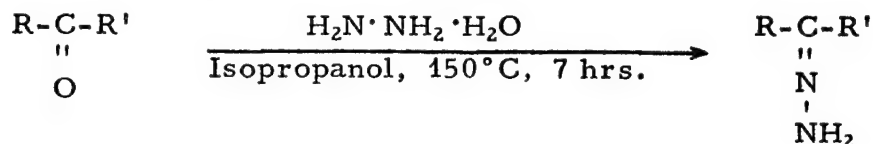
Listed in Table 14 are the aromatic hydrazones which were synthesized along with their characteristic melting points. The ketones benzanthrone and 2,2-dimethylbenzophenone could not be converted to hydrazones.

Table 14.   Melting Points of Synthesized Aromatics

| Compound | Lit. M.P. °C | Obs. M.P. °C |
|---|---|---|
| **A. Aromatic Hydrazones** | | |
| 9-Fluorenone hydrazone | 156 | 151 |
| Benzil hydrazone | 151 | 151 |
| 4-Chlorobenzophenone hydrazone | 106 | 100 |
| 4,4'-Dichlorobenzophenone hydrazone | 93 | 90 |
| 4-Bromobenzophenone hydrazone | α 104, β oil | -- |
| 4-Hydroxybenzophenone hydrazone | -- | 153 |
| 2,4-Dihydroxybenzophenone hydrazone | -- | -- |
| 4,4'-Dihydroxybenzophenone hydrazone | -- | 120 |
| 4-Methylbenzophenone hydrazone | 81 | 87 |
| 4,4'-Dimethylbenzophenone hydrazone | 110 | 101 |
| 4,4'-Dimethoxybenzophenone hydrazone | 86 | 85 |
| 4,4'-Bis(diethylamino)benzophenone hydrazone | -- | 123 |
| **B. Aromatic Diazo Compounds** | | |
| 9-Diazofluorene | 95 | 89 |
| 2-Diazo-2-phenylacetophenone | 79 | 63 |
| Diazodiphenylmethane | 32 | 32 |
| Diazodiphenylmethane, $d_{10}$ | -- | 29 |
| (p-Chlorophenyl)-diazophenylmethane | -- | -- |
| Bis(p-chlorophenyl)-diazomethane | 107 | 103 |
| (p-Bromophenyl)-diazophenylmethane | -- | -- |
| Diazophenyl-p-tolylmethane | 55 | 46 |
| Diazodi-p-tolylmethane | 101 | 95 |
| Diazobis(p-methoxyphenyl)-methane | 103 | 87 |
| 2-Diazo-1-acenaphthenone | 94 | 97 |
| 10-Diazo-9(10H)-phenanthrone | 109 | 104 |
| **C. Miscellaneous Aromatic Compounds** | | |
| Benzil azine | 202 | 203.5 |
| Fluorenone azine | 259 | 269 |
| 9-Chloro-9-phenylfluorene | 79 | 74 |

### b. Oxidation of Hydrazones to Diazo Compounds

The previously prepared hydrazones were subjected to treatment
with HgO using the method of Nenitzescu and Solomonica[7] to
form the diazo compounds required for this study.

$$
\begin{array}{c}
R\text{-}C\text{-}R' \\
\|\\
N \\
|\\
NH_2
\end{array}
\quad
\xrightarrow[\text{(C}_2\text{H}_5)_2\text{O, }25°\text{C, 30 min.}]{\text{HgO,} \quad \text{OH}^-}
\quad
\begin{array}{c}
R\text{-}C\text{-}R' \\
\|\\
N_2
\end{array}
$$
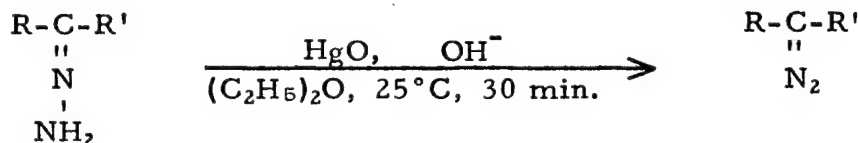
The diazo compounds and their melting points are listed in Table
14. Four of the hydrazones did not convert to the corresponding diazo
compounds. These are 4,4'-bis(diethylamino)benzophenone hydrazone and
the three hydroxy substituted hydrazones.

### c. Miscellaneous Diazo Compounds

Two additional diazo compounds were synthesized using the tech-
niques of Cava, Litle, and Napier.[8] These were 2-diazo-1-
acenaphthenone and 10-diazo-9(10H)-phenanthrone.



acenaphthene
quinone

SO$_2$N$_2$H$_3$

2-diazo-1-
acenaphthenone



phenanthrene
quinone

10-diazo-9(10H)-
phenanthrone
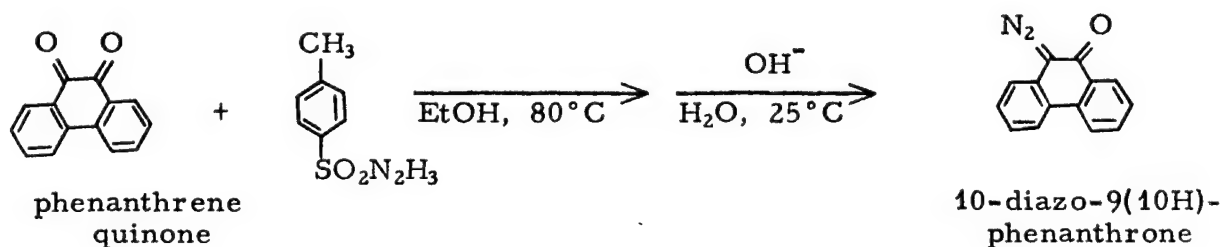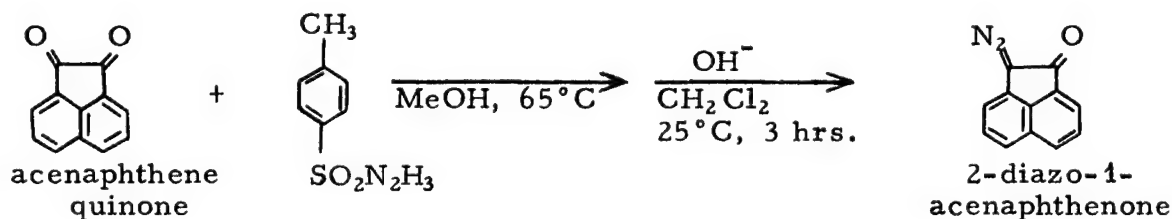
The melting-point data for these compounds are also listed in Table 14.

53

## 3.1.5.1.2. Miscellaneous Aromatics

### a. 9-Chloro-9-phenylfluorene

This compound was synthesized by use of the method of Cohen, Cohen, and Wang.[9]
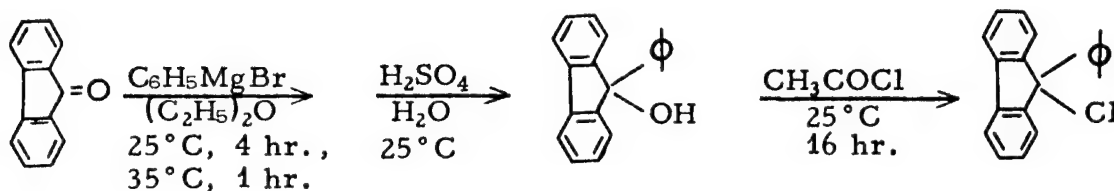


The pyrolysis of this compound will be investigated in an attempt to observe the thermal formation of the phenylfluorene radical.

### b. 9,9'-Bianthryl

This thermally reactive aromatic hydrocarbon was prepared by the method of Bell and Waring.[10]
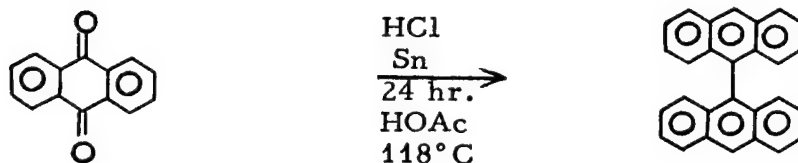


Bianthryl will be employed as a model compound for pyrolysis studies.

## 3.1.5.2. Synthesis of Aromatic Pyrolysis Reaction Products

Two compounds, benzil azine and fluorenone azine, were synthesized for comparison with the reaction products from the pyrolysis of diazobenzil and diazofluorene.

## a. Benzil Azine

Benzil azine was prepared by the method of Ritter and Wiedeman.[11]



Benzil — Benzil azine
Yield: 24 per cent
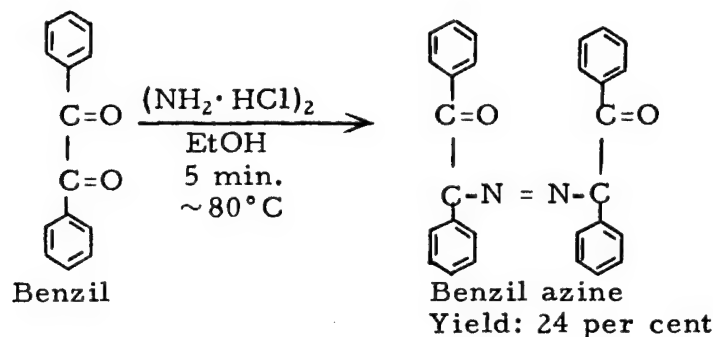
## b. Fluorenone Azine

Fluorenone azine was synthesized according to the technique of Cohen, Cohen, and Wang.[9]



Fluorenone — 9-Fluorenone hydrazone — 9-Fluorenone azine
Yield: 29.5 per cent
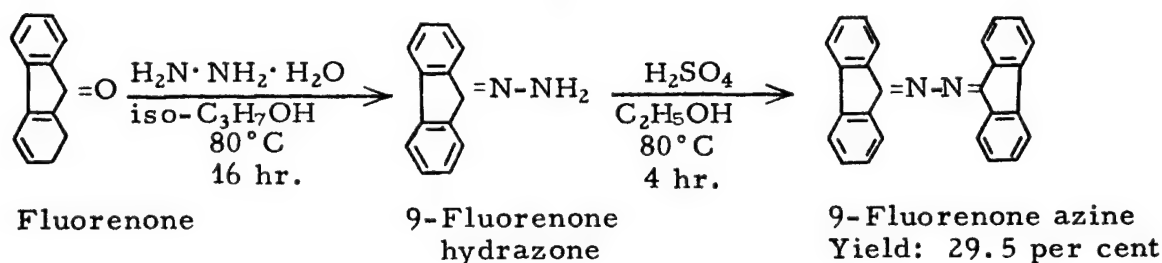
The infrared spectra of these compounds were obtained and compared with those of the pyrolysis products of diazobenzil and diazofluorene. Inspection of the spectra of benzil azine and those of 2-diazo-2-phenyl-acetophenone (diazobenzil) pyrolysis products shows no appreciable formation of benzil azine from the latter compound. A similar comparison of fluorenone azine and products of the pyrolysis of diazofluorene shows formation of some azine as well as $\Delta^{9,9'}$-bifluorene from the thermal decomposition of diazofluorene.

### 3.1.6. Electron Spin Resonance

### 3.1.6.1. Introduction

It is well known that free radicals are formed during the thermal decomposition and carbonization of all organic substances.[12,13] It has been strongly suspected that these free radicals are not merely minor reaction by-products, but are important chemical intermediates in the thermal reaction sequence. However, the precise nature and role of these radicals in the carbonization process have never been determined. It seems probable that the chemical structure of the free radical intermediates formed at the very early stages of pyrolysis controls the reaction paths and thus determines to a large extent the aromaticity, crystallinity,

55

and orientation properties of the resultant pitches and cokes. The physical and chemical properties of the coke are, in turn, of great importance in controlling the properties of the final products of graphitization.

Electron spin resonance (ESR) is a recently developed technique for detecting and identifying organic free radicals. The few reported cases in which ESR has been used to investigate the mechanism of a reaction by identifying the free radical intermediates have been described previously.[14]

Although a large number of ESR studies have been reported for pitches, cokes, and carbons of both natural and synthetic origin,[13] no detailed ESR studies of the carbonization mechanisms have been done. The reason why such studies were not possible was that the usual method of charring leads immediately to complex inhomogeneous radical-containing substances which show a single unresolved resonance line devoid of structure and almost devoid of information. The free radicals formed during carbonization cannot be identified from a single ESR line which is essentially identical to that exhibited by all solid organic radicals.

An investigation was conducted to determine whether carbonization could be carried out in such a way as to permit the use of ESR for identifying specific free radical intermediates directly. Identification is, of course, the first step in clarifying the role of free radicals in the mechanism of carbonization.

The first phase of this study has been reported previously.[14] It was shown that if the carbonization of pure organic compounds is carried out in an inert liquid matrix, the nuclear hyperfine structure required for identifying the intermediate radical species can be observed. The experimental technique and the results of a preliminary survey of the ESR of approximately 20 aromatic compounds were reported.[14]

Subsequent refinements of our ESR apparatus and techniques have provided a significant improvement in both sensitivity and resolution. The resultant more quantitative information has made it possible to identify some of the intermediate radicals and to propose detailed mechanisms for the initial pyrolysis reactions.

Section 3.1.6.1. describes the more detailed high resolution experiments on the model compound acenaphthylene, including the thermal formation and decomposition of the perinaphthenyl radical. The results of experiments on solid acenaphthylene cokes are also included. Section 3.1.6.2. discusses the thermal decomposition of aromatic diazo compounds. In Section 3.1.6.3., the ESR of the radical ion formed from hexamethylbenzene in sulfuric acid and other "acceptor" solvents is described.

## 3.1.6.2. Thermal Decomposition and Carbonization of Acenaphthylene

### 3.1.6.2.1. Formation of the Perinaphthenyl Radical

Using improved experimental techniques, primarily the magnet super-stabilizer and slow-sweep unit, it has been possible to examine in

greater detail the ESR spectrum of acenaphthylene pyrolyzed in m-quinquephenyl.

Upon heating acenaphthylene in m-quinquephenyl for a few seconds at 450°C, a light-orange solution is obtained. When cooled to 150°C, this solution exhibits an intense, well-resolved spectrum consisting of seven quartets of lines. The central part of the initial spectrum is shown in Figure 18. Note the weak signal due to a second "acenaphthylene" radical.
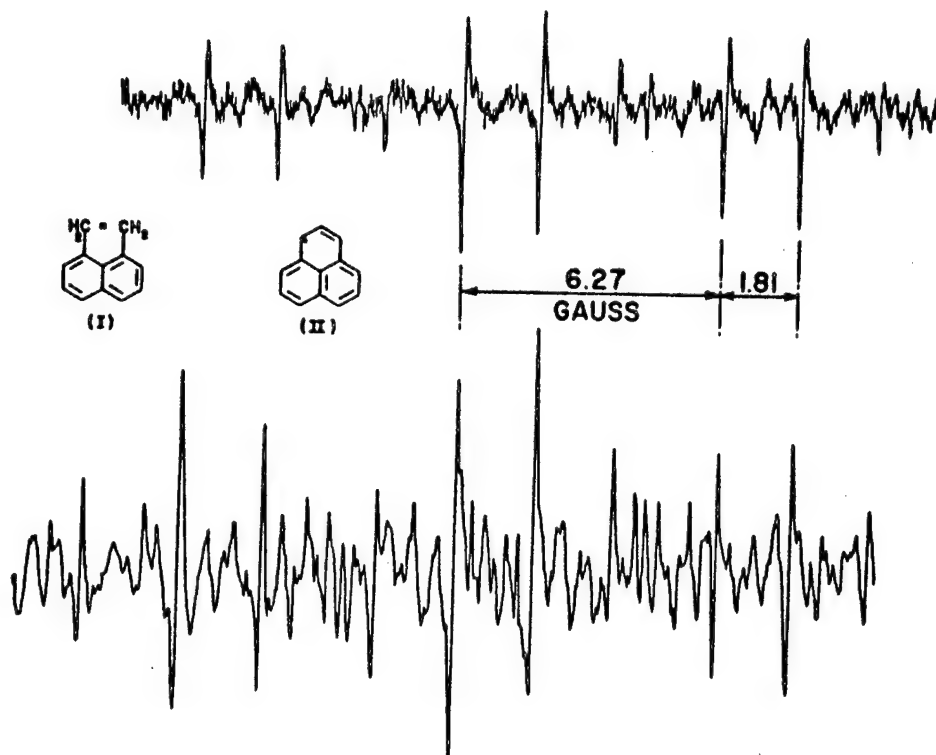


N-4869

Figure 18.  ESR for Radicals Formed During the Thermal Decomposition of Acenaphthylene in m-Quinquephenyl; Sample Heat-Treated at 400°C, Measured at 150°C; Upper Spectrum After Very Short Heating Time, Lower Spectrum After Longer Heating Time

We have identified the radical giving rise to the major signal as the perinaphthenyl radical (II). This species has been found in pyrolyzed petroleum products by Stehling and Bartz[15] and by Bennett[16] and was first synthesized by Sogo, et al.[17] Our coupling constants for the perinaphthenyl radical (6H, $a_1$ = 6.27 gauss and 3H, $a_2$ = 1.81 gauss) agree with those obtained by Bennett.

57

As the heat-treatment of acenaphthylene is continued at 400°C, the perinaphthenyl radical spectrum disappears and a much more complex and stable radical spectrum continues to grow. The lower half of Figure 18 shows an intermediate stage of the development of the second radical before perinaphthenyl has disappeared.

The relative thermal stability of the two radicals has been examined in somewhat greater detail. Figure 19 shows on an expanded scale the two lines of the central quartet of the ESR of perinaphthenyl. As shown in the lower portion of the figure, the lines are separated by $a_2 = 1.81$ gauss. In Figure 20, the same portion of the spectrum is
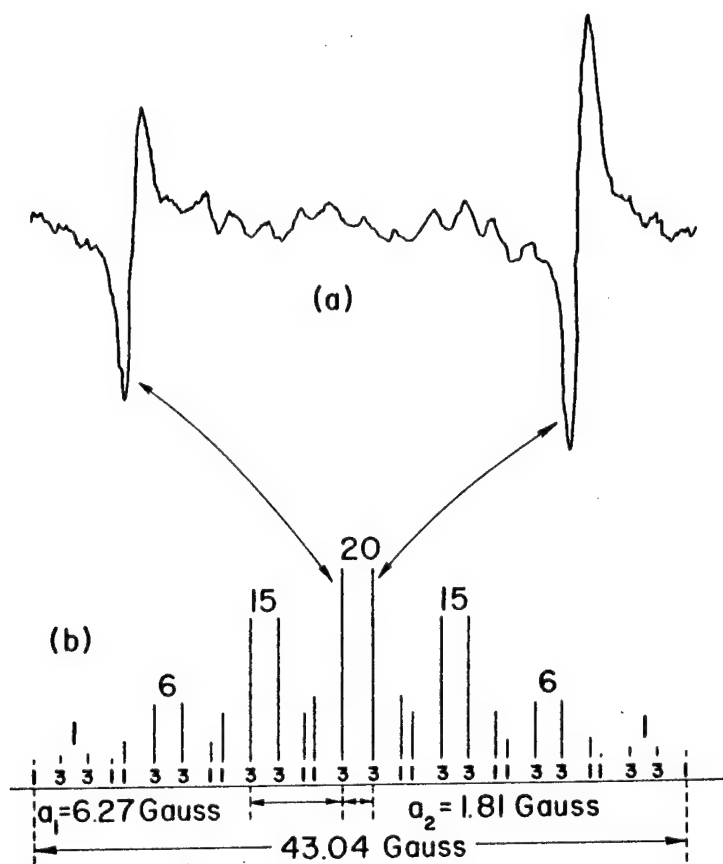


N-4085

Figure 19. Perinaphthenyl Radical from Heating 1:10 Solution of Acenaphthylene in m-Quinquephenyl for a few Seconds at 450°C, Measured at 180°C

swept repeatedly at 180°C. The perinaphthenyl peaks (P) decrease in intensity with time while the intensity of the second radical spectrum remains constant. The bottom spectrum was run approximately 30 minutes after the first. A small amount of the perinaphthenyl signal remained even after keeping the sample at 180°C for several hours.
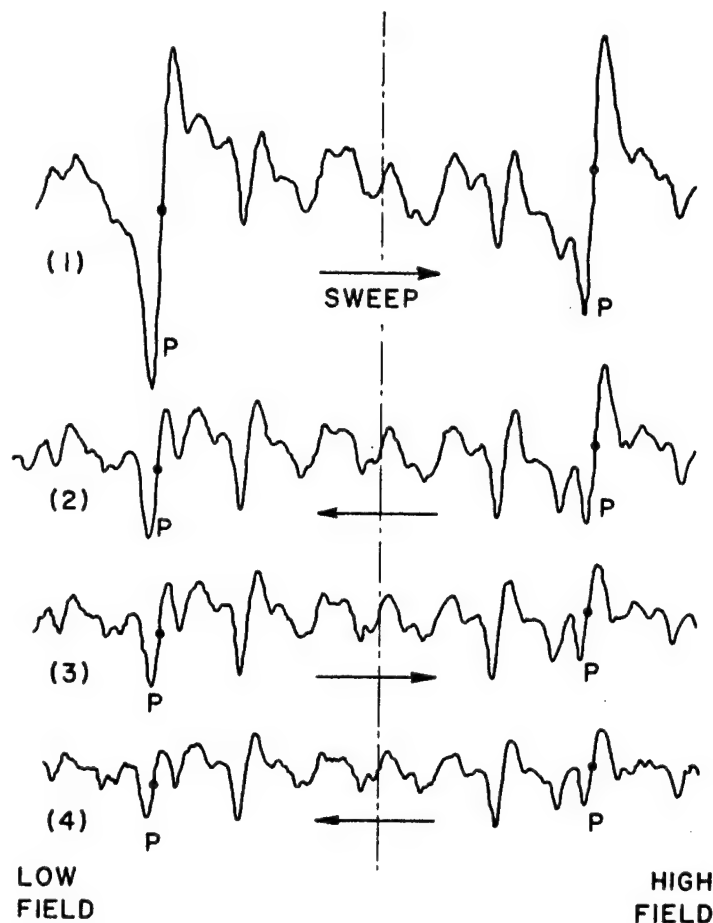
58

Figure 20.   Reactivity of Perinaphthenyl Radical at 180°C;
             P Denotes the Strong Lines of the Central Quartet

        The formation of perinaphthenyl from acenaphthylene can be vis-
ualized chemically through a carbon-carbon bond cleavage in the five-
membered rings of dimeric acenaphthylene, followed by rearrangement.[18]
Figure 21 illustrates how the acenaphthylene dimer is thought to rearrange
during the reaction step prior to the formation of zethrene (III). [19]

        The perinaphthenyl radical has also been observed from the pyroly-
sis of 4,5-methylene phenanthrene and polyvinyl chloride.  It is interesting
that the perinaphthenyl radical has not been detected during the carbonization
of unsubstituted aromatics. [13]  The three compounds mentioned above assist
in aromatic cyclization.

        The precise nature of the hydrocarbon solvent was also shown to
be unimportant in the production of the perinaphthenyl radical.  Solutions
of acenaphthylene in chromatographed quinquephenyl, deuterated quinque-
phenyl and p-terphenyl exhibited identical spectra for the radical.
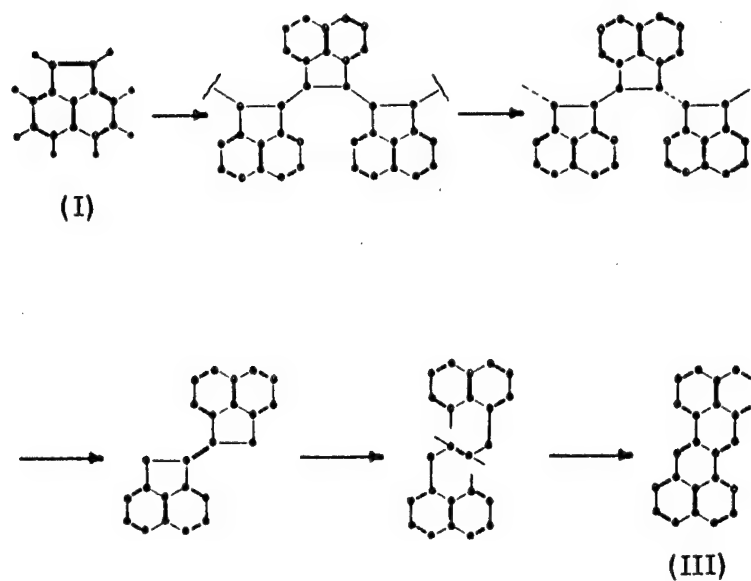
Figure 21. Possible Reaction Scheme for the Formation of Zethrene During the Early Stages of Carbonization of Acenaphthylene

### 3.1.6.2.2. The Second "Acenaphthylene" Radical

The most highly resolved ESR spectrum of thermally decomposed acenaphthylene yet obtained consisted of lines about 80 milligauss wide. The central portion of the spectrum is shown in Figure 22. Figure 22 represents approximately one-twelfth of the total spectrum. The two lines indicated by the arrows are the most intense lines of the central quartet of the spectrum of the perinaphthenyl radical.
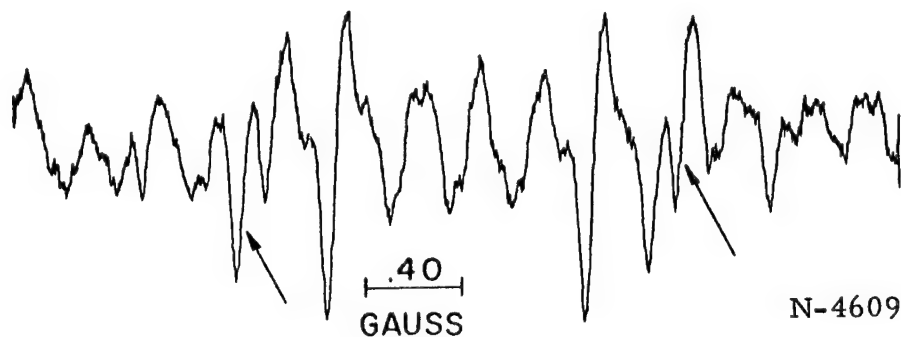


Figure 22. Portion of the High-Resolution Spectrum of Acenaphthylene in m-Quinquephenyl; Heated at 450°C for ~5 Minutes, Measured at 180°C

60

The resolution and signal-to-noise of the spectrum in Figure 22 leave much to be desired. Furthermore, the unreacted perinaphthenyl radical provides an additional complication. If one deletes the perinaphthenyl peaks, the line spectrum in the upper half of Figure 23 is obtained.

## ESR OF ACENAPHTHYLENE HEAT-TREATED IN $\phi_5$

CENTER          OBSERVED

COMPUTED

|     |               |       |
| --- | ------------- | ----- |
| 6H  | $a_1 = 4.08$  | GAUSS |
| 4H  | $a_2 = 3.28$  | "     |
| 2H  | $a_3 = 1.34$  | "     |
| 1H  | $a_4 = 1.08$  | "     |
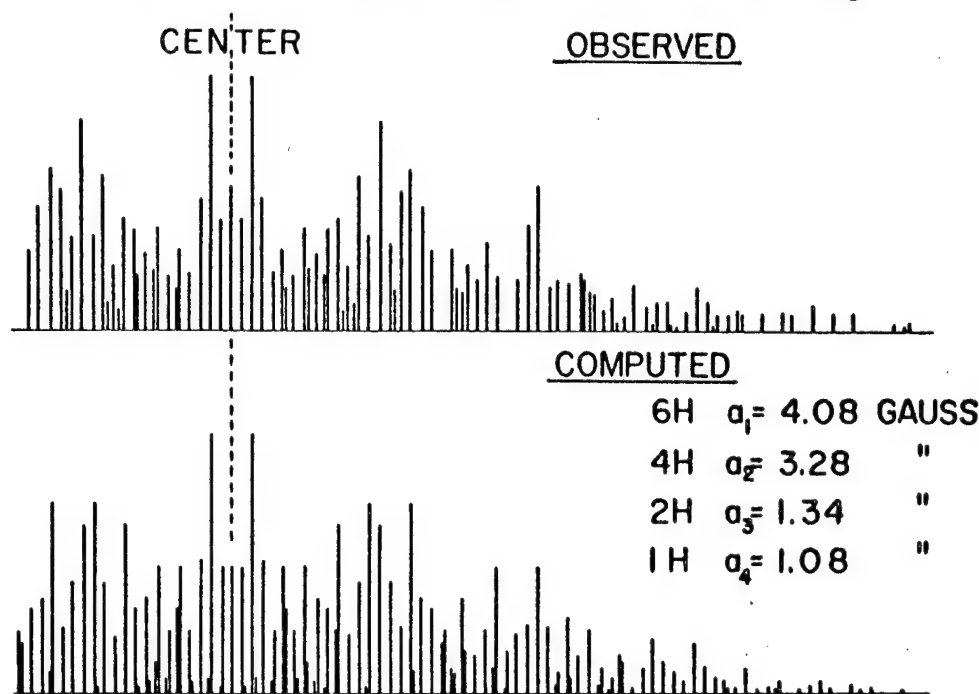
N-4373

Figure 23. Comparison of Experimental and Computed Line Spectra for Radical from Pyrolysis of Acenaphthylene in m-Quinquephenyl

The computed spectrum shown in the lower half of Figure 23 was obtained after a long trial-and-error procedure. The agreement is fairly good but by no means perfect. Many overlapping lines make any experimental line spectrum a poor approximation to the true situation as far as intensities are concerned. A more meaningful computed spectrum must account for linewidths and overlapping. An electron spin resonance spectrum simulation (SESRS) program is now being tried on an IBM 7094 computer. The output of the program will consist of plotted curves which could then be compared directly with Figure 22.

If the coupling constants indicated in Figure 23 are correct, the radical must contain altogether 13 protons. In an attempt to identify the radical, we have considered several possibilities. Zethrene (III) contains 14 protons so that the loss of a H atom would give a radical with 13 protons. The spin densities calculated from simple Hückel Molecular Orbital (HMO) theory are shown. Using a proportionality constant between spin densities and coupling constants of 30, the zethrene radical

61

.098 .070

.003 .003

.091 .064

.107

.107

.064 .091

.003 .003

.070 .098

(III)

.1 .1

0 0

.1 .1

0 0

.1 .1

.1 .1

0
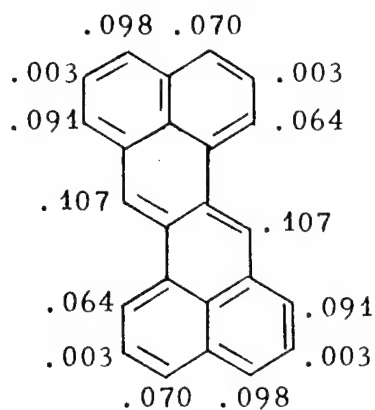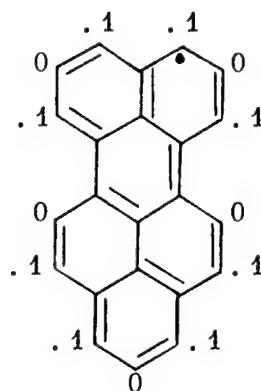
(IV)

would be expected to exhibit 6 proton splittings of around 3 gauss, 4 proton splittings around 2 gauss and 4 splittings close to zero. However, one of these protons would be missing (it is now known which one). The fit to the experimental values shown in Figure 23 is not very good. The main argument against zethrene is that the experiments show several groups of precisely equivalent protons, e.g., 6 of one kind, 4 of another. This is not very likely for zethrene where symmetry considerations do not demand this degree of equivalence. (Note that the HMO spin densities for zethrene all occur in pairs except for the .003). In addition, the experiment does not show 4 equivalent protons of very low spin density (.003), although there might be some question as to whether a (.003 x 30) = .09 gauss splitting could be resolved.

Another possibility considered was the periperylenyl radical (IV). After perinaphthenyl, this is the next larger member of the odd-carbon atom aromatic molecule series. Like perinaphthenyl, it has only two groups of equivalent protons, 8 and 5. The experimental results are completely inconsistent with this 13-proton radical.

A third possibility is a dimethyl-substituted perinaphthenyl radical (V) has 13 protons, six of which are exactly equivalent and which would have a fairly large splitting. The position between the two methyls would

CH₃ CH₃

(V)
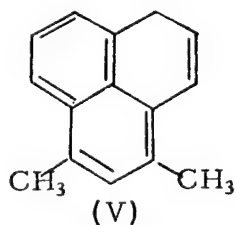
provide the single small splitting. The groups of 4 and 2 protons would be expected to result from the other rings; however, the magnitudes of the splittings differ somewhat from the expected values. Such a structure is also chemically reasonable, since the type of reaction required for its formation would be quite similar to those involved in the formation of the

62

perinaphthenyl radical (see Figure 21). Furthermore, methyl protons have been observed by NMR in the pyrolysis products of acenaphthylene. We plan to synthesize several substituted perinaphthenyl radicals (including the dimethyl) in order to clarify the identity of the radical.

### 3.1.6.2.3. Deuterated Acenaphthylene in m-Quinquephenyl

By replacing a particular proton having spin $\frac{1}{2}$ by its deuterium isotope of spin 1, the ESR hyperfine structure is altered in a precisely predictable manner, viz., each pair of lines goes into three lines with 0.1535 of the original spacing. Such isotopic substitution experiments are equivalent to "tagging" a particular molecular position. The role of that molecular site in a chemical reaction can then be determined unambiguously.

Previous preliminary experiments performed under medium resolution conditions[19] showed large differences in the ESR spectra of ordinary and deuterated acenaphthylenes when heat-treated in m-quinquephenyl ($\Phi_5$). These experiments have now been repeated under high resolution conditions using both ordinary and deuterated quinquephenyl solvents. The results can be summarized as follows.

a.

Acenaphthylene-$H_8$ exhibits the identical ESR spectrum in $\Phi_5$ ($H_{22}$) and $\Phi_5(D_{22})$. Both the perinaphthenyl and "acenaphthylene" radicals are observed. This proves that the solvent $\Phi_5$ is in fact inert with respect to these initial pyrolysis reactions.

b.

High resolution spectra for acenaphthylene-$D_6$ (VI) in $\Phi_5$ ($H_{22}$) and $\Phi_5(D_{22})$ are shown in Figure 24. Except for the broad back-



(VI)
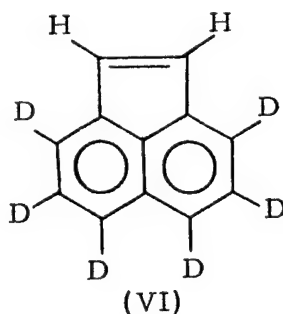
ground signal in b, the spectra are identical. This comparison again proves that the observed radical intermediates do not involve the solvent. These spectra may be due to partially deuterated perinaphthenyl radicals, "acenaphthylene" radicals, or a combination of the two.

c.

Acenaphthylene ($D_8$) in $\Phi_5(D_{22})$ gives a single unresolved line as would be expected for a totally deuterated complex free radical.

63
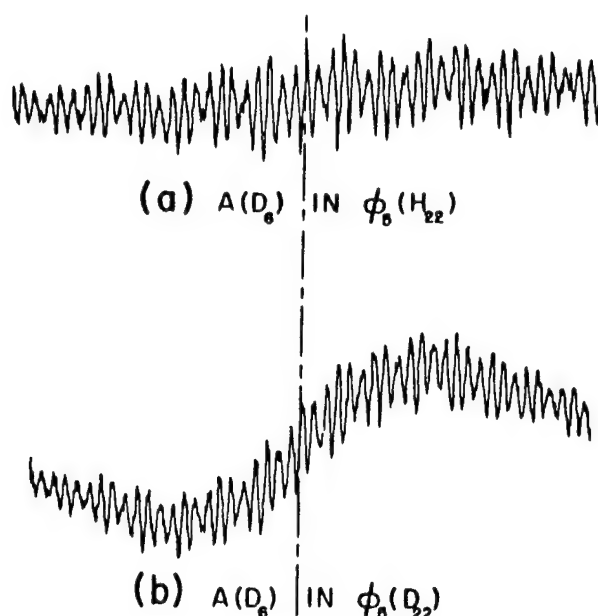
Figure 24. Experimental ESR Spectra of Radical Formed During Thermal Decomposition of (a) $D_6$-Acenaphthylene in Ordinary m-Quinquephenyl $\Phi_5(H_{22})$ and (b) $D_6$ Acenaphthylene in Deuterated m-Quinquephenyl, $\Phi_5(D_{22})$

d.

Acenaphthylene ($D_8$) in $\Phi_5(H_{22})$ gives a spectrum identical to those in Figure 24 for acenaphthylene ($D_6$). This totally unexpected result has only one reasonable explanation. There must be some exchange of the acenaphthylene deuterons with the solvent protons. However, it is evident that only the vinyl deuterons exchange, since the spectrum eventually observed is that for acenaphthylene-$D_6$. The aromatic deuterons of the acenaphthylene do not exchange with solvent, as proved by the identity of the spectra for acenaphthylene-$D_6$ in $\Phi_5(H_{22})$ and $\Phi_5(D_{22})$.

### 3.1.6.2.4. ESR of Solid Cokes of Ordinary and Deuterated Acenaphthylene

During the last 15 years, the variation of ESR properties of solid chars and cokes with heat-treatment temperature (HTT) has received considerable attention.[12,13] This activity has resulted from the suspected importance of the observed free radicals in carbonization and subsequent graphitization processes. Our recent experiments on charring processes in dilute liquid media have provided direct evidence for identifying these radicals and their role in the initial steps of carbonization. However, the products of later stages of carbonization which involve complex mixtures of extremely large free radicals are not soluble in any known solvents. Therefore, identification on a molecular basis is impossible. Even so, it has been shown that if these complex chars are prepared from a pure starting material with careful heat-treatment procedures, the unpaired

electrons and their molecular environment can, for ESR purposes, be considered identical. [20] Experiments on the variations of ESR properties of solid chars with heat-treatment temperature should, therefore, be amenable to at least some semiquantitative interpretation.

Linewidth and spin concentration are two of the most easily measured ESR parameters. Furthermore, their variation with HTT is similar for practically all charred organics. These two ESR properties are shown for charred sucrose in Figure 25.
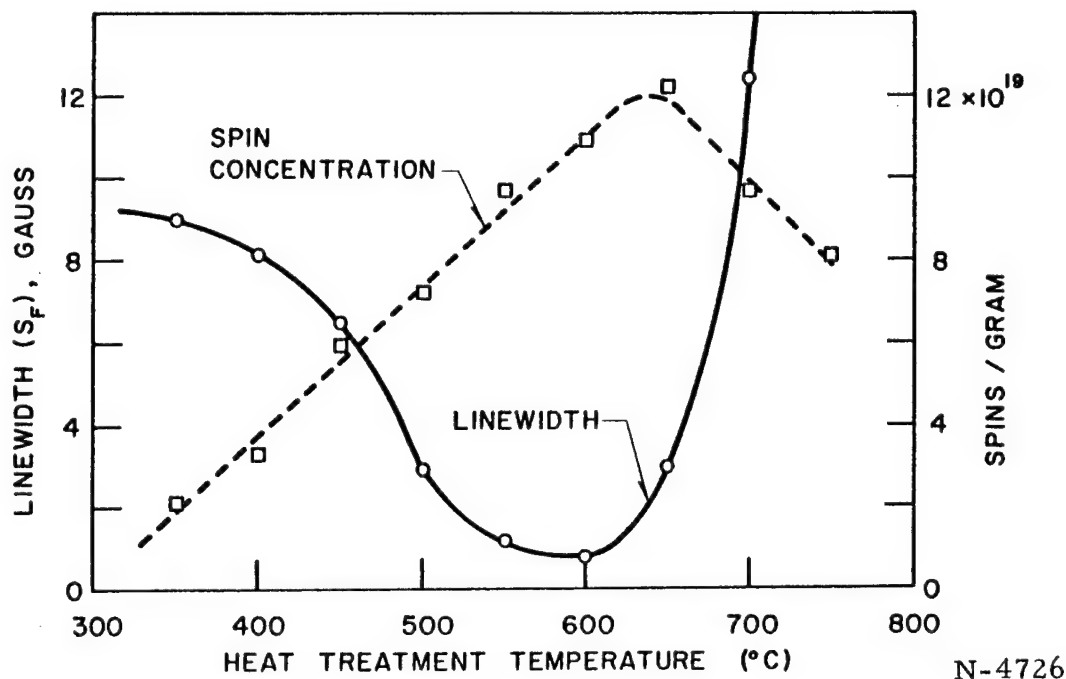


Figure 25. Linewidth and Spin Concentration Versus Heat-Treatment Temperature for Charred Sucrose

The observed behavior has been explained qualitatively by a number of investigators. [13] As the carbonization proceeds, both the number and the size of the aromatic free radicals increase. The slow change of linewidth with heat-treatment temperature (HTT) in the 300 to 400°C region strongly suggests that the linewidth mechanism is probably due to proton hyperfine interaction, which should be independent of radical concentration. As the size and number of radicals increase, the nuclear hyperfine interaction is averaged out by electron delocalization; finally, the ESR line becomes quite narrow due to intermolecular exchange interactions. There have been no satisfactory explanations for the linewidth behavior above a HTT of 600°C.

It has been recognized for some time that deuterium substitution (deuterium has $\sim\frac{1}{3}$ the magnetic moment of the proton) experiments should

65

yield concrete experimental evidence for the above mechanism in the HTT region where the char still contains significant amounts of hydrogen. However, the unavailability of suitable deuterated organics has been the major obstacle.

We have found one such suitable aromatic compound which has been obtained in completely deuterated form and which can be conveniently charred at low temperatures, viz., acenaphthylene. Figure 26 shows the results of our first experimental comparison of the linewidth behavior of the two acenaphthylenes. The significant point is that at very low charring temperatures (very low radical concentration), the ESR linewidth for the deuterated acenaphthylene is $\frac{1}{3}$ to $\frac{1}{4}$ that for ordinary acenaphthylene. This result is unambiguous proof that the cause of the linewidth in very low temperature chars is nuclear hyperfine interaction.
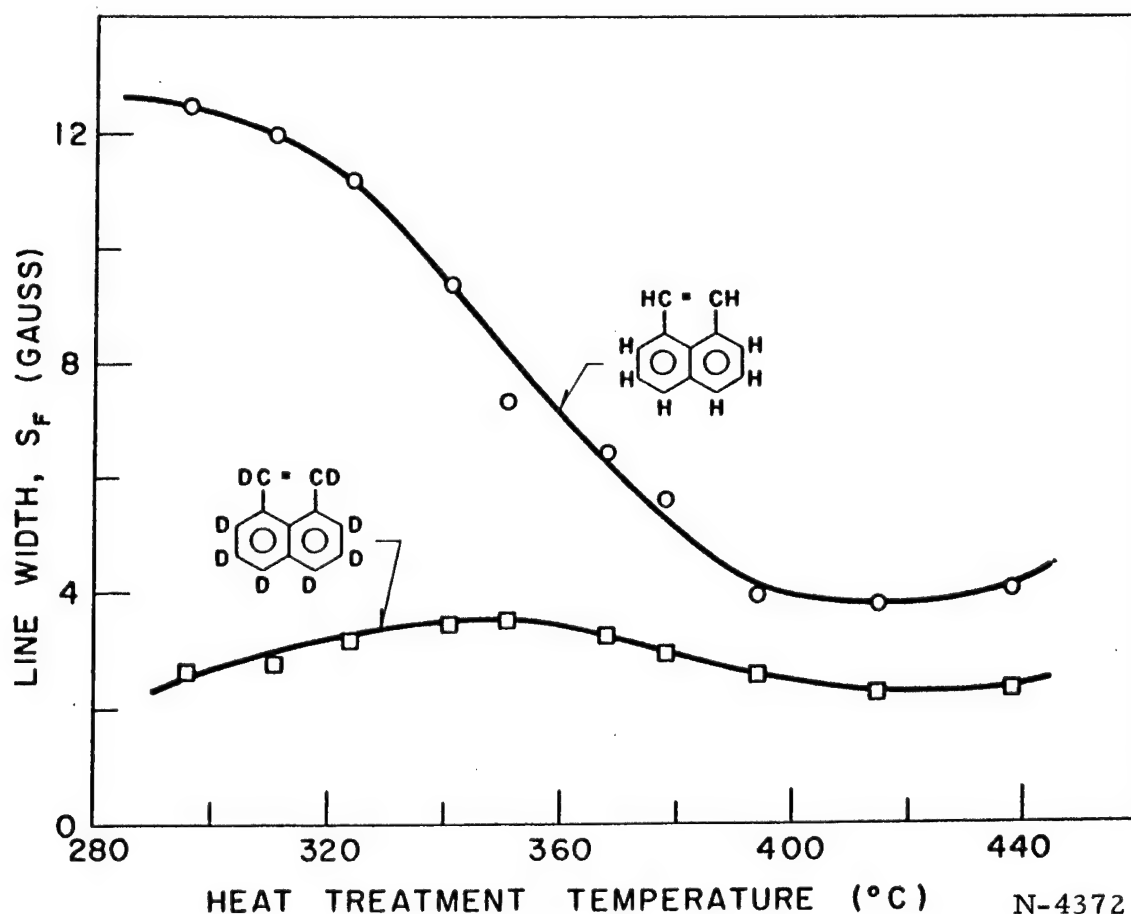


Figure 26.  Linewidth Versus Heat-Treatment Temperature for Ordinary and Deuterated Acenaphthylene

The slight increase in linewidth for the deuterated material may be due to electron dipole-dipole interactions as the radical concentration increases.  The apparent plateau around 400°C HTT for both materials is

66

not understood, since the linewidth minimum in Figure 25 is much deeper and occurs at much higher HTT. Acenaphthylene is known to exhibit a much sharper line at around 600°C HTT.[21]

The experimental procedure for obtaining the results in Figure 26 proved to be somewhat inadequate. The samples were heated in sealed tubes for one hour, measured, then reheated to the next higher temperature. Redistillation of the carbonaceous volatiles into the bottom of the tube and possible $O_2$ degassing from the Pyrex tube were not eliminated. In view of the interesting but not very well understood results at the higher HTT region in Figure 26, the experiments should be repeated in a more controlled manner and extended to higher HTT.

### 3.1.6.3. Thermal Decomposition of Aromatic Diazo Compounds

The formation of stable free radical entities appears to occur quite generally during the carbonization of aromatic hydrocarbons. The discrete identification of these radical intermediates is made difficult by the inability to chemically identify their specific complex reaction products. Numerous reaction paths are available at the high temperatures necessary for the formation of these radical species.

We have therefore attempted to apply our ESR method to the study of organic compounds which decompose at low temperatures to form discrete and stable reaction products. The expectation is that an understanding of these simpler radical reactions will help clarify the more complex radical processes in carbonization.

Aromatic diazo compounds decompose at relatively low temperatures yielding radical intermediates. The first step in the thermal reaction of an organic diazo compound (VII) is postulated to involve the loss of nitrogen with the resultant formation of a reactive carbene (VIII).

$$\underset{(VII)}{\underset{R'}{\overset{R}{>}}CN_2} \quad \overset{\Delta}{\rightarrow} \quad \underset{(VIII)}{\underset{R'}{\overset{R}{>}}C:} \quad + \quad N_2 \uparrow$$

The carbene (VIII) generally reacts either electrophilically (electrons paired) or as a radical (electrons unpaired). The most usual products of the pyrolysis of (VII) in inert media are the dimer (IX) or the azine (X). Isomerizations and hydrogen abstractions have also been observed.

$$\underset{(IX)}{\underset{R}{\overset{R}{>}}C = C\underset{R}{\overset{R}{<}}} \qquad \underset{(X)}{\underset{R}{\overset{R}{>}}C = N - N = C\underset{R}{\overset{R}{<}}}$$

67
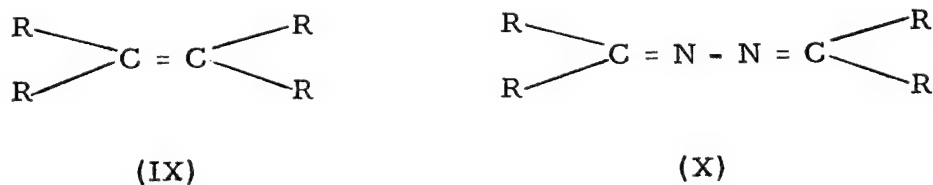
We have studied the thermal decomposition of diazo compounds in dilute solution in biphenyl at temperatures between 100 and 200°C. Under these conditions, fairly long-lived free radicals are observed.

### 3.1.6.3.1. Diphenyldiazomethane ($\Phi_2CN_2$)

In a previous report,[14] the ESR of thermally decomposed diphenyldiazomethane in biphenyl was reported and the 35-line spectrum tentatively explained in terms of $\Phi_2CN\cdot$ fragment. Since the spectrum was incompletely resolved, the assignment remained ambiguous. These experiments were later repeated using new high resolution and slow sweep techniques. Additional sharp peaks were resolved for a solution which had been heated to 185°C and quenched to 85°C. Concentration, thermal history, and the temperature of measurement were all found to be important in determining the extent of resolution obtained. Part of the difficulty was that the radical concentration was apparently a function of temperature.

We have again repeated several of these experiments in more dilute systems. Figure 27 shows the center portion of the ESR spectrum of



$\underset{\text{GAUSS}}{\overline{\text{0.4}}}$     N-5043
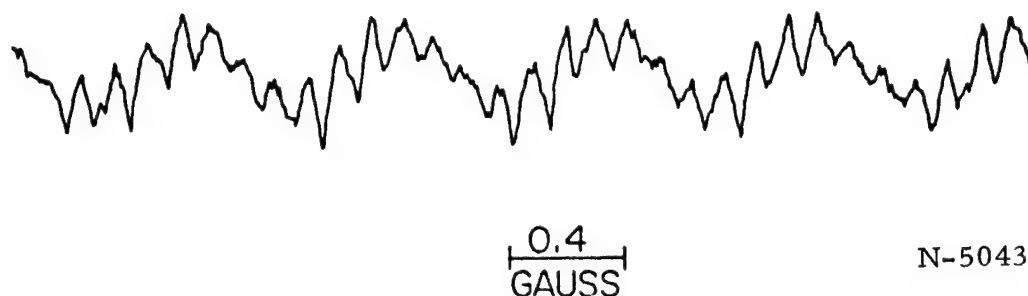
Figure 27.   ESR of Diphenyldiazomethane Thermally
Decomposed in Biphenyl at 185°C

a well-degassed 1:100 solution of $\Phi_2CN_2$ in $\Phi_2$, heated and measured at 185°C. The sharp lines are approximately 50 milligauss wide. Figure 28 shows the experimental line spectrum which contains more than 60 lines. We have not yet been able to reduce this spectrum to coupling constants. It is also not clear whether the gently rolling broad peaks ($\sim 0.8$ gauss wide) are due to a second radical species or to the simple overlap of the sharp components. Other curves in which the unresolved peaks are much larger than the resolved peaks suggest that there are two species present. Simulated curves obtained from the "Simulation of Electron Spin Resonance Spectra" (SESRS) computer program should clarify this question.

68
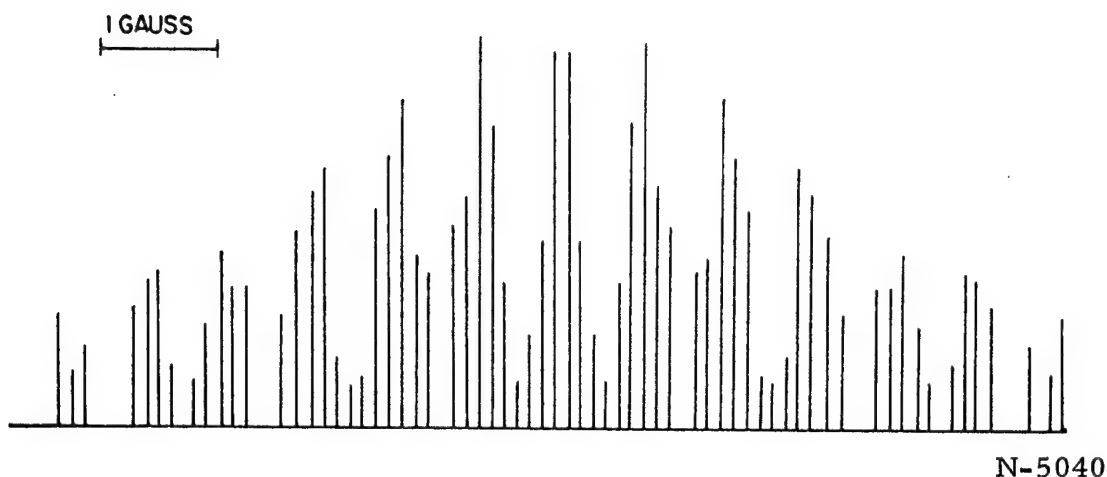
Figure 28.   Experimental Line Spectrum for the High
             Resolution $\Phi_2CN_2$ Spectrum in Figure 27

Further investigation into the nature of these radicals included a
number of experiments with completely deuterated $\Phi_2CN_2$ dissolved in both
ordinary and deuterated biphenyl.   Figure 29 shows essentially the entire
ESR curve for a 1:10 solution of deuterated $\Phi_2CN_2$ in $\Phi_2$(H), heated   and
measured at $\sim 140°C$.   The ESR was identical when $\Phi_2$(H) was replaced by
$\Phi_2$(D), showing that there is no proton (or deuterium) exchange with the
solvent.
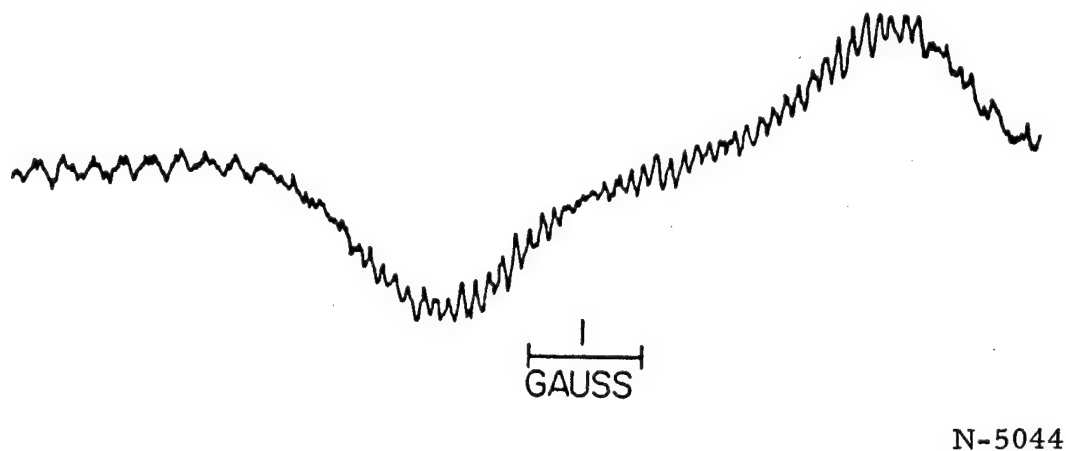


Figure 29.   ESR of Deuterated $\Phi_2CN_2$ Thermally Decom-
             posed in Biphenyl at 140°C

The broad humps in Figure 29 are very suggestive of a nitrogen
splitting in which each of the three 1:1:1 components are inhomogeneously
broadened by one or more small deuterium splittings.   In fact,  if we add
the derivatives of three equally intense Gaussian curves in which the peak-
to-peak linewidth $\Delta H_i$ is 1.18 times the spacing between lines $\Delta H_p$, we ob-
tain the solid curve in Figure 30.   This curve has been calculated with
considerable accuracy by Lebedev, et al.[22]   The dashed curves are only

approximate and were drawn to show qualitatively how the three curves add to yield the single solid curve. The fit of the computed curve to the experimental curve in Figure 29 is quantitative. The nitrogen coupling constant $a_N$ is, therefore, about 1.4 gauss, or $\frac{1}{3}$ the peak-to-peak separation on the solid curve in Figure 30. This assignment is also consistent with the three equivalent groups of partially resolved lines which occur with relative intensities of 1:1:1.
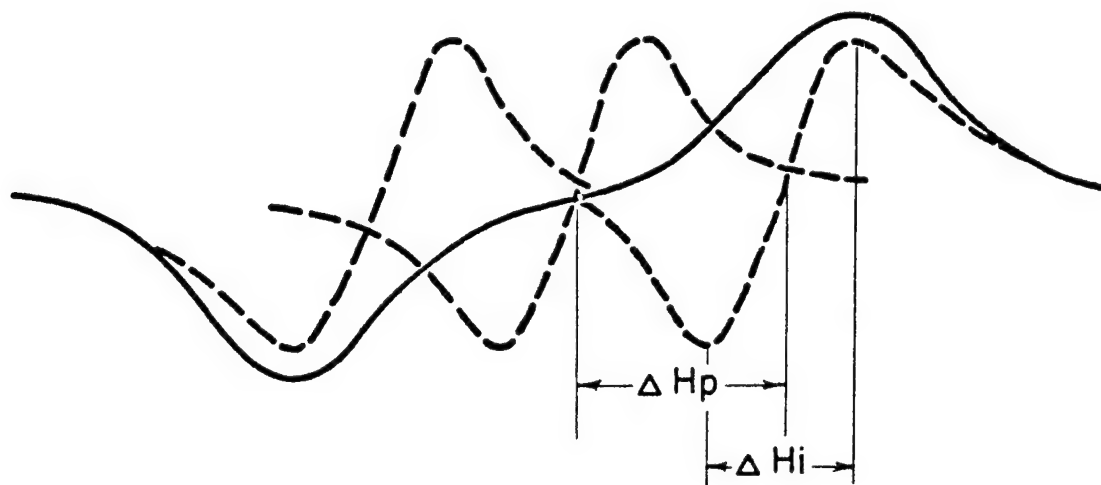


N-5039

Figure 30.   ESR Curve Computed for the Sum
of Three Gaussian Distributions

From the partially resolved deuterium hyperfine lines in Figure 29, one can make a good guess at the larger proton coupling constant from which these lines were derived. Since the spacing of these lines is ~0.1 gauss, the corresponding proton splitting must have been some multiple of $0.10/0.15 \cong 0.7$ gauss. The hyperfine lines in the wings of the curve in Figure 29 show that this multiple must be at least 2 and is probably as large as 4. Proof for the correct assignment will come eventually from SESRS calculations and more detailed analyses of the spectra for both ordinary and deuterated diphenyldiazomethane.

The inhomogeneously broadened humps in Figure 29 came from a D-splitting equal to or less than the component linewidths of ~100 milligauss. The excellent fit of Figure 29 with Figure 30 (which was based on a sum of Gaussian distributions) is further evidence for an inhomogeneous mechanism of line broadening caused by small hyperfine splittings. It may be that the 0.7 gauss basic separation observed previously is the important coupling constant.[19]

Although there are still some aspects of the ESR spectra of $\Phi_2CN_2$ which are not clear, we now suggest the following tentative coupling constants:

70

$$1 \text{ N}, a_N = 1.4 \text{ gauss},$$

$$6 \text{ H}, a_{o,p} = 1.4 \text{ or } 2.8 \text{ gauss},$$

and $\qquad 4\text{H}, a_m = 0.7 \text{ gauss.}$

This assignment, which is still consistent with a $\Phi_2CN\cdot$ fragment, remains to be proved by constructing both line spectra and SESRS spectra for ordinary and deuterated $\Phi_2CN_2$.

3.1.6.3.2.   9-Diazofluorene

The ESR spectrum of the radical from the decomposition of 9-diazofluorene is shown in Figure 31.   The resolution is by no means com-
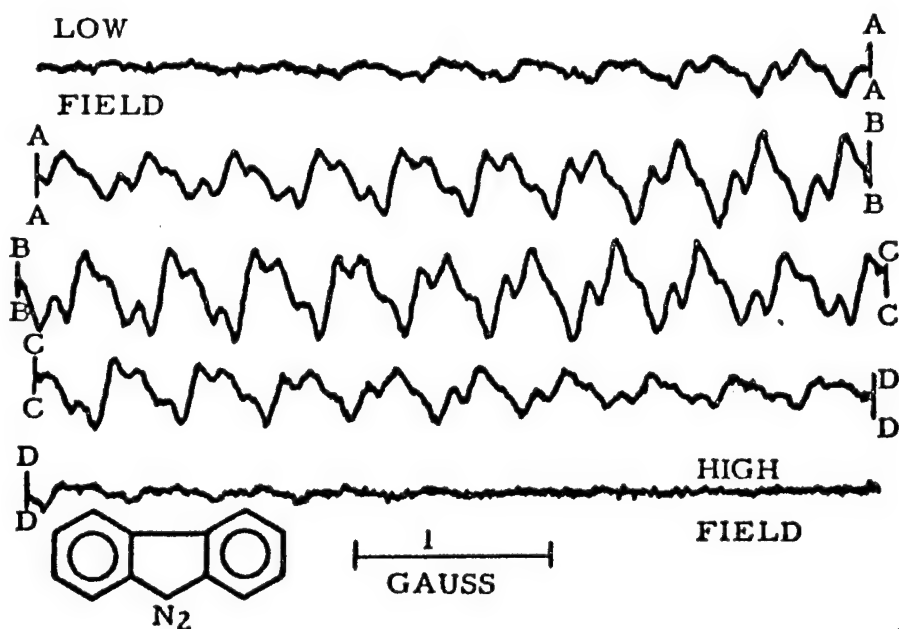


N-4067

Figure 31.   ESR Curve for a 1:10 Solution of
Diazofluorene in Biphenyl at 190°C

plete, but is considerably better than that obtained previously.[14] This spectrum has been tentatively reduced to coupling constants and a comparison of experimental and computed line spectra is shown in Figure 32. Again, the incomplete resolution in Figure 31 makes the uniqueness of the assignment in Figure 32 somewhat doubtful.   An SESRS comparison will be required before we can be sure that the radical does, in fact, contain 12 protons.   The radical could conceivably contain nitrogen, as was found for $\Phi_2CN_2$.

71
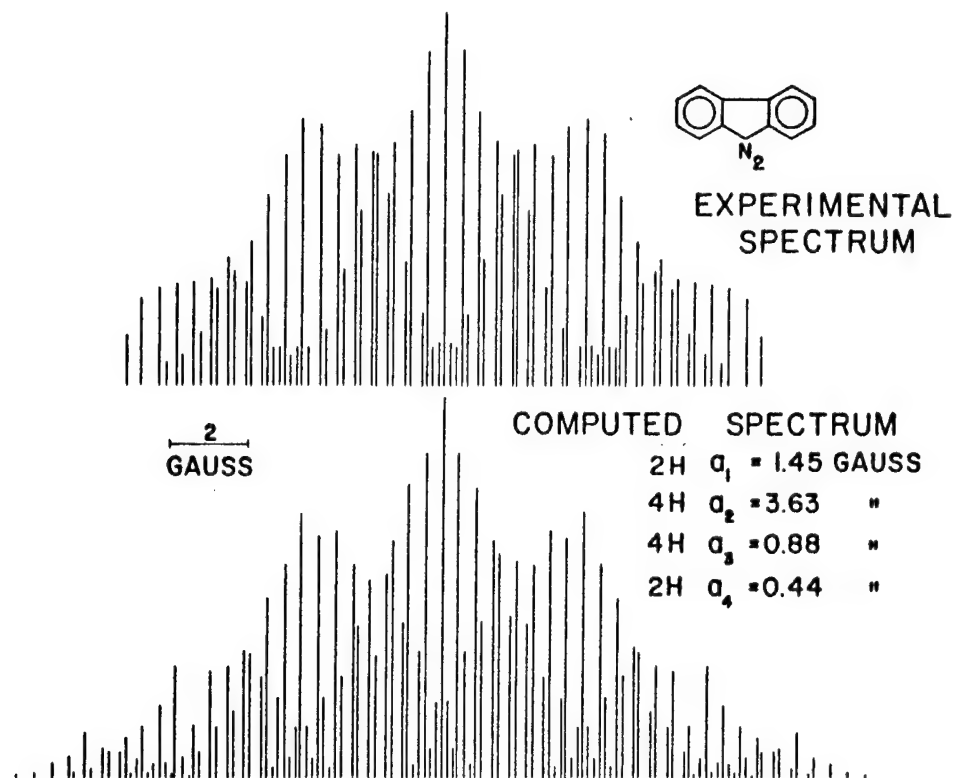
Figure 32. Comparison of Experimental and Computed
ESR Line Spectra for 9-Diazofluorene

### 3.1.6.3.3. Diazobenzil

The upper half of Figure 33 shows the ESR spectrum for diazo-
benzil decomposed in biphenyl at 150°C. The lines were approximately
100 milligauss wide. The line spectrum in the lower half of the spectrum
was computed for a 10-proton system with the coupling constants shown.
There can be no question about the assignment in this case.

These coupling constants are consistent with those expected from
a symmetrical diphenyl-substituted radical species. It is believed that the
reactive carbene formed by the thermal elimination of nitrogen from diazo-
benzil rearranges to form either a benzil (XI) or a ketene-type (XII) radical.

It is interesting that the resonance spectrum from decomposed
diazobenzil appears identical with that recently reported by Dehl and
Fraenkel[23] for the benzil anion, except that our coupling constants are about
three times larger. Further work concerning the identification of the rad-
icals from the thermal decomposition of diazo compounds is in progress.

72
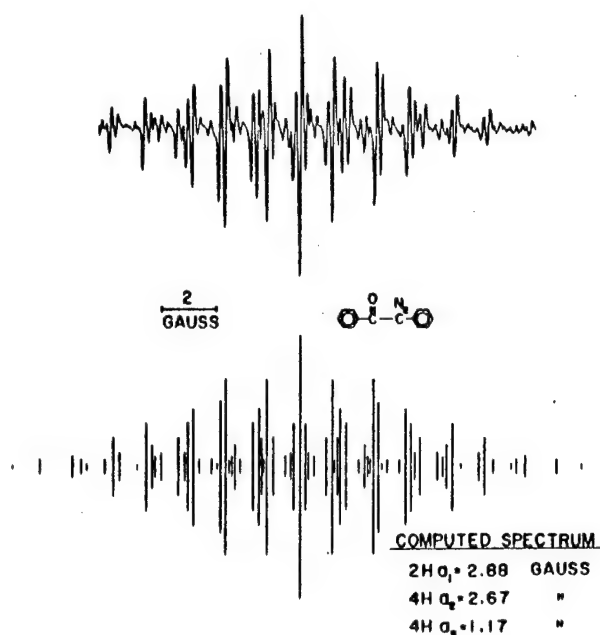
Figure 33.  Comparison of Experimental and Computed Spectra
of Radical from Thermal Decomposition of Diazo-
benzil in Biphenyl



(XI)                    (XII)
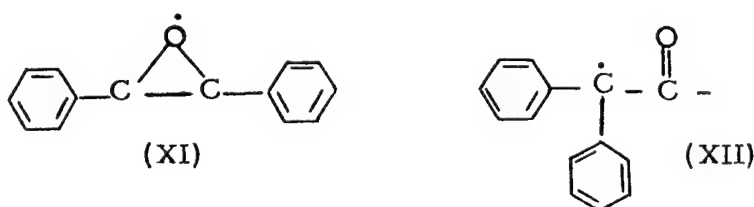
### 3.1.6.4.  Electron Spin Resonance of Solutions of Hexamethylbenzene (HMB) in Sulfuric Acid

One of the important methods of determining electron distributions
in aromatic molecules is to form the paramagnetic cation or anion and then
to study the ESR hyperfine structure of the paramagnetic species.  Informa-
tion about electron densities is useful in predicting the course of thermal
reactions of these molecules.  Because of the known importance of methyl
groups in the pyrolysis of aromatics, it was of interest to study the electron
distribution in a methylated aromatic radical.  Since benzene is the simplest
aromatic hydrocarbon, we have investigated the ESR of hexamethylbenzene
in sulfuric acid with the expectation that the low ionization potential of the
molecule might make radical-ion formation energetically favorable in this
medium.

73

## 3.1.6.4.1.  Spectra and Coupling Constants

Figure 34 shows half of the ESR spectrum of HMB in $H_2SO_4$ run under fairly high resolution conditions.  This complex pattern was not



Figure 34.    ESR Spectrum of a Solution of Hexa-
methylbenzene in Sulfuric Acid

expected, since if the six methyl groups were equivalent, the 18 protons would simply give rise to 19 equally spaced lines having a binominal distribution of intensities.   Figure 35 shows the entire experimental line
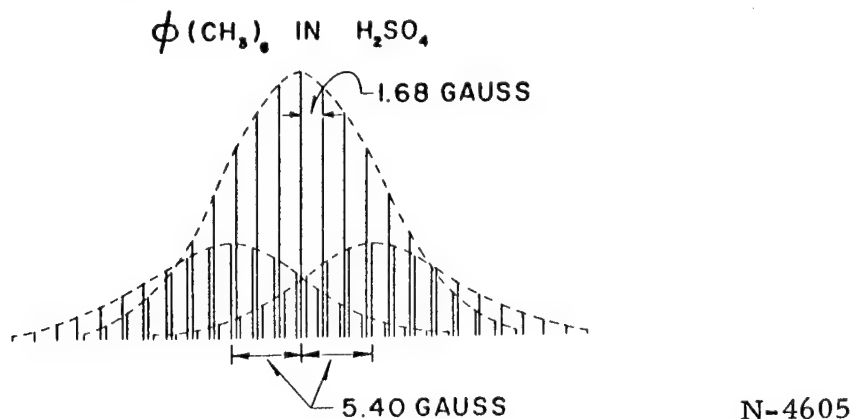


Figure 35.    Experimental Line Spectrum for $\Phi(CH_3)_6$ in $H_2SO_4$; Line Positions and Intensity Taken from Spectrum in Figure 34

spectrum. A total of 63 lines was observed. Note that they fall into 3 groups with an intensity ratio of 1:2.8:1.

Let us first consider just the center groups, since the relative intensities of corresponding lines in each group are identical. The lines and bars in Figure 36 represent the experimental intensities for the center group. It can be seen that the drop-off in intensity of the lines for both 18 and 36 equivalent protons is much too rapid. These numbers would be expected for monomer and dimer radical species. On the other hand, a choice of 12 protons with $a_1 = 3.36$ gauss and 6 protons with $a_2 = 1.68$ gauss gives excellent agreement with the observed spectrum. This assignment may not be unique; however, improved signal-to-noise could permit an unambiguous count of the total number of lines in the wings and thus lead to a unique assignment.

$\phi(CH_3)_6$  IN  $H_2SO_4$



EXPERIMENT

12 H  $a_1 = 3.36$ G
6 H  $a_2 = 1.68$ G

36 H  $a_1 = 1.68$ G

18H  $a_1 = 1.68$ G

N-4606
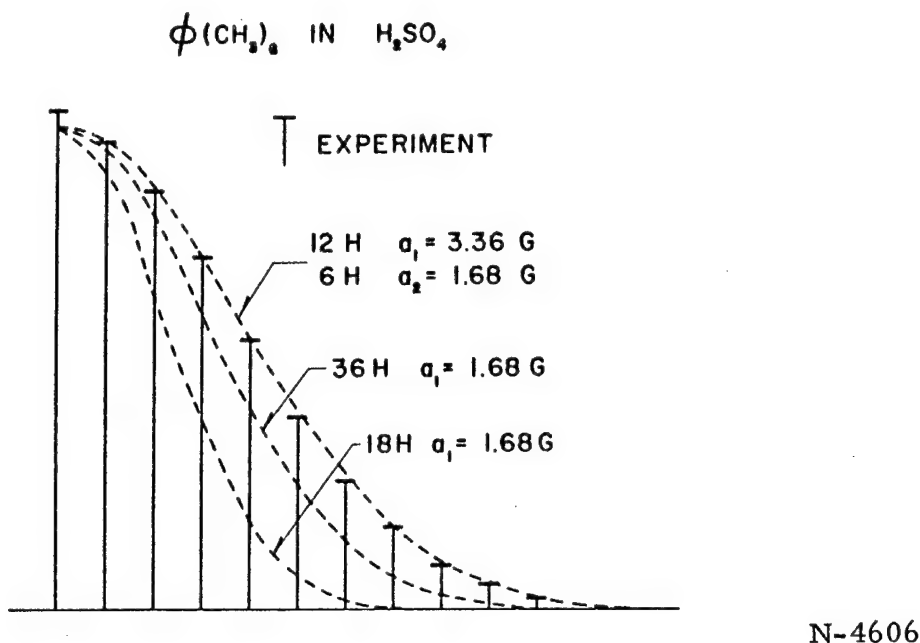
Figure 36. $\Phi(CH_3)_6$ in $H_2SO_4$; Comparison of Experimental Intensities with Those Computed for 3 Different Sets of Coupling Constants

The 3 identical groups of lines are somewhat of a mystery. The ratios of intensities of the groups shown in Figure 35, viz., 1:2.8:1, are not too different from a 1:2:1 distribution which would be expected for two equivalent protons with a 5.40 gauss coupling constant. It was noted that the ESR lines belonging to the outer groups were perhaps 6 to 10 per cent wider than those in the central groups. A 10 per cent increase in width would mean ~20 per cent decrease in height so that the 1:2.8:1 ratio would become more like 1:2.3:1.

75

If there are two equivalent protons with a 5.4-gauss splitting, their most reasonable origin is the $H_2SO_4$ solvent. Therefore, replacing the solvent with $D_2SO_4$ should alter these groups in the following predictable manner. The ratio of the deuterium coupling constant $a_D$ to the proton coupling constant $a_H$ is given by:

$$\frac{a_D}{a_H} = \frac{\mu_D I_H}{\mu_H I_D} = \frac{0.8574(\frac{1}{2})}{2.7927(1)} = 0.1535,$$

so that the 5.4-gauss splitting would become 0.83 gauss. This is almost identical to half the 1.68 gauss methyl proton splitting. Figure 37 shows
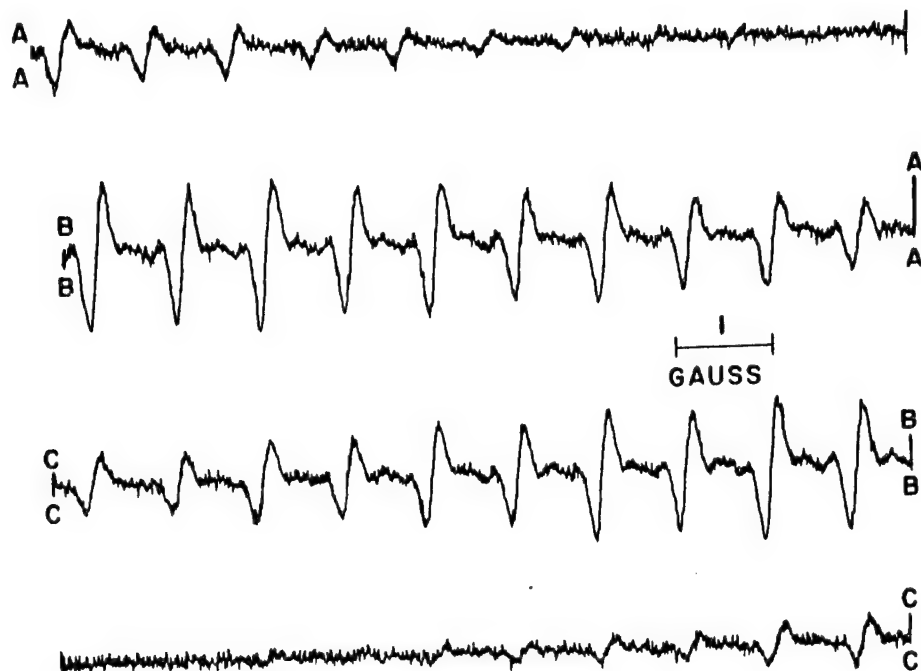


Figure 37.   ESR Spectrum of a Solution of $\Phi(CH_3)_6$ in $D_2SO_4$

the ESR spectrum for $\Phi(CH_3)_6$ in $D_2SO_4$. The predicted 0.83-gauss splitting is evident, there being no sign of the previous 3 groups of lines shown in Figure 35. In Figure 38, a comparison of experimental and computed line spectra is shown. The alternation in intensity is a result of the 1:2:3:2:1 distribution of intensities for two equivalent deuterons of spin 1. The slight asymmetry of the ESR lines in Figure 37 is probably due to the 10-milligauss difference between $(\frac{1}{2})$ (1.68) = 0.84 and 0.1535 (5.40) = 0.83 gauss.

76

$\phi(CH_3)_6$ IN $D_2SO_4$

CENTER

— EXPERIMENTAL

| COMPUTED SPECTRUM

12 H   $a_1$= 3.36 GAUSS

6 H   $a_2$= 1.68 GAUSS

2 D   $a_3$= 0.84 GAUSS

└0.84 GAUSS

N-4608
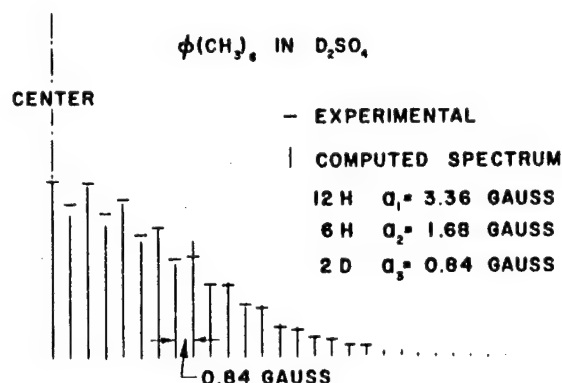
Figure 38.   Comparison of Experimental and Computed Intensities for $\Phi(CH_3)_6$ in $D_2SO_4$

### 3.1.6.4.2.   Linewidths and Temperature Dependence

As stated in Section 3.1.6.4.1, the linewidths in the outer groups of lines (see Figure 35) were about 10 per cent larger than those in the inner groups.   The anomalous intensity variation could then be explained on the basis of some selective line broadening mechanism.

According to theories of McConnell,[24] Kivelson,[25] and others, the tumbling of a free radical molecule (with its anisotropic g-value) modulates the interaction of the electron spin with the dc magnetic field and affects both $T_1$ and $T_2$.   In McConnell's theory, $T_2$ depends on both even and odd powers of the nuclear quantum number M and is inversely proportional to both the tumbling correlation time and the related viscosity.

The ESR spectrum of $\Phi(CH_3)_6$ in $H_2SO_4$ was run at several temperatures in order to determine if the observed intensity discrepancies were in fact the result of such relaxation phenomena.   The results are shown in Figure 39.   Note that although the strong lines (M=O) are about the same intensity at all three temperatures, the smaller satellites (M = ± 1) decrease in intensity and broaden as the temperature is lowered and the resulting viscosity increases.   For the center triplet, the ratios of intensities of the center line to that of the small satellites are 1.6, 2.3, and 4.6 for 54°C, 27.5°C, and -2°C, respectively.   If the three groups of lines for the two equivalent protons had a 1:2:1 ratio of intensities, the corresponding center line-to-satellite intensity ratio would be 1.37.   Thus, at high temperatures, the spectrum seems to be approaching this limiting value.   Within experimental error, the M = +1, M = -1 peaks have the same heights (and thus widths) so that the broadening mechanism depends only on even powers of M.   It was also found that the addition of trifluoroacetic acid to a solution of the radical in $H_2SO_4$ lowered the room-temperature viscosity slightly and lowered the intensity ratio in the center triplet from 2.3 to 2.0.

77
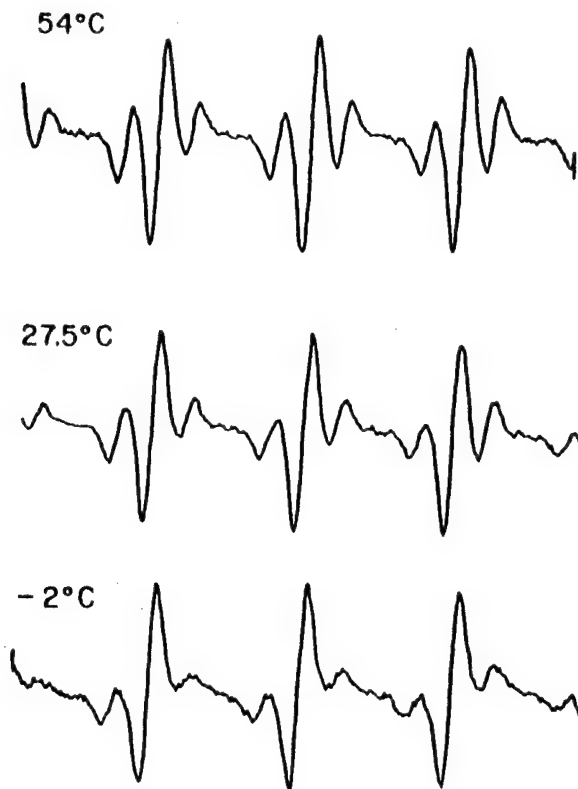
Figure 39. ESR of Hexamethylbenzene in $H_2SO_4$ at 3 Temperatures

N-5042

McConnell has suggested that the symmetry in behavior of +M and -M lines implies that the hyperfine tensor and the g-tensor have the same principal axes. This information may be useful in deciding between possible structures of the observed free radical.

### 3.1.6.4.3. Hexamethylbenzene in Molten Iodine

Since Kommandeur [26] found that perylene in molten $I_2$ gave the ESR spectrum of the perylene radical cation, a similar experiment was tried with $\Phi(CH_3)_6$. The spectrum obtained for a 0.003 molar solution of $\Phi(CH_3)_6$ in $I_2$ at 125°C ($I_2$ melts at 114°C) is shown in Figure 40. The 21-line spectrum is incompletely resolved. However, the 1.71-gauss splitting is within experimental error, identical to the basic splitting (1.68 gauss observed for $\Phi(CH_3)_6$ in $H_2SO_4$. Because of the poor resolution, it is not certain whether the additional 2-proton splitting (a = 5.40 gauss) found in $H_2SO_4$ solution is present in $I_2$ solution. The reason for this uncertainty is that since 5.40 is nearly 3 times the basic 1.7-gauss splitting, good resolution would be required to separate the lines (see Figure 35). However, the total width of the spectrum is consistent with the 2-proton splitting. The explanation for the poor resolution is not clear, although Kommandeur found a similar result for perylene in $I_2$. The ESR results for $\Phi(CH_3)_6$ in molten $I_2$ suggest that the radical is identical to that formed in $H_2SO_4$ except that the two equivalent protons may be absent.

78

$$\overset{4}{\underset{\text{GAUSS}}{\rule{1.5cm}{0.4pt}}}$$
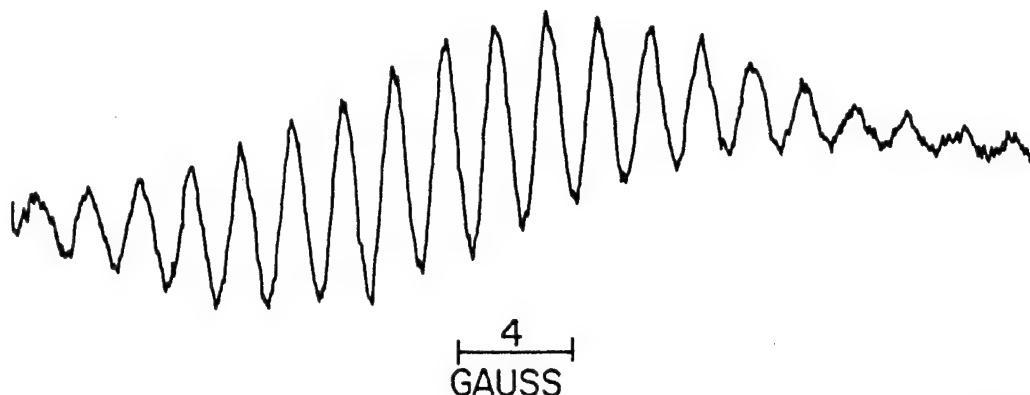
N-5041

Figure 40.   ESR of a 0.003 Molar Solution of Hexa-
methylbenzene in Molten Iodine at 125 °C

### 3.1.6.4.4.   g-Factors of the Hexamethylbenzene Radical Ion in Various Solvents

The g-factors for hexamethylbenzene in $H_2SO_4$, $I_2$, and another
acceptor solvent $SbCl_5$ were 2.0026, 2.0057, and 2.0042, respectively.
The ESR for the $SbCl_5$ system consisted of a single, unresolved broad line
which may be due to precipitated or colloidal solids.   The 2.0042 may,
therefore, reflect crystalline anisotropy rather than an average molecular
property.   On the other hand, the molten $I_2$ system is a true solution (hyper-
fine structure is observed) indicating that the high g-factor is significant.
It is known that iodine attached to an aromatic ring gives rise to a large
positive g-shift because of the large spin-orbit coupling parameter of iodine.[27]
The 2.0057 g-factor suggests, therefore, that the $I_2$ must interact strongly
with the free radical.   The strong interaction is also present in the system
perylene-iodine which was studied by Kommandeur.[26]   We have measured
the g-factor for this system and find the perylene radical cation to have the
remarkably high g-value of 2.0090 ± .0003.   The mechanism for such a
large g-shift caused by solvent interactions alone is not understood at pres-
ent.

The measured g-factor of 2.0024 for $\Phi(CH_3)_6$ in $H_2SO_4$ was evidence
that the $H_2SO_4$ did not oxidize the hydrocarbon to a semiquinone.   This state-
ment was based on measurements of various semiquinones made by Blois.[27]
We have now measured the g-factor of duroquinone in $H_2SO_4$ (with added $Na_2$-
$S_2O_6$) and have indeed found the expected high g-value of 2.0034.   Therefore,
the radical formed from $\Phi(CH_3)_6$ in $H_2SO_4$ does not contain oxygen.

### 3.1.6.4.5.   Identity of the Radical

From a careful consideration of Figures 35 and 36, the best pos-
sible assignment of coupling constants for $\Phi(CH_3)_6$ in $H_2SO_4$ seems to be:

79

$$2\ H,\ a_1 = 5.40\ \text{gauss},$$
$$12\ H,\ a_2 = 3.36\ \text{gauss},$$
$$6\ H,\ a_3 = 1.68\ \text{gauss}.$$

On the basis of this assignment and the proof from the $D_2SO_4$ experiment that only the 2H's originated from the solvent, we were led to the idea of complex formation, i.e., a distorted $\Phi(CH_3)_6$ cation strongly complexed with one molecule of $H_2SO_4$. Although this idea seems appealing, there are at least two points which make this viewpoint rather tenuous. First, not one of the many previously investigated aromatic radical cations in $H_2SO_4$ shows any evidence of complex formation with the solvent. Second, it is unlikely that a proton splitting as large as 5.40 gauss could arise from protons which are not directly chemically bound to the aromatic system.

A more likely possibility is the pentamethylbenzyl radical (XIII).
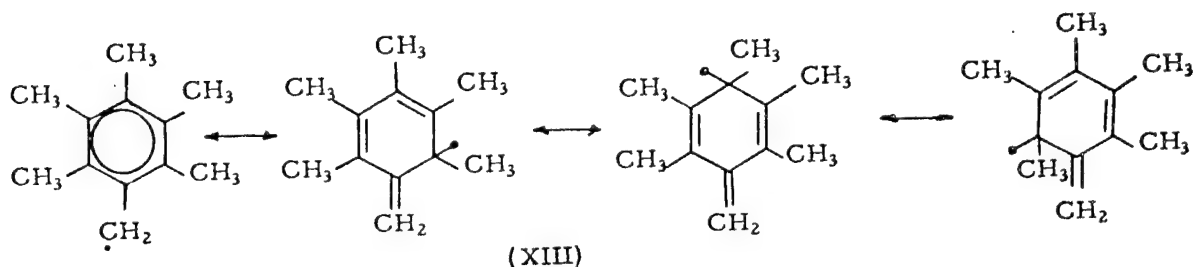


(XIII)

The formation of (XIII) in $H_2SO_4$ and $I_2$ can be visualized through the direct loss of a hydrogen atom from HMB or more likely by a 1-electron oxidation followed by the loss of a proton. This radical is expected to be quite stable by virtue of the resonance structures shown above. Furthermore, the protons at the $CH_2$ position would possess considerable olefinic character and should be readily exchangeable in $D_2SO_4$.

Although no spin density calculations have been made for (XIII), theoretical[28,29] and experimental[30] studies have been carried out on the unsubstituted benzyl radical. Our coupling constants are in agreement with a qualitative extension of this theory to the radical (XIII).

### 3.1.7. Nuclear Magnetic Resonance (NMR)

### 3.1.7.1. Introduction

The key problem in elucidating the mechanisms of carbonization and thermal decomposition reactions resides in the chemical identification of discrete reaction intermediates and reaction products. The preceding section has described the use of ESR spectroscopy to identify the free radical intermediates formed during the thermal decomposition of pure organic compounds. Of at least equal importance in understanding the reaction

80

process is the identity of the diamagnetic pyrolysis products. One of the most promising techniques for characterizing such materials is that of High Resolution Nuclear Magnetic Resonance (NMR). As applied to the proton, this technique permits the classification of hydrogens in organic materials and can serve additionally as a definitive structural tool.

The acquisition of a Varian A-60 NMR spectrometer in our laboratory allows our application of the NMR method to the study of carbonization reactions. Emphasis can thus be placed on the investigation of the hydrogen transfer and hydrogen rearrangement reactions shown to be important during the early phases of carbonization.[3]

The investigations performed in this period involved: the use of NMR to measure spectra of model aromatic compounds for reference purposes, the application of NMR to elucidate pyrolysis reactions, and the study and characterization of complex graphite raw materials by NMR.

## 3. 1. 7. 2.   Experimental

All spectra were obtained with a Varian A-60 NMR spectrometer. The spectra of model compounds were usually determined for dilute solutions in $CCl_4$. In several instances $CS_2$ proved to be a more effective solvent and was therefore employed. All chemical shift data are given in parts per million, ppm, relative to $Si(CH_3)_4$ as an internal standard ($\delta$ values). Comparison of $\delta$ values in $CS_2$ and $CCl_4$ for a variety of the hydrocarbons showed the absence of any solvent effect of aromatic proton chemical shifts between these solvents.

Pitches and pyrolysis products were examined as saturated solutions in $CCl_4$ or $CS_2$. High-temperature spectra were obtained with the use of a Varian High-Temperature Probe. All spectra were recorded by standard high-resolution NMR methods. For improved resolution, most of the aromatic proton peaks were recorded on expanded scale.
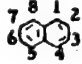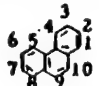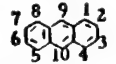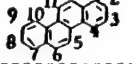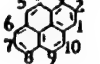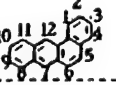
## 3. 1. 7. 3.   Nuclear Magnetic Resonance Spectra of Model Aromatic Compounds

As with the other spectroscopic methods, the interpretation of NMR spectral data must rely on comparison with those obtained for model systems. Surprisingly little published information, however, is available for the polynuclear aromatics, the structures of particular interest to our pyrolysis studies. The most inclusive compilation has been made by Pople, Bernstein, and Schneider.[31] These authors have provided chemical shift data for aromatic hydrogens in various types of polynuclear aromatic molecules. More recently, Jonathan, Gordon, and Dailey[32] have considered in some detail the proton NMR spectra for some selected polynuclear aromatic systems. Freyman, Dvolaitsky, and Jacques[33] have compiled chemical shift data for alkyl substituents in naphthalene, phenanthrene, and chrysene. Chamberlain[34] has summarized some chemical shift data for hydrogens associated with aromatic structures.

81

These data have been utilized for the classification of hydrogen distributions by NMR in aromatic materials such as petroleum oils and asphalts.[35] For the purposes of this present program, however, it was deemed necessary to obtain more precise and extensive data relating to chemical shifts of hydrogens associated with particular aromatic structures. Special attention has been placed on the polynuclear aromatic systems of interest in our current studies.

In the course of the present investigation, NMR spectra have been determined for about 60 aromatic and substituted aromatic hydrocarbons. The NMR chemical shift data are summarized in Table 15. Listed are $\delta$ values for protons of methyl groups substituted in 8 different aromatic ring systems. The position of substitution and the corresponding chemical shift are both indicated. Additional structures are given in Table 23.

Table 15.  Chemical Shifts ($\delta$) of Aromatic $CH_3$ Groups

| | | Methyl Subst. | $\delta$ ppm |
|---|---|---|---|
| 1. Benzene |  | 1 | 2.37 |
| | | 1,2 | 2.25 |
| | | 1,3 | 2.30 |
| | | 1,4 | 2.28 |
| | | 1,3,5 | 2.25 |
| | | 1,2,4,5 | 2.15 |
| | | 1,2,3,4,5 | 2.13, 2.18 |
| | | 1,2,3,4,5,6 | 2.17 |
| 2. Naphthalene |  | 1 | 2.68 |
| | | 2 | 2.50 |
| | | 1,2 | 2.47, 2.57 |
| | | 1,5 | 2.70 |
| | | 1,6 | 2.50, 2.63 |
| | | 2,3 | 2.40 |
| | | 2,3,6 | 2.38, 2.47 |
| 3. Phenanthrene |  | 1 | 2.73 |
| | | 2 | 2.53 |
| | | 3 | 2.62 |
| | | 4 | 3.03 a |
| | | 9 | 2.72 b |
| 4. Anthracene |  | 2 | 2.55 |
| | | 9 | 3.05 |
| | | 9,10 | 3.05 |
| 5. Chrysene |  | 3 | 2.60 c |
| | | 1,2 | 2.59, 2.41 c |
| | | 3,4 | 2.65, 2.21 c |
| 6. Pyrene |  | 1 | 2.93 |
| | | 2 | 2.80 |
| | | 4 | 2.87 |
| 7. Benz(a)anthracene |  | 7 | 3.10 |
| | | 7,12 | 3.02, 3.30 |
| 8. Fluorene |  | 1 | 2.35 |
| | | 2 | 2.40 |
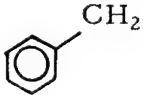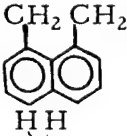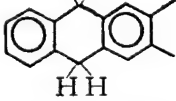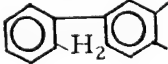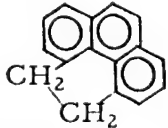
a) Data of Ref. 36
b) Data of Ref. 37
c) Data of Ref. 33

82

Table 16 gives the chemical shifts of $CH_2$ protons in various forms of substitution on aromatic rings. These data are schematically summarized in Table 17 which illustrates the $\delta$ values for various kinds of aromatic $CH_2$ groups.

Table 16.    Chemical Shifts of $CH_2$ Groups
on Aromatic Rings

| Compound | $\delta\ CH_2$, ppm |
|---|---|
| Ethylbenzene | 2.43-2.82 |
| 1-Ethylnaphthalene | 2.70-3.15 |
| 2-Ethylnaphthalene | 2.77 (center) |
| 1,2-Dihydronaphthalene | 2.20-2.45 |
| | 2.62-2.92 |
| Tetralin | 2.56-2.75 |
| Acenaphthene | 3.30 |
| 5-Bromoacenaphthene | 3.24, 3.31 |
| 9,10-Dihydroanthracene | 3.86 |
| 9,10-Dibenzylanthracene | 3.97 |
| 5,12-Dihydronaphthacene | 4.02 |
| 4,5-Methylenephenanthrene | 4.15 |
| Fluorene | 3.83 |
| 2-Methylfluorene | 3.77 |
| 9-Methylfluorene | 3.65-4.03 |
| 9-Ethylfluorene | 3.85 |
| 9-(2-Ethylhexylfluorene) | 3.87 |
| 1,2-Benzofluorene | 4.06 |
| 2,3-Benzofluorene | 4.05 |

Table 17.    Summary of Chemical Shifts of
Structural Types of $CH_2$ Groups
on Aromatic Rings

| Structure Type | $\delta$ ppm |
|---|---|
|  | 2.43-3.15 |
|  | 3.30 |
|  | 3.86-4.02 |
|  | 3.77-4.06 |
|  | 4.15 |

83

In Table 18, the δ values for several types of tertiary hydrogens α to aromatic rings are listed. Tables 19 and 20 give chemical shift data for $CH_3$ and $CH_2$ protons not directly adjacent to the aromatic ring. The δ values of several miscellaneous proton species associated with aromatic rings systems are compiled in Table 21.

Table 18. Chemical Shifts of CH Groups
on Aromatic Rings

| Compound | δ CH, ppm |
|----------|-----------|
| Triphenylmethane | 5.46 |
| 9,9'-Bifluorenyl | 4.78 |
| 9-Bromofluorene | 5.88 |
| 9-(2-Ethylhexylfluorene) | 3.87 |
| 9-Ethylfluorene | 3.85 |
| 9-Methylfluorene | 3.65-4.03 |

Table 19. Chemical Shifts on Nonaromatic
$CH_3$ Groups

| Compound | δ $CH_3$, ppm |
|----------|---------------|
| Ethylbenzene | 1.12-1.36 |
| 1-Ethylnaphthalene | 1.18-1.50 |
| 2-Ethylnaphthalene | 1.30 (center) |
| 9-Ethylfluorene | 0.67 |
| 9-(2-Ethylhexylflourene) | 0.86, 0.95 |
| 9-Methylfluorene | 1.39-1.53 |

Table 20. Chemical Shifts of Nonaromatic $CH_2$ Groups

| Compound | δ ppm |
|---|---|
| 9-Ethylfluorene | 2.10 |
| 9-(2-Ethylhexylfluorene) | 1.26 |
| 1,2-Dihydronaphthalene | 2.62-2.92* |
| Tetralin | 1.60-1.84 |

* Large downfield shift caused by adjacent vinyl group.

Table 21. Miscellaneous Hydrogens Associated with Aromatic Rings

| Compound | δ ppm |
|---|---|
| Allyl Benzene | 3.26, 3.38, 4.90 (olefinic protons) |
| 1-Allylnaphthalene | 3.72-3.82, 4.90-6.40 (olefinic protons) |
| Acenaphthylene | 6.98 |
| 1,2-Dihydronaphthalene | 5.80-6.45 (vinyl protons) |

The NMR data for the aromatic protons of the model compounds are summarized in Table 22. The spectrum type is shown in the first column. The δ values and the number of line components resolved are given in the third and fourth columns. Finally, in the last column the specific proton assignments are designated. In only a few cases have these assignments been unambiguously confirmed. However, all assignments are based on a systematic study of the substitution patterns of the various polynuclear aromatic ring systems. In nearly all the ring structures investigated, the self-consistencies achieved in this manner are felt to make the specific proton assignments reliable. The assignments are also consistent with those of other investigators.[31,32]

85

# Table 22. Chemical Shifts of Aromatic Ring Protons

| Spectrum Type | Aromatic | δ Aromatic - H, ppm | Resolved* Components | Protons |
|---|---|---|---|---|
| A | Ethylbenzene | 7.02 | 1 | ------- |
| A | Allylbenzene | 7.15 | 1 | ------- |
| A | Tetraphenylethylene | 7.02 | 1 | ------- |
| $A_2B_2C$ | Triphenylmethane | 6.98-7.06 | 3 | ------- |
| $A_2B_2$ | Naphthalene | 7.28-7.50 | 6 | 2, 3, 6, 7 |
| | | 7.62-7.83 | 6 | 1, 4, 5, 8 |
| $ABX_2Y_2$ | 1,2-Dimethylnaphthalene | 7.08-7.99 | 17 | |
| ABC | 1,5-Dimethylnaphthalene | 7.18-7.41 | 4 | 2, 3, 6, 7 |
| | | 7.68-7.82 | 4 | 4, 8 |
| ----- | 1-Ethylnaphthalene | 7.22-7.77 | ~11 | ------- |
| ----- | 1-Allylnaphthalene | 7.22-8.02 | ~18 | ------- |
| $ABCX_2$ | 2,3,6-Trimethyl-naphthalene | 7.22 | 1 | 1, 4 |
| | | 6.89-7.45 | 6 | 5, 7, 8 |
| ----- | 1,2-Dihydronaphthalene | 6.95-7.09 | 3U | ------- |
| ----- | 1,2,3,4-Tetrahydro-naphthalene | 6.80 | 1 | ------- |
| ABC | Acenaphthylene | 7.40-7.78 | 8 | ------- |
| ABC | Acenaphthene | 7.02-7.58 | 8 | ------- |
| ABCXY | 5-Bromoacenaphthene | 6.91-7.78 | 12 | ------- |
| ABCDX | Phenanthrene | 7.67 | 1 | 9, 10 |
| | | 7.45-7.90 | 16 | 1, 2, 3, 6, 7, 8 |
| | | 8.55-8.80 | 5 | 4, 5 |
| ABCX | 4,5-Methylene-phenanthrene | 7.43-7.78 | 10 | 1, 2, 3, 6, 7, 8 |
| | | 7.68 | 1 | 9, 10 |
| ----- | 2-Methylphenanthrene | 7.21-7.84 | 14 | 1, 3, 6, 7, 8 |
| | | 7.56 | 1 | 9, 10 |
| | | 8.48-8.72 | 5 | 4, 5 |
| ----- | 3-Methylphenanthrene | 7.25-7.78 | 17 | 1, 2, 6, 7, 8 |
| | | 7.58 | 1 | 9, 10 |
| | | 8.38-8.78 | 5 | 4, 5 |
| $A_2B_2X$ | Anthracene | 7.33-7.56 | 5 | 2, 3, 6, 7 |
| | | 7.83-8.03 | 5 | 1, 4, 5, 8 |
| | | 8.38 | 1 | 9, 10 |
| $A_2B_2$ | 9,10-Dimethylanthracene | 7.33-7.55 | 4 | 2, 3, 6, 7 |
| | | 8.13-8.34 | 4 | 1, 4, 5, 8 |
| $A_2B_2$ | 9,10-Dihydroanthracene | 7.12-7.16 | 2 | |
| $A_2B_2X$ | 9-Methylanthracene | 7.33-7.54 | 8 | 2, 3, 6, 7 |
| | | 7.86-8.32 | U | 1, 4, 5, 8 |
| | | 8.24 | 1 | 10 |
| ----- | 2-Methylanthracene | 7.12-7.32 | 5 | 3, 6, 7 |
| | | 7.49-7.81 | 6 | 1, 4, 5, 8 |
| | | 8.03-8.09 | 2 | 9, 10 |
| ----- | 9-Phenylanthracene | 7.17-7.58 | 10 | 2, 3, 6, 7 |
| | | 7.85-8.05 | 4 | 1, 4, 5, 8 |
| | | 8.40 | 1 | 10 |
| $A_2B_2$ | 9,10-Dibenzylanthracene | 7.08 | | Benzyl |
| | | 7.19-7.45 | 4 | 2, 3, 6, 7 |
| | | 8.02-8.30 | 4 | 1, 4, 5, 8 |
| ABX | Pyrene | 7.91 | 1 | 4, 5, 9, 10 |
| | | 7.85-7.95 | 3 | 2, 7 |
| | | 7.98-8.15 | 3 | 1, 3, 6, 8 |
| ----- | 1-Methylpyrene | 7.79 | 1 | 2 |
| | | 7.91 | 1 | 4, 5, 9, 10 |
| | | 7.88-8.10 | 4 | 3, 6, 7, 8 |
| ----- | 2-Methylpyrene | 7.68 | U | 7 |
| | | 7.74 | 1 | 4, 5, 9, 10 |
| | | 7.83 | 1 | 1, 3 |
| | | 7.77-7.98 | 4 | 6, 8 |
| ----- | 4-Methylpyrene | 7.48 | 1 | 2 |
| | | 7.70 | 1 | 5, 9, 10 |
| | | 7.59-7.83 | 6 | 1, 3, 6, 7, 8 |
| ABCD | Fluorene | 7.13-7.53 | 10 | 4, 5 |
| | | 7.63-7.80 | ~5 | 1, 2, 3, 6, 7, 8 |
| ABCD | 9,9'-Dibromofluorene | 7.23-7.59 | 15 | 4, 5 |
| | | 7.74-7.95 | 7 | 1, 2, 3, 6, 7, 8 |
| ABCD | 9-Bromofluorene | 7.20-7.47 | 11 | 4, 5 |
| | | 7.53-7.67 | 6 | 1, 2, 3, 6, 7, 8 |
| ABCD | 9,9'-Bifluorenyl | 6.89-7.33 | 11 | 1, 2, 3, 6, 7, 8 |
| | | 7.46-7.62 | 6 | 4, 5 |
| ABCX | 9,9'-Bifluorylidene | 7.07-7.33 | 6 | 2, 3, 6, 7 |
| | | 7.54-7.70 | 5 | 4, 5 |
| | | 8.28-8.41 | 5 | 1, 8 |

(Continued)
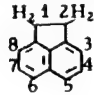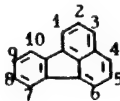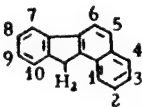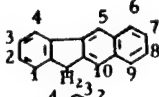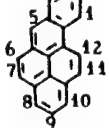
Table 22. (Continued)

| Spectrum Type | Aromatic | δ Aromatic - H, ppm | Resolved* Components | Protons |
|---|---|---|---|---|
| ABCX | 9-Methylfluorene | 7.14-7.53 | 12 | 1,2,3,6,7,8 |
| | | 7.54-7.72 | 6 | 4,5 |
| ABCD | 9-Ethylfluorene | 7.13-7.55 | 14 | 1,2,3,6,7,8 |
| | | 7.57-7.71 | 6 | 4,5 |
| - - - - - | 2-Methylfluorene | 6.99-7.45 | 10 | 1,3,6,7,8 |
| | | 7.49-7.71 | 6 | 4,5 |
| - - - - - | Benz(a)anthracene | 7.35-7.58 | 6 | 2,3,9,10 |
| | | 7.61 | 1 | 5,6 |
| | | 7.67 | 1 | 7 |
| | | 7.71-8.05 | U | 4,8,11 |
| | | 8.22 | 1 | 1,12 |
| | 7,12-Dimethylbenz- (a) anthracene | 7.18-7.54 | 6 | 2,3,9,10 |
| | | 7.64 | 1 | 5,6 |
| | | 7.78 | 7 | 4,8,11 |
| | | 7.95-8.16 | | |
| | | 8.21 | 1 | 1 |
| - - - - - | Fluoranthene | 7.17-7.54 | 8 | 7,8,9,10 |
| | | 7.60-7.88 | 11 | 1,2,3,4,5,6 |
| - - - - - | Benzo(a)fluorene | 7.18 7.47 | 9 | 7,8,9,10 |
| | | 7.64-7.90 | U | 1,2,3,4 |
| | | 7.77 | 1 | 5,6 |
| - - - - - | Benzo(b)fluorene | 7.29-7.58 | 6 | 1,2,3,4 |
| | | 7.68-7.96 | 6 | 6,7,8,9 |
| | | 8.10 | 1 | 5,10 |
| - - - - - | Benzo(a)pyrene | 7.39-7.60 | 6 | 2,3 |
| | | 7.72-7.91 | 6 | 4,7,8,9,10,11 |
| | | 8.42-8.62 | 6 | 1,5,6,12 |
| - - - - - | Coronene | 8.69 | 1 | - - - - - |

*U designates unresolved.

(Concluded)

Table 23.   Additional Structural Formulae of Polynuclear Aromatic Ring Systems

| | | |
|---|---|---|
| (1) | Acenaphthene |  |
| (2) | Fluoranthene |  |
| (3) | Benzo(a)fluorene |  |
| (4) | Benzo(b)fluorene |  |
| (5) | Benzo(a)pyrene |  |

87

Examples of NMR spectra for representative aromatic compounds are illustrated in Figure 41.
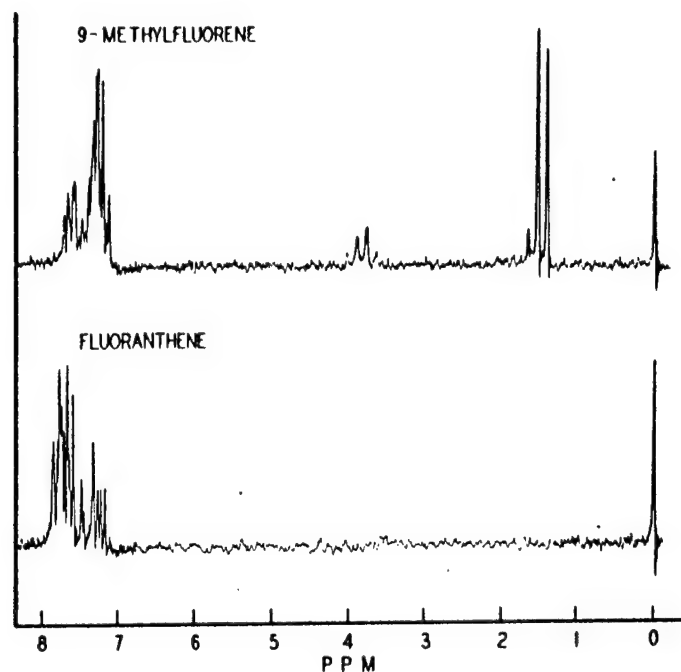


Figure 41.   NMR Spectra of Representative
Aromatic Hydrocarbons

In general, two kinds of quantitative information are available from high-resolution proton magnetic resonance; the chemical shift and the spin-spin coupling between interacting nuclei. The chemical shift is dependent on the proton type and reflects its molecular environment. The spin-spin coupling interaction provides definitive information regarding the neighboring protons in the molecule. Both kinds of information are important in structure verification.

In this initial study, emphasis has been placed on the determination of chemical shifts for various aromatic proton types. The more difficult task of computing spin-spin coupling constants will be restricted to systems of specific interest to our chemical studies.

### 3.1.7.3.1.   Chemical Shifts of Aromatic Methyl Groups

The chemical shifts of protons are known to be composites of a variety of effects,[31] a local paramagnetic contribution, a local diamagnetic contribution, and a magnetic anisotropy effect of neighboring atoms. The latter can be further subdivided into a diamagnetic contribution and a paramagnetic contribution. The first two terms are believed to be sensitive to the electron density about the proton. The neighbor-anisotropy effect in organic molecules is largely influenced by bond hybridizations. Additionally, in aromatic compounds, circulating ring currents involving the π elec-

88

trons lead to large downfield proton shifts. Jonathan, Gordon, and Dailey[32] have recently calculated aromatic proton shifts, $\sigma_\pi$, with the aid of molecular orbital theory for a number of aromatic systems. These authors employed a refined ring-current model for polynuclear aromatic systems. Fair quantitative agreement was found for measured and calculated aromatic proton screening constants. This comparison, however, was made difficult in a number of instances by the inability to assign peaks to specific protons due to the complications of spin-spin splitting.

Maclean and Mackor[36] showed that for a limited series of methylated aromatics, the chemical shift of the methyl group could be related to the respective proton shift in the unsubstituted aromatic hydrocarbon. Recently Durand, Parello and Buu-Hoi[37] have obtained methyl chemical shifts for some methylated polynuclear aromatic hydrocarbons and found a poor relation between computed and experimental shifts.

Our data in Table 15 show the variation of proton chemical shifts for aromatic methyl groups in a variety of aromatic ring systems. The examples provided encompass a total range in $\delta$ values of about 1.1 ppm. The marked dependence of the methyl peak position on the type of substitution make these NMR measurements useful in ascertaining aromatic structure. The methyl proton shifts can be compared directly with the ring proton screening constants computed by Jonathan, et al.[32] with the use of the ring-current model. This correlation is shown in Figure 42 which com-
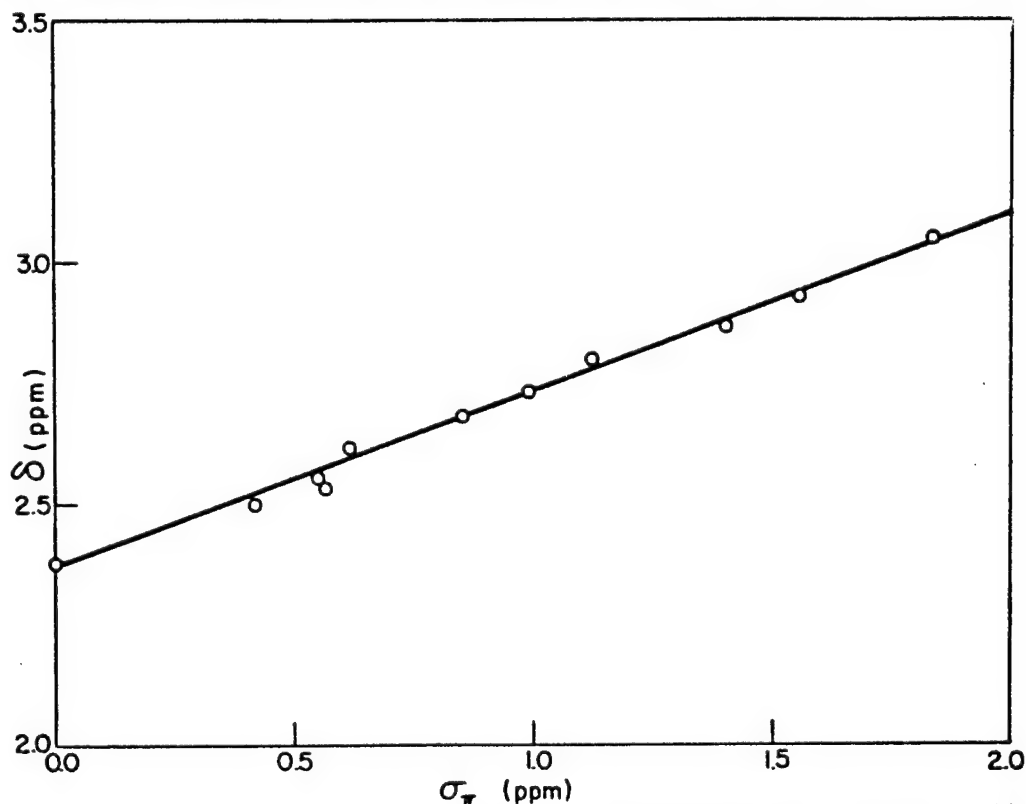


N-5037

Figure 42.   Comparison of $\delta CH_3$ for Methylated Aromatics Versus $\sigma_\pi$ for Unsubstituted Aromatics

89

pares the δ values in ppm for the methyl protons in methyl derivatives of benzene, naphthalene, anthracene, phenanthrene, and pyrene with the calculated values of the aromatic protons, $\sigma_\pi$, in ppm relative to benzene.

A precise relationship is obtained between these two sets of parameters. These results show that:

a.

The methyl protons of aromatic methyl groups as well as the ring protons are predominantly influenced by ring-current shifts. The magnitude of these shifts appear to be quite well estimated by the calculations of Jonathan, et al.

b.

The methyl proton shifts are a much more accurate means of determining these ring-current effects than the ring proton shifts, since the former do not show any spin-spin splitting effects and can be recorded as single sharp peaks.

c.

NMR measurements should be useful for predicting the position of substitution of methyl groups in polycyclic aromatics by a comparison of theoretical and experimental screening constants.

### 3.1.7.3.2. Chemical Shifts of Aromatic Methylene Groups

Summarized in Table 17 are some δ values for the more common kinds of aromatic methylene substituents. These substituents, which are generally important in carbonization products and raw materials, exhibit characteristic chemical shifts which can be readily employed in structural verifications.

The chemical shifts for the various methylene protons appear to be influenced by both electron density considerations and steric effects. The latter are effectively demonstrated by the large downfield shift of the protons in 4,5-methylenephenanthrene.

### 3.1.7.3.3. Chemical Shifts of CH Groups on Aromatic Rings

Tertiary hydrogen adjacent to the aromatic ring is not a common structural feature of the aromatic molecules present in carbon raw materials. Several examples of some available compounds of this type are given in Table 18.

### 3.1.7.3.4. Chemical Shifts of Nonaromatic $CH_3$ and $CH_2$ Groups

The δ values of $CH_3$ groups and $CH_2$ removed from the aromatic ring by one or more atoms are similar to those found for aliphatic compounds. As expected, the distant aromatic ring has only a minor effect on

the screening constants. Some examples of such compounds are provided in Tables 19 and 20.

### 3.1.7.3.5. Miscellaneous Protons Associated with Aromatic Rings

Some miscellaneous proton types associated with aromatic rings are compiled in Table 21.

### 3.1.7.3.6. Chemical Shifts of Aromatic Protons

Attempts at quantitative correlative prediction of aromatic proton chemical shifts in polynuclear aromatics have met with little success.[31,32] The varying contributions to the proton screening constants discussed earlier make such predictions difficult.

The aromatic proton chemical shift data for a variety of polynuclear aromatic systems are summarized in Table 22. It is seen that the proton chemical shifts are markedly influenced by both the position of substitution and the aromatic ring type. The $\pi$-electron density which contributes to the circulating ring currents is a major factor. The protons of benzene and benzene derivatives are chemically shifted upfield with respect to the protons of the more condensed aromatics.

The positions of the individual proton peaks are further complicated by spin-coupling interaction from neighboring protons. This situation is made somewhat less complex by the apparent absence of interactions between protons in different fused rings in the systems examined. The proton pattern of each ring can therefore be handled individually by the useful methods of spectral analysis. In polynuclear systems, however, the individual ring patterns can superimpose, making the overall spectrum quite difficult to interpret.

A precursory analysis of the aromatic proton patterns for a variety of aromatic structural types is given in Table 22. When possible, the expected spectrum type has been designated. The chemical shift designations have been made with respect to the individual protons. Since the individual proton patterns are spread out by spin-spin splitting, the range in ppm is given for each peak. This value would be the most useful parameter in analyzing complex mixtures. A very brief discussion of the individual ring systems follows.

#### a. Benzene

All of the benzene derivatives studied show the aromatic proton $\delta$ values to be in the vicinity of 7.0-7.1 ppm.

#### b. Naphthalene

The spectrum is typical $A_2B_2$ type. The two types of protons are readily distinguished, $\beta$ protons with $\delta = 7.28$-$7.50$ and $\alpha$ protons with $\delta = 7.62$-$7.83$. Alkyl substitution in the naphthalene ring such as in

91

the methyl naphthalenes and acenaphthene is seen to shift the aromatic peaks upfield presumably by increasing the electron density in the aromatic ring.

### c. Phenanthrene

The phenanthrene protons fall between 7.45-7.90 ppm in a complex manner. Of special interest is the large downfield chemical shift of the 4,5 protons. These are found at 8.55-8.80 ppm. This shift has been attributed to a direct steric interaction.

Again, methyl substituents are seen to induce slight upfield shifts for the phenanthrene ring protons.

### d. Anthracene

Anthracene can be treated as an $A_2B_2X$ system. The 1,4,5,8 protons are found considerably downfield from the 2,3,6,7 protons. The large downfield shift of the 9,10 protons (8.38 ppm) is consistent with the reactivity at these positions.

Methyl substitution in the 9 and 10 positions shifts the 1,4,5,8 protons even further downfield presumably through a direct steric effect. The 2,3,6,7 protons remain unaltered. Methyl substitution in the 2 position shifts the aromatic protons upfield in the expected manner.

### e. Pyrene

The entire ABX pattern of pyrene falls between 7.85 and 8.15 ppm. Methyl substitution is again seen to shift the aromatic protons by an electronic effect.

### f. Fluorene

The fluorene protons generally fall between 7.10-7.80 ppm. Substitution in the 9 position does not appreciably alter these values. Alkyl substituents directly on the benzenoid ring shift the aromatic peaks in the expected manner.

The effects of direct steric interaction is dramatically evidenced in bifluorylidene in which a large downfield shift is found for the 1, 1', 8, 8' protons.

### g. Benz(a)anthracene

As expected, a complex pattern is observed for benz(a)anthracene. Of interest is the downfield shift (8.22 ppm) for 2 protons assigned at the 1 and 12 positions in analogy with the 4,5 proton assignment in phenanthrene.

92

### h. Fluoranthene

Fluoranthene exhibits an extremely complex pattern. More detailed study is necessary for a precise assignment.

### i. Benzo(a)pyrene

The proton assignments for this hydrocarbon are shown in Table 22. A peak corresponding to 4 protons is found far downfield. This peak definitely includes the sterically interacting 1 and 12 protons and, additionally, probably includes the 5 and 6 protons. The 2 proton peaks at 7.39-7.60 have been assigned to the 2 and 3 protons.

### j. Coronene

The protons of coronene are all equivalent and, hence, only a single line is observed. The large downfield shift for the proton signal, 8.69 ppm illustrates the ring-current effect in this large condensed aromatic molecule.

### 3.1.7.4. NMR Spectra of Reaction Products

The data of the previous section permit the classification of the chemical shifts of aromatic and alkylated aromatic protons according to proton type. This information can then be directly applied to the investigation of organic pyrolysis products. In such materials only the $CCl_4$ or $CS_2$ soluble portions can be examined. Furthermore, since many of these materials contain paramagnetic constituents, only semi-high resolution proton spectra can be obtained. In several instances, the pyrolysis products consist of or can be separated into single pure compounds. In such case, the NMR method can allow specific structural identification. This section summarizes the use of NMR to investigate both kinds of materials.

### 3.1.7.4.1. Acenaphthylene and Acenaphthylene-D6 Pyrolytic Residues

NMR spectra were obtained for both the volatile and nonvolatile products of pyrolysis at 400°C for acenaphthylene and acenaphthylene-D6. Since the deuterium magnetic resonance will not be observed, this technique offers a specific means for following the course of the two olefinic hydrogens in the pyrolysis sequence.



Acenaphthylene-D6

93
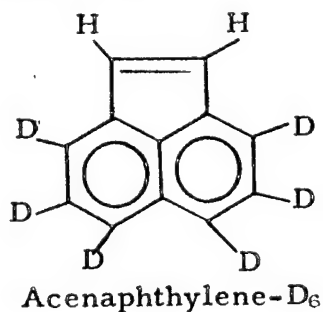
The peak at 3.27 ppm for the acenaphthene aliphatic protons was observed in all the materials. Aromatic proton peaks at 7.40 ppm were observed for the $D_6$-acenaphthylene. These results provide evidence for incorporation of the side-chain protons in the converted aromatic product. This mechanism has been proposed for the formation of zethrene from acenaphthylene.[3]

Both the $D_6$-acenaphthylene and the fully protonated acenaphthylene gave peaks at 6.82 ppm which are associated with a side-chain olefinic structure (different from acenaphthylene-6.95 ppm). A peak at 3.04 ppm in the nondeuterated acenaphthylene can be attributed to methyl group formation by ring splitting.

### 3.1.7.4.2. Chromatographed Fractions of Pyrolyzed Acenaphthylene

Some of the highly colored chromatographed fractions from pyrolyzed acenaphthylene appear to be free radicals in nature, since no NMR spectra could be obtained for these substances. Other fractions gave unusual spectra consisting of a mixture of sharp and broad lines indicating a partial polymer nature (Figure 43). The dominance of acenaphthenic and aromatic methyl hydrogens in some of the fractions shows the importance of cleavage of the 5-membered ring and hydrogen abstraction by radical intermediates.
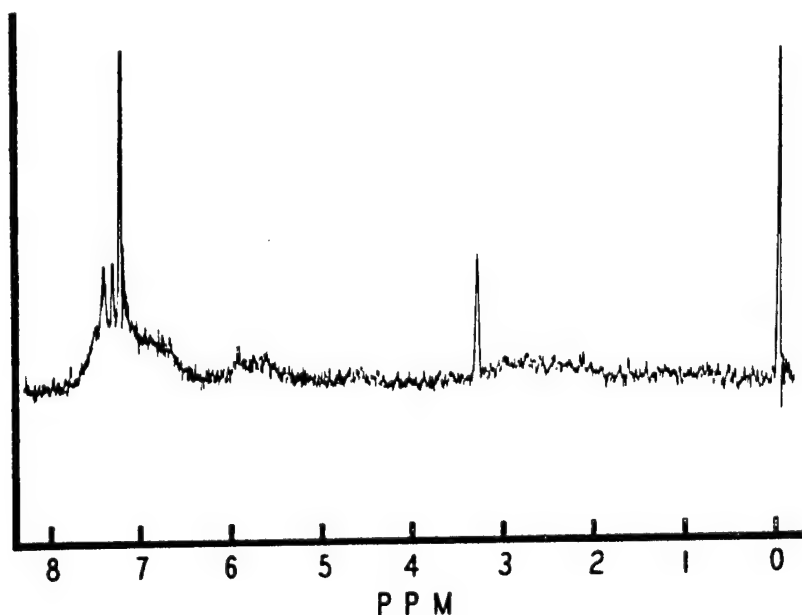


N-5067

Figure 43. NMR Spectrum of Pyrolysis
Products of Acenaphthylene

### 3.1.7.4.3. Pyrolyzed Fluoranthene

NMR Examination of fluoranthene pyrolysates and the "fluoranthene pitch" shows that the $CS_2$ soluble portions possesses the basic fluor-

anthene structure. This result is consistent with our earlier conclusion that fluoranthene initially undergoes direct thermal dimerization. There is no evidence of aliphatic material in these products.

### 3.1.7.4.4. Pyrolyzed Diazofluorene

The pyrolysis product of diazofluorene at 200°C was confirmed by NMR to be predominantly $\Delta^{9,9'}$-bifluorene.

### 3.1.7.4.5. Pyrolyzed Diazobenzil

The NMR spectrum of the 200°C pyrolysis product of diazobenzil shows that most of the nitrogen is not retained in the reaction products. A symmetric aromatic structure is indicated. Furthermore, a slight aliphatic peak at 4.83 ppm demonstrates some hydrogen abstraction by the radical intermediate.

### 3.1.7.5. Nuclear Magnetic Resonance of Aromatic Ions

NMR spectra were obtained for several aromatics in ionizing media. These investigations were designed to supplement the ESR research on radical and radical ion intermediates in pyrolysis.

#### a. Acenaphthylene-Acid Systems

NMR spectra of acenaphthylene in glacial acetic acid showed only slight evidence of protonation in the 5-membered ring. Much higher resolution spectra could be obtained for acenaphthylene in $CH_3COOH$ than in $CCl_4$. The use of $CH_3COOH$ as an NMR solvent for aromatics will be explored. No spectrum could be obtained, however, for the dark green solution of acenaphthylene in $H_2SO_4$, indicating that a radical-ion is formed in this solvent.

#### b. 2, 3, 6-Trimethylnaphthalene-$H_2SO_4$

ESR measurements demonstrated that the colored solution of 2, 3, 6-trimethylnaphthalene in $H_2SO_4$ is not paramagnetic. NMR spectra indicate that this hydrocarbon protonates in $H_2SO_4$, probably at the 1 position to yield the ion (I).



(I)
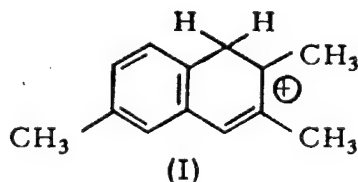
Although the methyl protons are quite distinct in $H_2SO_4$, the ring protons are extensively broadened, probably resulting from the proton exchange with the solvent.

95

## c.  Hexamethylbenzene-$H_2SO_4$

Maclean and Mackor[36] examined the NMR of hexamethylbenzene (HMB) in HF.  At -85°C, they observed the spectrum of (II); at room temperature, they obtained a single peak due to proton exchange within the ion.
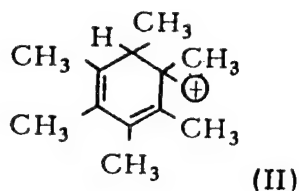


HMB in $H_2SO_4$ at room temperature gives a single proton peak at 2.35 ppm, a value which represents only a slight shift from the normal methyl resonance of HMB (2.14 ppm) in inert solvents.  The single peak may be due to neutral HMB molecules dissolved in $H_2SO_4$ or to rapidly exchanging ions of structure (II).

## d.  Hexamethylbenzene-$D_2SO_4$

HMB dissolves very slowly in $D_2SO_4$.  As solution continues, the small proton peak of the residual $H_2SO_4$ in $D_2SO_4$ is observed to grow, indicating an exchange between the methyl hydrogens and solvent deuterons.  A single proton peak is found for HMB in $D_2SO_4$ (cf. the similar condition for $H_2SO_4$).  This peak is considerably shifted, however, to 4.10 ppm.  If $D_2SO_4$ is added to a solution of HMB in $H_2SO_4$, both peaks at 2.35 and 4.10 ppm are observed.  Although the chemical shift in $D_2SO_4$ cannot be explained, it may be associated with complex exchanges between HMB and solvent.

## e.  Hexamethylbenzene-$I_2$

HMB has been found to yield a paramagnetic species in molten $I_2$. NMR spectra have now been obtained for HMB in molten $I_2$ in order to ascertain whether any chemical iodination of the methyl groups is occurring.  HMB in molten $I_2$ yields a single broadened methyl peak at 2.65 ppm, which may be attributed to neutral hexamethylbenzene molecules dissolved in $I_2$.  No evidence of chemical reaction could be observed.

## f.  Pyrene-Chloranil

The aromatic hydrocarbon pyrene is known to form a charge transfer complex with chloranil in solution.  When these two compounds are melted together, a green species is produced.  NMR measurements have been made for a 1:1 mixture of pyrene and chloranil at 180°C. Initially, the high resolution spectrum of pyrene is observed.  Within 15 minutes, however, this spectrum broadens and disappears.  These results

demonstrate that the green species is likely a radical-ion produced by electron transfer from pyrene to chloranil. The formation of this species presumably leads to the broadening of the NMR spectrum.

### 3.1.7.6. Nuclear Magnetic Resonance Spectra of Pitches

### 3.1.7.6.1. Commercial Coal Tar Pitches

NMR spectra have been measured on commercial coal tar pitches in $CCl_4$ solution. Two pitch types, 30-medium pitch and a lower melting 15-vacuum pitch, were included. From an NMR standpoint the soluble portion of comparable pitches from the same supplier are extremely similar. All the pitches exhibited a large broad aromatic region at 7.0 to 8.0 ppm. In a number of samples the aromatic region from 8.0 to 8.8 ppm (hindered protons of the phenanthrene type) was also pronounced. In some preparations actual resolution of distinct aromatic proton peaks could be discerned.

The aliphatic proton content of the pitch solutions varied from about 10 to 20 per cent. The aliphatic protons were predominantly in the form of methyl groups on medium-size fused ring systems (2.2 to 2.7 ppm). Slight peaks at 3.0 ppm (reactive aromatic methyl and methylene groups) and 3.3 to 3.9 ppm (hydrogenated ring systems and acenaphthenes) were also observed in many instances.

No improved resolution could be observed for a commercial coal tar pitch (P-98) examined as a pure melt at 130°C. Under these conditions, only a single broad aromatic and single broad aliphatic peak could be discerned.

These preliminary results confirm the composition of coal tar pitches to be mixtures of fused polycyclic aromatic hydrocarbons. Substitution seems to be largely in the form of methyl groups and to a lesser extent hydroaromatic rings. In selected cases, the NMR method can discern differences in aromatic composition as well as measure resolved individual aromatic proton peaks.

### 3.1.7.6.2. Synthetic Pitch from Acenaphthylene

#### a. CS₂ Solution

When acenaphthylene pitch[32] is dissolved in $CS_2$, a semi-resolved spectrum can be obtained. A split aromatic proton peak representing about 82 per cent of the total hydrogen and a sharp aliphatic peak for the methylene $CH_2$ groups consisting of about 18 per cent of the protons are observed. A small methyl peak is also evident. The acenaphthylene pitch differs appreciably from the commercial coal tar pitches in that the aliphatic protons are still to a large extent bound up in the 5-membered acenaphthenic ring. Spectra of higher heat-treated acenaphthylene do show the more conventional $CH_3$ absorptions as further ring degradation ensues.

## b.  150°C Spectrum

When acenaphthylene pitch is heated above its melting point, the NMR spectrum obtained in Figure 44 is observed.  The aromatic and aliphatic peaks have been considerably broadened in the spectrum of the pure molten pitch.  This broadening does not abate as the temperature is raised to 200°C.  The high-temperature spectrum of the acenaphthylene pitch closely resembles that of the commercial 30-medium pitch.
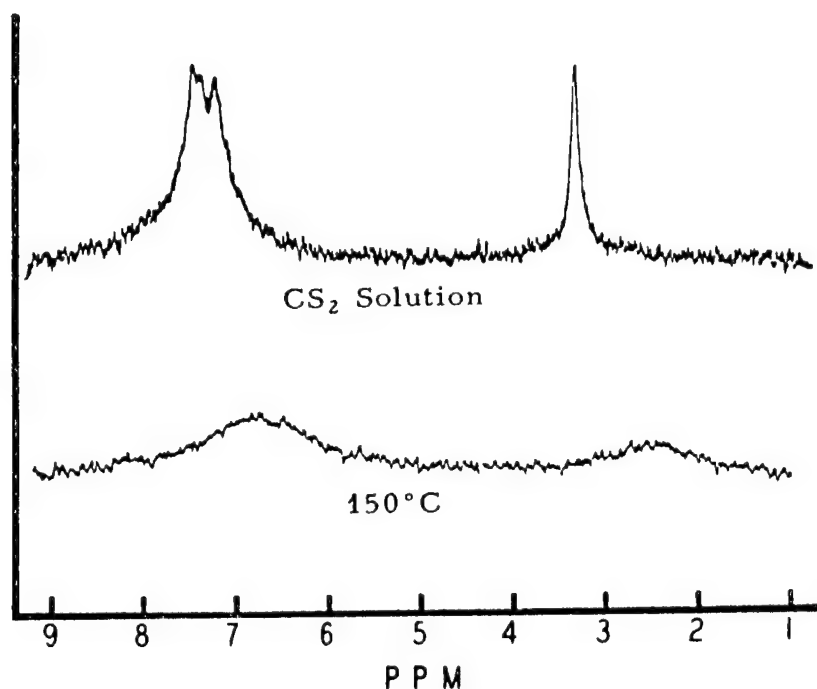


N-5068

Figure 44.  NMR Spectrum of Acenaphthylene Pitch

It appears, therefore, that the $CS_2$ insoluble portion of acenaphthylene pitch consists to a large extent of aromatic hydrocarbon free radicals.  The solubility of these radicals in the molten pitch causes the broadening effects observed.  The large upfield shift of the center of gravity of the aliphatic proton peak relative to the aromatic proton peak indicates that large methylated aromatic species are also being brought into solution.

### 3.1.7.6.3.  Experimental Pitches from Lawrenceburg (M-176 and M-177)

Two experimental pitches from Lawrenceburg (M-176, a low-temperature pitch, and M-177, a high-temperature pitch) were investigated by NMR.  The $CS_2$ spectra showed considerable differences.  M-176 was highly aliphatic, the aromatic/aliphatic ratio being 32/68.

The aliphatic hydrogen distribution relative to the total hydrogen was:

> 13% - CH₃ (not α-to aromatic ring),
> 20% - CH₂ (not α-to aromatic ring),
> and   33% - CH₂ and CH₃ α-to aromatic ring.

When M-176 was examined at 150°C to 190°C, the entire spectrum broadened extensively. This effect is again attributed to the dissolution of free radicals.

M-177, on the other hand, was highly aromatic, resembling a typical 30-medium pitch. The aromatic/aliphatic ratio was 80/20, the aliphatics being present mainly in the form of aromatic methyls.

## 3.1.8.  Ultraviolet and Visible Absorption Spectroscopy

### 3.1.8.1.  Introduction

Ultraviolet and visible absorption spectroscopy are important techniques for the characterization and structural identification of aromatic hydrocarbons. For the aromatic hydrocarbons, relationships have been derived between aromatic structure and electronic absorption in the ultraviolet and visible spectral regions.[39] With the use of such relationships, spectroscopic techniques can be employed in a routine manner for studying pyrolysis products. In this report an additional structural feature which influences the electronic absorption spectra of aromatics has been considered; namely, the effects of substituent groups.

A significant feature of the aromatic and substituted aromatic hydrocarbons is their ability to readily undergo oxidation and reduction. These processes lead to the formation of stable aromatic radicals and ions. Spectroscopic studies of these entities can provide considerable information relating to aromatic structure and reactivity. Furthermore, aromatic radicals are believed to be important intermediates in pyrolysis.

Aromatic ions and radicals are readily formed by dissolution of the hydrocarbon in concentrated sulfuric acid.[40] The most extensive work in this area has involved the use of electron spin resonance to study the aromatic radical ions produced in this manner.[41] The initial step in this process is believed to consist of a direct protonation of the aromatic ring to form a carbonium ion (II) which then undergoes oxidation to the radical ion (III).

$$\text{ArH} \underset{}{\overset{+H^{\oplus}}{\rightleftharpoons}} \text{ArH}_2^{\oplus} \underset{}{\overset{-H\cdot}{\rightleftharpoons}} \text{ArH}\cdot^{\oplus}$$

$$\text{(I)} \qquad\qquad \text{(II)} \qquad \text{(III)}$$
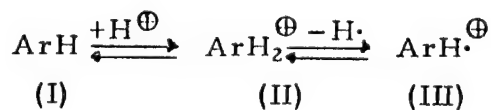
Electron spin resonance measurement of the radical ion (III) yields sig-
nificant information relating to aromatic electronic structure.[39-41] Ultra-
violet and visible electronic spectra of such solutions are expected to
exhibit absorption bands characteristic of (I) and (III). The nature and
formation of these bands should be diagnostic of aromatic structure. In
view of our interest in aromatic structure and in aromatic radicals as in-
termediates in carbonization, we have examined the spectral behavior of
a variety of polycyclic aromatics in $H_2SO_4$. Both the effects of structural
variation and ring substitution were considered.

### 3.1.8.2. Experimental

The sulfuric acid solutions were made up initially to 1 g/l in 98
per cent $H_2SO_4$ and diluted further with 98 per cent $H_2SO_4$ as necessary.
The spectra were run immediately after preparing the solutions (0 hours)
and at various later times, depending on the speed of reaction. The scan-
ning time for each spectrum was approximately 30 minutes. All spectra
were obtained with a Beckman DK spectrophotometer employing 1 cm
silica cells.

### 3.1.8.3. Results

#### a. Effects of Substituents on the Electronic Spectra of Aromatics

Listed in Table 24 are the wavelengths of the long-wavelength "p"-
bands[39] for a series of substituted anthracenes in cyclohexane
solution. The spectral ionization potentials have been computed in the last
column by the method reported previously.[1,2]

In Table 25 are comparable data for some substituted pyrene
derivatives. These data show the influence of substitution on the spectral
parameters.

#### b. UV-Visible Spectra of Polynuclear Aromatics in $H_2SO_4$

Table 26 summarizes the spectral data for a variety of polynuclear
aromatics in $H_2SO_4$ solution. In all cases new broad absorption
bands were formed in the visible spectral region. The wavelengths of the
maxima of these bands are shown in the last column of Table 26. The ap-
pearance and intensity of the spectral absorptions are dependent on time
due to the equilibria represented in the equation on the preceding page.

Figure 45 illustrates typical UV spectra of some of the aromatics
and substituted aromatics in cyclohexane solution. The spectra exhibit
characteristic sharp bands and absorptions which generally occur between
the 200- and 600-mμ region.

In Figure 46 are shown some representative spectra for polynu-
clear aromatics in $H_2SO_4$ solution. In all cases, new broad absorption bands
are evident. These extend through the whole visible region of the spectrum
and in some cases to 1000 mμ. Figure 47 illustrates the effect of time on

Table 24.  Long-Wavelength "p"-Band and Derived Ionization Potential
for Substituted Anthracenes in Cyclohexane Solution

| Compound | p-Band (mμ) | Ionization Potential (e.v.) |
|---|---|---|
| Anthracene | 376 | 7.22 |
| 2-Methylanthracene | 377 | 7.21 |
| 2-Phenylanthracene | 383 | 7.16 |
| 9-Phenylanthracene | 383 | 7.16 |
| 1-Aminoanthracene | 386 | 7.14 |
| 9-Methylanthracene | 386 | 7.14 |
| 9,9'-Bianthryl | 389 | 7.12 |
| 9-Bromoanthracene | 389 | 7.12 |
| 9, 10-Diphenylanthracene | 393 | 7.09 |
| 2-Aminoanthracene | 395 | 7.08 |
| 9, 10-Di-1-naphthylanthracene | 395 | 7.08 |
| 9, 10-Dibenzylanthracene | 398 | 7.06 |
| 9, 10-Dimethylanthracene | 398 | 7.06 |
| 9, 10-Dichloroanthracene | 401 | 7.04 |
| 9, 10-Dibromoanthracene | 402 | 7.03 |
| 9-Nitroanthracene | 418 | 6.93 |

Table 25.  Long-Wavelength "p"-Band and Derived Ionization Potential
for Substituted Pyrenes in Cyclohexane Solution

| Compound | p-Band (mμ) | Ionization Potential (e.v.) |
|---|---|---|
| Pyrene | 335 | 7.56 |
| 2-Methylpyrene | 337 | 7.54 |
| 4-Methylpyrene | 337 | 7.54 |
| 1-Methylpyrene | 344 | 7.48 |
| 1-Chloropyrene | 344 | 7.48 |
| 1-Bromopyrene | 347 | 7.45 |
| 1-Pyrenamine | 358 | 7.36 |
| 1-Nitropyrene | 371 | 7.25 |

Table 26. New Visible and UV Absorption
Bands of Aromatics in $H_2SO_4$

| Compound | Time (Hours) | Wavelengths (mμ) |
|---|---|---|
| Anthracene | 0 | 417s, 560w, 660w, 711s |
| 9,9'-Bianthryl | 1 | 475s, 577w, 630w, 732s |
| 9-Bromoanthracene | 0 | 710w, 790w |
| 9,10-Dibenzylanthracene | 0 | 442s, 535w, 627w |
|  | 3 | 423w, 625w, 713s |
| 9,10-Dibromoanthracene | 3-1/2 | 430w, 465s, 545w, 650w, 698s |
|  | 24 | 465s, 698s |
| 9,10-Dichloroanthracene | 24 | 439s, 610w, 675s |
| 9,10-Dimethylanthracene | 0 | 410s, 540w, 590w, 663s |
|  | 2 | 420s, 510w, 540s, 590s, 663s |
| 9,10-Di-1-naphthylanthracene | 3 | 420w, 545w, 597w, 658w, 704w |
| 9,10-Diphenylanthracene | 0 | 410s, 610w |
|  | 30 | 430w, 530w, 588w, 637w, 743w |
| 9-Methylanthracene | 0 | 410s, 584w, 635w, 685s |
|  | 3 | 410w, 584w, 635w, 685w |
| 9-Nitroanthracene | 23 | 468w, 550w |
| 2-Phenylanthracene | 0 | 505s, 631w, 685s, 752s, 870w |
|  | 3-1/2 | 438w, 558s, 750w, 860w |
| 9-Phenylanthracene | 0 | 417s, 540w, 583w, 652w, 707w |
|  | 3-1/2 | 707w |
| Acenaphthylene | 3 | 625s |
| Naphthacene | 0 | 458s, 600s, 740s, 851s, 929w, 985w |
| Pyrene | 1 | 385w, 440w, 527w, 629w |
| 2-Methylpyrene | 0 | 360s, 397w, 447s, 505w574w, 801w |
|  | 5 | 371s, 393w, 473s, 549w, 803w |
| 1-Methylpyrene | 0 | 373s, 396w, 450w, 464s, 473w, 780w |
|  | 1 | 374s, 398w, 785s |
| 1-Pyrenamine | 1 | 423w, 610w |
|  | 5 | 440w, 600w |
| 1-Nitropyrene | 1 | 468s, 584w |
| 2,3,6-Trimethylnaphthalene | 72 | 409w, 503s, 600w |
| 9,9'-Bifluorene | 0 | 715w |
| 3-Bromofluorene | 5 | 367w, 378w, 403s, 920s |
| 9-Bromofluorene | 0 | 391w, 403s, 474s, 583w |
| 9,9-Dibromofluorene | 5-1/2 | 387w, 404s, 489w, 585w, 845w, 886s |
| 9-Ethylfluorene | 1-1/2 | 402s, 519s |
| 9-Fluorenone | 1 | 401s, 520w, 630w, 860w, 904s |
| 2-Fluorenol | 0 | 388w, 403w, 825s |
| 3-Fluorenol | 5 | 404w |
| 9-Fluorenol | 1 | 401w, 479w, 642w |
| 2-Methylfluorene | 5 | 451w, 531s |
| 9-Methylfluorene | 1 | 403s, 585s |

s = strong
w = weak

102
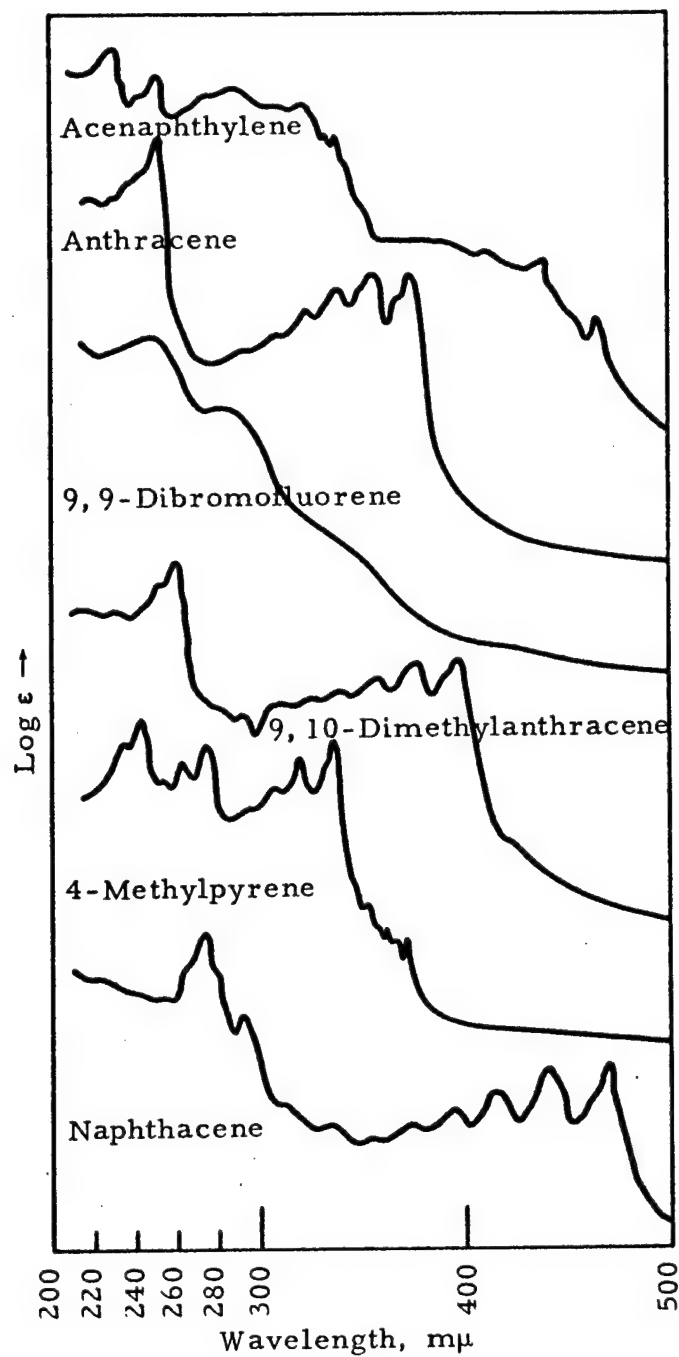
Figure 45. Ultraviolet Spectra of Various
Aromatics in Cyclohexane

N-4490

103
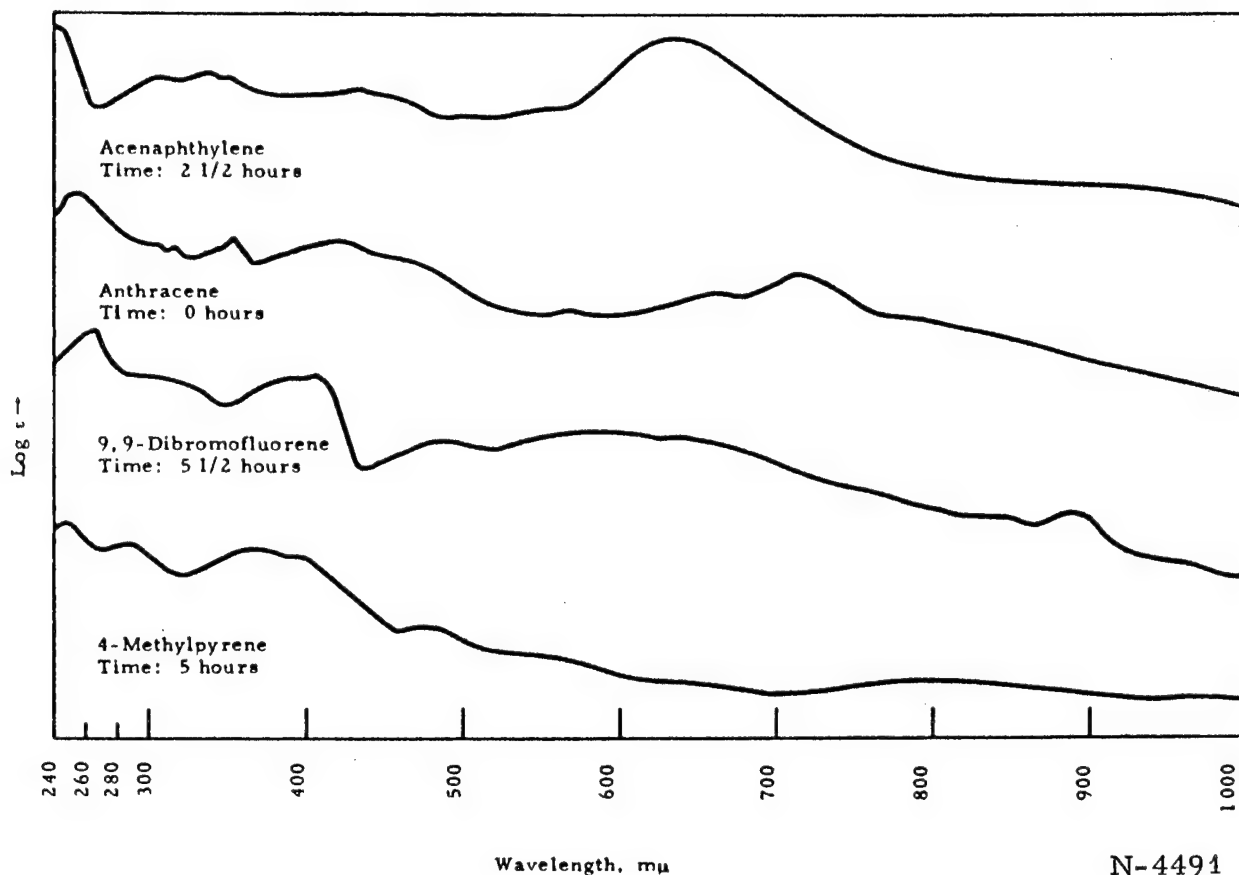
Figure 46. Ultraviolet and Visible Spectra of Various
Aromatics in Concentrated Sulfuric Acid

N-4491

the $H_2SO_4$ spectra of two aromatics. The changes can be interpreted in terms of the aforementioned equation. During the initial stages of solution, the spectral transformations appear reversible. Dilution of the concentrated $H_2SO_4$ solution with water results in reprecipitation of the original aromatic material. With continued time, additional irreversible reactions of oxidation and sulfonation transpire.

### c. UV-Visible Spectra of Hexamethylbenzene in $H_2SO_4$ and $SbCl_5$

UV-visible spectra have been obtained for hexamethylbenzene (HMB) in 98 per cent $H_2SO_4$ and for HMB + $SbCl_5$ in $CH_2Cl_2$. These systems are of interest from the standpoint of ESR investigations which are discussed in a previous section. The UV-visible spectra are given in Figure 48.
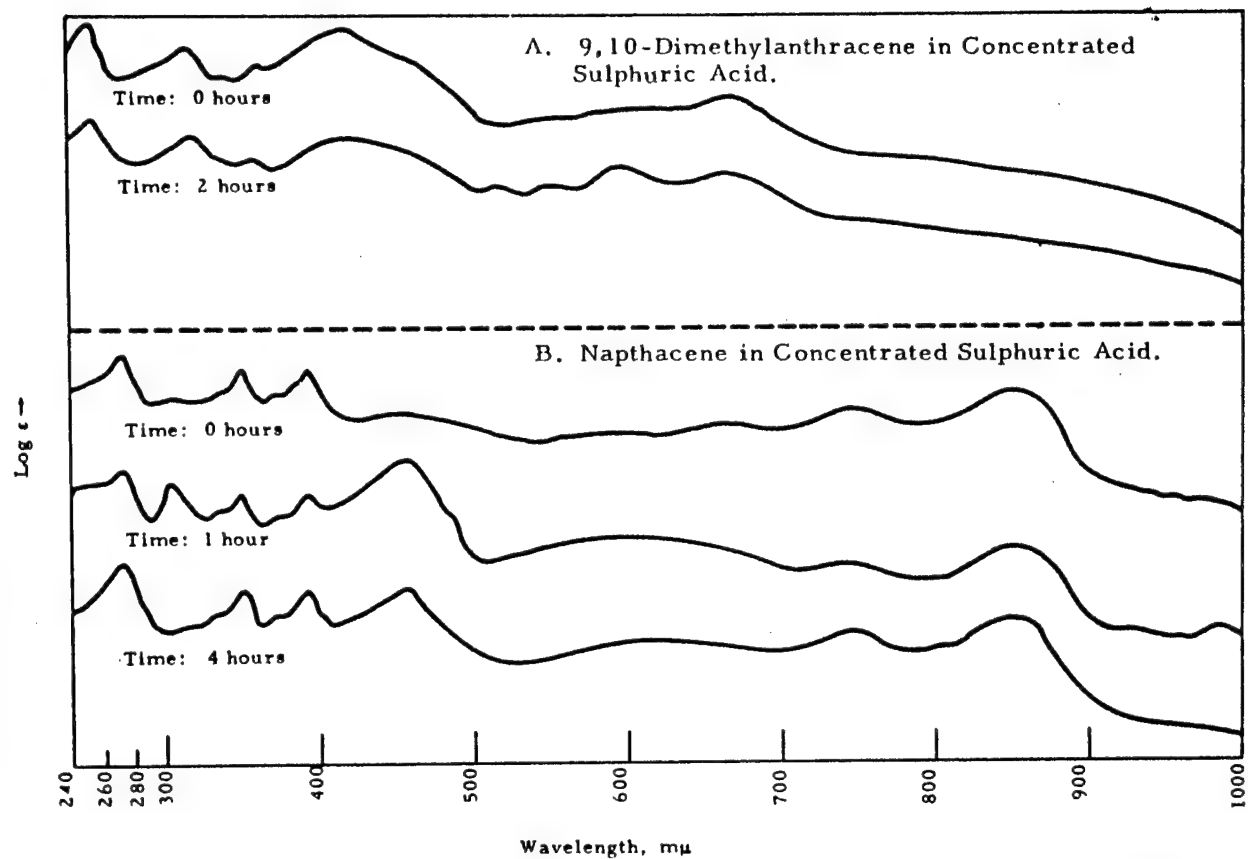
Figure 47. Ultraviolet and Visible Spectra of 9, 10-
Dimethylanthracene and Naphthacene
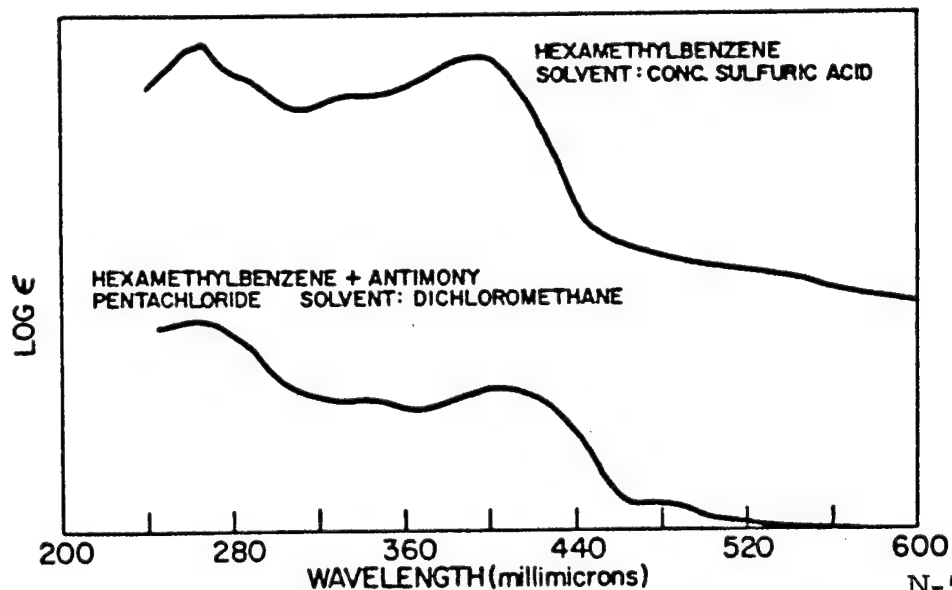


N-5038

Figure 48. UV-Visible Spectra of Hexamethyl-
benzene in Oxidizing Media

105

### 3.1.8.4. Discussion

#### a. Substituent Effects on Ultraviolet Spectra of Polynuclear Aromatics

All substituents on the ring in both anthracene and pyrene are seen to shift the "p"-band to longer wavelengths. The magnitude of this effect appears to be related to the increased resonance stabilization by the substituent group. This effect is also additive as evidenced by the di-substituted anthracene derivatives where the change in wavelength is approximately twice that of the corresponding mono-substituted material. Substituents have also been shown to increase the thermal reactivity of polynuclear aromatic systems.[1,2]

#### b. Spectra of Substituted Anthracenes in $H_2SO_4$

The behavior of nearly all the anthracene derivatives in concentrated $H_2SO_4$ is qualitatively similar. On dissolution, an intense band between 410 and 500 mμ develops immediately. With time, usually three or four characteristic bands between 530 and 750 mμ develop as the first formed band diminishes.

This behavior can be attributed to the initial formation of a carbonium ion species with subsequent oxidation to the radical-ion.
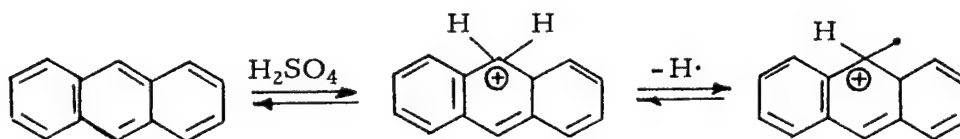


The stability of these ionic species is influenced by the substituent. Substitution in the 9,10-positions (the most reactive ring sites) stabilizes these intermediates from irreversible reaction by the $H_2SO_4$ solvent. For example, the spectrum of the anthracene radical-ion persists for only one hour in $H_2SO_4$, whereas that of 9,10-diphenylanthracene persists for several days.

#### c. Spectra of Substituted Pyrenes in $H_2SO_4$

All of the pyrene derivatives included in Table 26 react similarly in $H_2SO_4$. A band between 425 and 475 mμ is observed immediately on dissolution. This band can be assigned to an initially formed protonated ion. Pyrene has been shown to exhibit an absorption at 450 mμ in a protonating, nonoxidizing medium.[40] With increased time, bands at longer wavelengths, 500 to 800 mμ, develop. These can be attributed to radical ion species.

106

## d. Spectra of Fluorene Derivatives in $H_2SO_4$

The behavior of fluorene derivatives in $H_2SO_4$ is of interest since
the fluorene ring system is a nonalternant aromatic. Formation
of radical ions is expected to be more difficult for fluorene than for the
alternant aromatics. Fluorene itself does not react with $H_2SO_4$; however,
a variety of substituted fluorenes do. These substituents apparently in-
crease the stability of the ionic species. The wavelengths of the newly
formed absorption bands for such ring systems are shown in Table 26.
All the compounds exhibit absorption in the vicinity of 400 mμ which may
be indicative of a carbonium ion entity. It is not yet certain that the
bands at longer wavelength are those of a radical ion. ESR measure-
ments are expected to clarify this point. Radical ions of the fluorene
type would be of extreme interest since accurate electron density mea-
surements could be derived for such entities.

## e. Spectra of Miscellaneous Aromatics in $H_2SO_4$

### Acenaphthylene

Acenaphthylene gives rise to an intense blue-green solution
in $H_2SO_4$ which results in a single broad absorption band at
625 mμ. It has not been possible to observe a NMR spectrum for this
solution so this intermediate is believed to possess radical character. ESR
measurements are planned for this system.

### Naphthacene

Naphthacene provides an excellent example of the protona-
tion, oxidation sequence in $H_2SO_4$. The series of spectra in
Figure 47 shows the initial formation of bands at 458 and 600 mμ which
can be assigned to a simple carbonium ion. With time, these decrease
in intensity while additional bands at longer wavelengths resulting from
a radical-ion species increase.

### 2, 3, 6, -Trimethylnaphthalene

This compound dissolves in $H_2SO_4$ very slowly to form a high-
ly colored solution. 2, 3, 6-Trimethylnaphthalene has been
found to protonate to yield a nonradical ion without subsequent oxidation.

## f. Hexamethylbenzene (HMB) in $H_2SO_4$ and $SbCl_5-CH_2Cl_2$

The spectra shown in Figure 48 demonstrate that identical radical
and ionic species are formed with HMB in both media. This re-
sult is consistent with ESR studies discussed in an earlier section.

107

## 3.2. Bench-Scale Investigations

While previous bench-scale effort[43] has centered around pre-
paring low thermal expansion materials for applications where thermal
shock resistance is important, there is a definite need for a graphite with
high-temperature oxidation resistance. For applications of this type, con-
siderable attention has been given to protecting graphite by coating with
oxidation resistant materials.

In successful applications of coatings to graphite, it is desirable
to have a close match between the thermal expansions of the substrate and
the coating. Where there is a large mismatch, the coating may crack
from thermal cycling. In addition, the anisotropy of most graphites
causes thermal expansion differences within the substrates themselves.

As reported previously,[44] grade RVC graphite has been devel-
oped as a successful substrate for silicon carbide coatings. Grade RVC
has an isotropic* thermal expansion closely matching that of silicon car-
bide.

Various "use conditions" require the utilization of coatings other
than silicon carbide in conjunction with graphite substrates. These coat-
ings have thermal expansions considerably higher than that of silicon car-
bide. Niobium carbide has been selected for comparison in this inves-
tigation because of its comparatively high thermal expansion coefficient
among the metallic carbides. Isotropic graphite substrates having thermal
expansions greater than that of grade RVC are required for use with these
coatings. Two methods of producing the high thermal expansion coke re-
quired for production of these graphites have been investigated to date.
These are: (a) seeding of coker charge stocks with finely divided carbon-
aceous materials; and (b) coking of air-blown charge stocks.

## 3.2.1. Seeding Experiments

Raw cokes are formed through a polymerization reaction in which
relatively small molecules combine to form larger molecules under given
conditions of time, temperature, and pressure. If the arrangement of the
carbon atoms (crystallites) approaches that of a graphite lattice, the coke
is said to be well ordered and exhibits a high degree of anisotropy in ther-
mal expansion. In the seeding process, a finely divided carbonaceous
material which interferes with the growth of the well-ordered crystallites,
is added to the coker charge stock. The fabricated graphite billets then
exhibit relatively high** and isotropic thermal expansions.

The seeded cokes were processed either by coking in a pressure
autoclave at a pressure of 50 lbs./in.$^2$ gauge, or by coking in beakers at
·atmospheric pressure; and then the cokes were calcined to 1000°C and
mixed with coal tar pitch. Extruded rods, $\frac{5}{8}$ inch in diameter by 6 inches

---

* Approximately Equal with- and across-grain values
** 3 to 6 x $10^{-6}$/°C near room temperature

in length, and molded billets, 3 inches in diameter by 3 inches in length, were formed, baked, and graphitized.  Physical property measurements were made on samples obtained from the graphitized material.

### 3.2.1.1.  Rubber and Ink Blacks as Seed Materials

Work with high thermal expansion cokes had indicated that graphitized molded billets processed from a coke containing approximately 15 weight per cent Mogul-A carbon black and 85 weight per cent vacuum residuum exhibited with-grain and across-grain thermal expansion values (30-100°C) of 4.79 and 4.72 x $10^{-6}$/°C, respectively.  These values decreased as the amount of carbon black was increased.  Coked vacuum residuum which was not seeded had with- and across-grain thermal expansions of 1.82 and 2.62 x $10^{-6}$/°C, respectively.  When thermatomic black was added to gilsonite selects, a solid asphaltic hydrocarbon, the thermal expansions of the resulting billets were lower than the values obtained from billets produced from nonseeded gilsonite cokes.

### 3.2.1.1.1.  Vacuum Residuum Charge Stock

Work continued under the present contract has resulted in isotropic high thermal expansion materials.  These materials were produced from a vacuum residuum coker charge stock seeded with rubber and ink carbon blacks.  These blacks are formed by the partial combustion or thermal decomposition of natural gas or liquid petroleum fractions, and are available in a wide range of particle sizes. (Property data of the carbon blacks are shown in Table 27.)  Seeding vacuum residuum with blacks of smaller particle diameter, greater surface area, and higher content of chemisorbed oxygen results in an increase in thermal expansion of the graphitized billets, as shown in Table 27.  With the higher surface area blacks, the thermal expansion increases with increasing amounts of black until a maximum is reached beyond which thermal expansion gradually decreases.  Figure 49 shows this effect for three blacks used to seed vacuum residuum.

The use of Carbolac-1, one of the smallest diameter, largest surface area carbon blacks commerically available, as a seed for vacuum residuum resulted in the highest thermal expansion.

### 3.2.1.1.2.  Gilsonite Charge Stock

Gilsonite selects is a source of high thermal expansion coke. Graphitized molded billets made from this coke have with-grain and across-grain thermal expansion values (30-100°C) of 5.19 and 5.15 x $10^{-6}$/°C, respectively.  The use of Mogul-A carbon black as a seed was found to increase the thermal expansion values slightly (Table 28).

High volume shrinkages (10 to 15 per cent) which occur during the graphitization of billets processed using calcined high thermal expansion cokes make the fabrication of large-size graphite articles difficult.  Graphitization of the filler ingredient prior to extrusion or molding reduces this

Table 27. Comparison of Thermal Expansion Characteristics and Carbon Black Properties for Cokes Produced by the Addition of Carbon Blacks to Vacuum Residuum Charge Stock

| Calculated Calcined Coke Composition | Extruded Rod Thermal Expansion* $10^{-6}/°C$ (30–100°C) W.G.** | Carbon Black Properties | | | | |
| --- | --- | --- | --- | --- | --- | --- |
| | | Process | Type | Particle Diameter, mμ | Surface Area sq. meters/g | Chemisorbed Oxygen Content |
| 82.1 wt. % Vacuum Residuum<br>17.9 wt. % Elftex-8 | 4.28 | Oil Furnace | Rubber (High Absorption) | 29 | 85 | 1.0 |
| 84.1 wt. % Vacuum Residuum<br>15.9 wt. % ELF-6 | 4.62 | Channel | Rubber (Easy Processing) | 29 | 105 | 1.6 |
| 84.8 wt. % Vacuum Residuum<br>15.2 wt. % Mogul-A | 4.80 | Channel | Color and Ink (Long Flow) | 28 | 295 | 8.7 |
| 88.0 wt. % Vacuum Residuum<br>12.0 wt. % Carbolac-2 | 4.84 | Channel | Color and Ink (High Color) | 12 | 850 | 11.2 |
| 91.4 wt. % Vacuum Residuum<br>8.6 wt. % Carbolac-1 | 5.07 | Channel | Color and Ink (High Color) | 9 | 950 | >11.2 |

* Thermal expansion values measured on graphitized billets.

** W.G. = With Grain
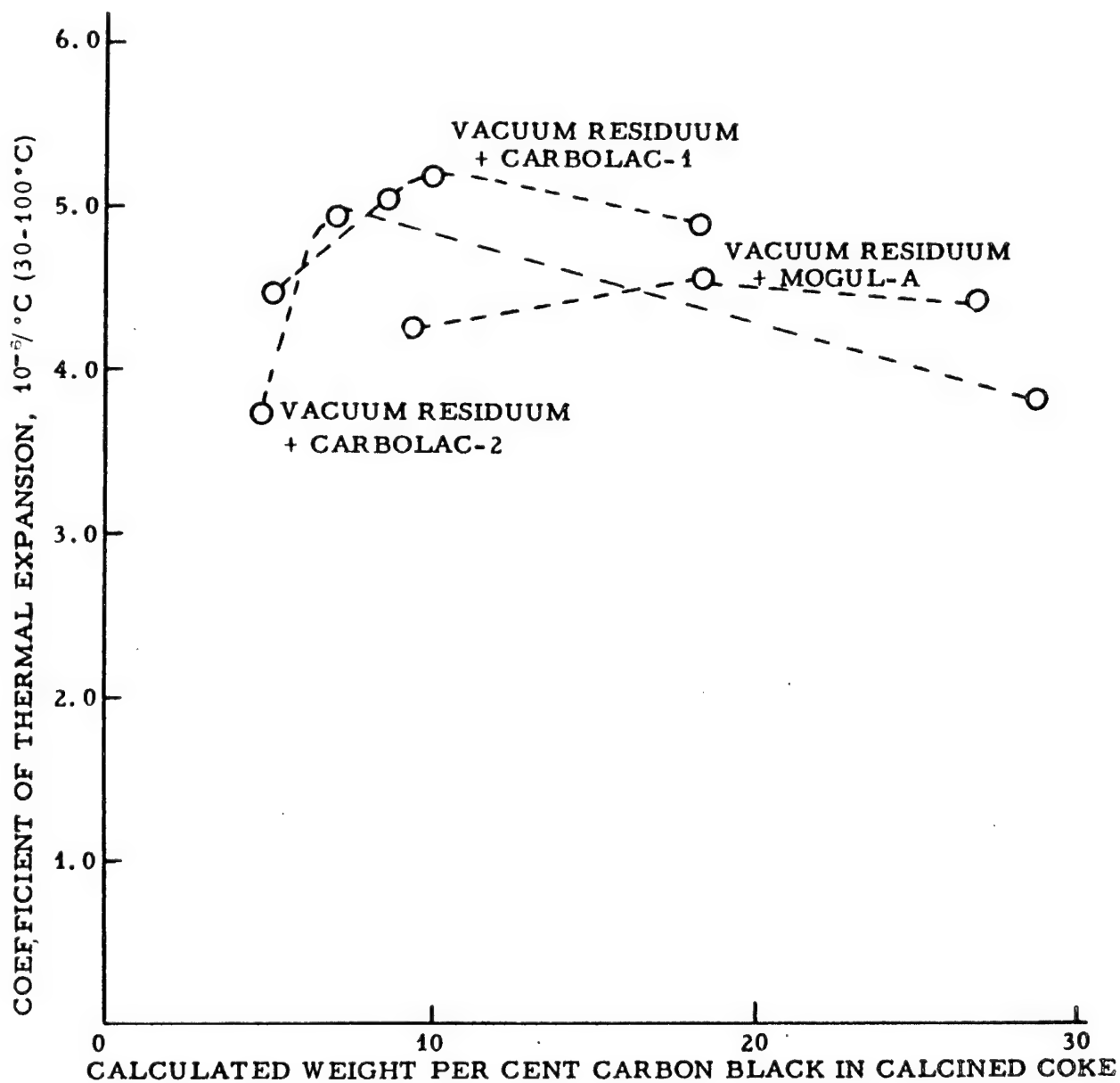
Figure 49. Coefficient of Thermal Expansion (30-100°C)
Versus Carbon Black Concentration in Cal-
cined Coke

L-865

111

shrinkage. The effects of the use of graphitized filler material on graphitized billet properties have been studied. Table 28 presents property data for graphitized molded billets using filler materials calcined to 1000 °C or graphitized at 2800°C. A drop in the 30 to 100°C thermal expansion and shrinkage during graphitization resulted from the use of graphitized filler. The high-temperature thermal expansion did not suffer drastically from the use of the graphitized filler but remained close to that of niobium carbide (Figure 50).

Table 28. Processing and Property Data of Molded Graphite Billets, Gilsonite and Gilsonite-Mogul-A Seeded Coke

| Run No. | 44 | 48 | 48A | 48B |
|---|---|---|---|---|
| Coking Equipment | Autoclave | Autoclave | Pot Furnace | Pot Furnace |
| Pressure, lbs./in.$^2$ gauge | 50 | 50 | atm. | atm. |
| Calculated Coke Composition | 100% Gilsonite Selects | 87 wt. % Gilsonite Selects 13 wt. % Mogul-A Carbon Black | | |
| Filler Material Heat-Treatment Temperature | 1000°C | 1000°C | 1000°C | 2800°C |
| Bulk Density, g/cc | | | | |
| Green | 1.70 | 1.59 | 1.52 | 1.67 |
| Baked | 1.55 | 1.42 | 1.48 | 1.60 |
| Graphitized | 1.67 | 1.60 | 1.57 | 1.57 |
| Per Cent Weight Loss Bake to Graph. | 5.1 | 5.2 | 8.0 | 2.0 |
| Per Cent Volume Shrinkage Bake to Graph. | 12.1 | 16.5 | 13.6 | 2.1 |
| Thermal Expansion, $10^{-6}$/°C (30-100°C) | | | | |
| With Grain | 5.19 | 5.46 | 5.22 | 4.35 |
| Across Grain | 5.15 | 5.44 | 5.26 | 4.41 |
| Specific Resistance, $10^{-4}$ Ω-cm | | | | |
| With Grain | 10.39 | 14.15 | 18.84 | 18.13 |
| Across Grain | 10.66 | - | 18.84 | 18.42 |
| Flexural Strength, lbs./in.$^2$ | | | | |
| With Grain | 3460 | 3390 | 3250 | 1740 |
| Across Grain | 2850 | 2580 | 3680 | 1670 |

48A - PROCESSED USING 87 WT. %
GILSONITE, 13 WT. % MOGUL-A
BLACK COKE; CALCINED TO
1000°C PRIOR TO USE

48B - PROCESSED USING SAME BASE
MATERIAL, BUT GRAPHITIZED
TO 2800°C PRIOR TO USE

O - NbC
■ - 48A (W.G.)
▲ - 48A (A.G.)
□ - 48B (W.G.)
△ - 48B (A.G.)
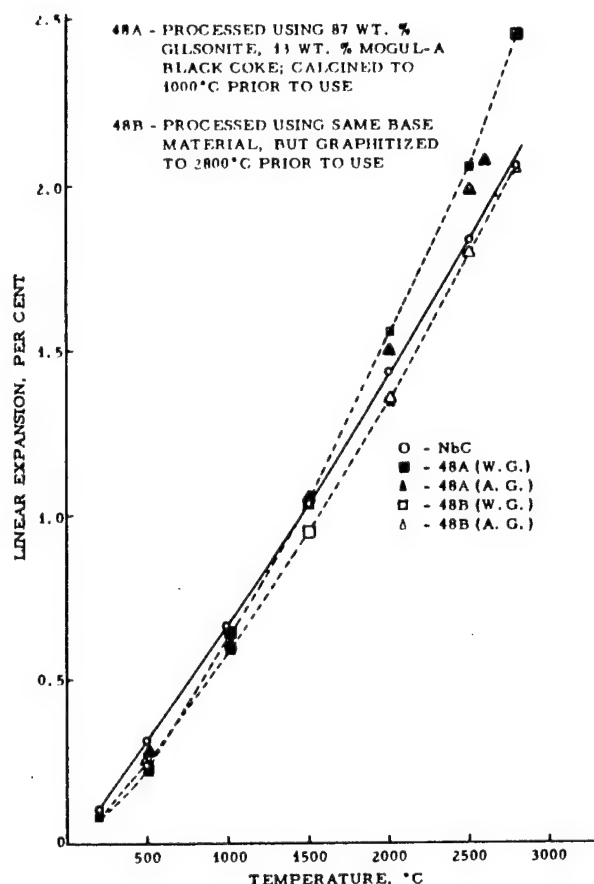
L-163

Figure 50. High-Temperature Thermal Expansion Characteristics of Graphitized Molded Billets Produced from Carbon-Seeded Cokes, as Compared to Niobium Carbide

### 3.2.1.1.3. Thermal Tar and Slurry Oil Charge Stocks

Thermal tar and slurry oil coking charge stocks, known to produce cokes having low thermal expansion values in the with-grain direction, have been seeded with Carbolac-1. The properties of extruded and molded graphitized billets processed with beaker-coked materials of the above types are presented in Table 29. The results indicate that high thermal expansion levels may be obtained by seeding coking charge stocks which normally yield either low or moderate thermal expansion cokes.

### 3.2.1.2. Acetylene Black as a Seed Material

Recent experiments have included the investigation of acetylene black as a seed for coking charge stocks. Cokes seeded with acetylene black have produced graphitized billets with the highest level of thermal expansion observed to date. Acetylene black has an average particle diameter of 50 mμ and a surface area of approximately 64 square meters per gram which is considerably larger and smaller, respectively, than many of the channel blacks whose effectiveness has already been discussed.

113

Table 29. Comparative Thermal Expansion Data,
Seeded and Nonseeded Thermal Tar

| Calculated Composition of Calcined Beaker Coke | Extruded Billet Thermal Expansion, $10^{-6}/°C$ (30-100°C) | Molded Billet Thermal Expansion, $10^{-6}/°C$ (30-100°C) | |
|---|---|---|---|
| | W. G. | W. G. | A. G. |
| 100 wt. % Slurry Oil | 0.67 | - | - |
| 81 wt. % Slurry Oil  19 wt. % Carbolac-1 | 4.50 | 4.40 | 4.40 |
| 100 wt. % Thermal Tar | 0.47 | - | - |
| 82 wt. % Thermal Tar  18 wt. % Carbolac-1 | 4.82 | 4.83 | 4.83 |

The reason for this anamolous behavior is not known but a possible explanation is a free radical reaction in the early stages of the thermal history, initiated by surface-adsorbed hydrogen, yielding a cross-linked structure. Acetylene black may contain considerable hydrogen adsorbed during the hydrogen quench used in its preparation. Other carbon blacks are prepared using either an air or water quench.

The results of seeding vacuum residuum with acetylene black are shown in Table 30. Thermal expansion values appear to remain high in the 11- to 23-per cent black concentration range. Flexural strength values also remain high in this range.

For successful large-size billet fabrication, graphitization of the filler material would be necessary; however, high-temperature thermal expansion may suffer. Figure 51 shows thermal expansion data for samples from graphitized billets which were produced using 1000°C calcined and 3000°C graphitized acetylene black-seeded vacuum residuum materials. As with gilsonite, the thermal expansion of the billets made from the graphitized filler did not suffer drastically but in fact, above 1500°C, was higher than niobium carbide.

Additional experiments indicate that acetylene black is an effective seed for atmospheric residuum and thermal tar coker charge stocks. Thermal tar normally yields a low thermal expansion coke; atmospheric residuum yields a coke which has a thermal expansion approximately 30 per cent lower than vacuum residuum. Figure 52 shows the thermal expansion versus black concentration in calcined cokes from the three charge stocks. Regardless of the type of charge stock, graphitized billet thermal expansion values are comparable for similar acetylene black concentrations.

The desirable physical and thermal properties of graphite produced from the small-scale trial of acetylene black seeded cokes has

114

Table 30. Graphitized Billet Data for Seeded and Control Coking Charges; Seeding of Coking Charge Stocks by Acetylene Black

| Composition of Charge Stock | Calculated Composition of Calcined Coke | Method of Coking | Extruded ⅛-inch Diameter Graphitized Billet Data | | Molded 3-Inch Diameter Graphitized Billet Data | | | | | |
|---|---|---|---|---|---|---|---|---|---|---|
| | | | Specific Resistance Ω-cm x $10^{-4}$ | Thermal Expansion (30-100°C) $10^{-6}$/°C | Specific Resistance Ω-cm x $10^{-4}$ | | Thermal Expansion (30-100°C) $10^{-6}$/°C | | Flexural Strength lbs./in.$^2$ | |
| | | | W.G. | W.G. | W.G. | A.G. | W.G. | A.G. | W.G. | A.G. |
| 98.8 wt. % Vacuum Residuum 1.2 wt. % Acetylene Black | 93.2 wt. % Vacuum Residuum 6.8 wt. % Acetylene Black | Beaker (Atmospheric Pressure) | 8.77 | 4.33 | - | - | - | - | - | - |
| 97.6 wt. % Vacuum Residuum 2.4 wt. % Acetylene Black | 89.1 wt. % Vacuum Residuum 10.9 wt. % Acetylene Black | " | 14.22 | 5.43 | - | - | - | - | - | - |
| 97.0 wt. % Vacuum Residuum 3.0 wt. % Acetylene Black | 87.0 wt. % Vacuum Residuum 13.0 wt. % Acetylene Black | " | 15.39 | 5.81 | - | - | - | - | - | - |
| 96.4 wt. % Vacuum Residuum 3.6 wt. % Acetylene Black | 85.0 wt. % Vacuum Residuum 15.0 wt. % Acetylene Black | " | 21.10 | 5.47 | 18.73 | 20.28 | 5.50 | 5.43 | 3491 | 2928 |
| 95.9 wt. % Vacuum Residuum 4.1 wt. % Acetylene Black | 81.2 wt. % Vacuum Residuum 18.8 wt. % Acetylene Black | " | 20.64 | 5.51 | 17.88 | 19.19 | 5.39 | 5.53 | 3974 | 2887 |
| 94.3 wt. % Vacuum Residuum 5.7 wt. % Acetylene Black | 76.4 wt. % Vacuum Residuum 23.6 wt. % Acetylene Black | " | 19.53 | 5.31 | 19.40 | 20.34 | 5.36 | 5.32 | 4269 | 3367 |
| 96.9 wt. % Vacuum Residuum 3.1 wt. % Acetylene Black | 88.7 wt. % Vacuum Residuum 11.3 wt. % Acetylene Black | Pressure Autoclave (50 lbs./in.² g) | 20.70 | 5.28 | 21.49 | 21.75 | 5.48 | 5.43 | 3581 | 2726 |
| 93.3 wt. % Vacuum Residuum 6.7 wt. % Acetylene Black | 82.2 wt. % Vacuum Residuum 17.8 wt. % Acetylene Black | " | 18.84 | 5.58 | 19.30 | 22.54 | 5.57 | 5.68 | 3026 | 2475 |
| 94.3 wt. % Vacuum Residuum 5.7 wt. % Acetylene Black | 81.5 wt. % Vacuum Residuum 18.5 wt. % Acetylene Black | " | 24.60 | 5.46 | 19.62 | 20.63 | 5.64 | 5.56 | 3818 | 3657 |
| 100 wt. % Vacuum Residuum | 100 wt. % Vacuum Residuum | " | 7.25 | 1.28 | 11.34 | 15.02 | 2.06 | 3.60 | 1386 | 1051 |

Figure 51. High-Temperature Thermal Expansion Characteristics of With-Grain Samples from Extruded Billets Produced from Acetylene Black-Seeded Vacuum Residuum Materials Produced in Pressure Autoclave, as Compared to Niobium Carbide
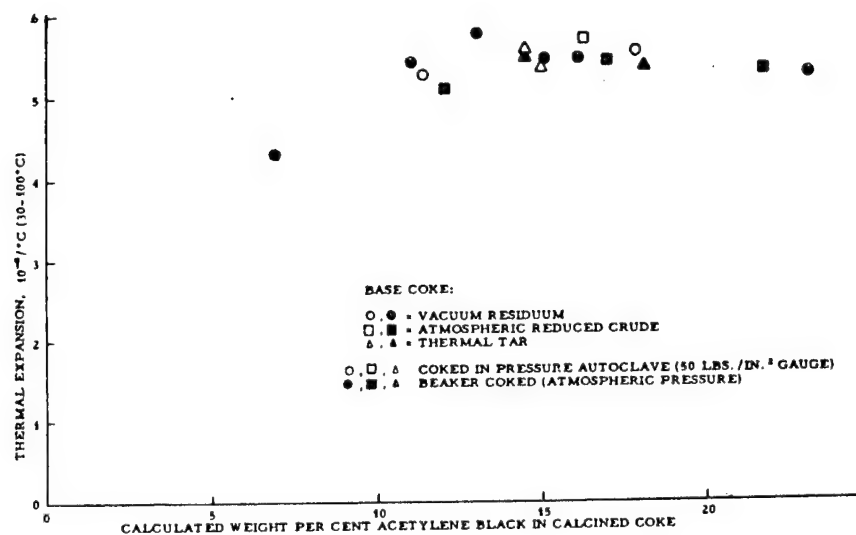


Figure 52. Thermal Expansion Versus Per Cent Acetylene Black in Calcined Coke, Relationships for With-Grain Samples from Graphitized Extruded Billets

116

prompted the investigation of the use of this black in experimental coker trials. For continuous operation, a uniform dispersion, free of agglomerates, is required. To minimize pumping difficulties and to prevent excessively high furnace pressures, a dispersion having viscosity characteristics similar to vacuum residuum is desired. Compared to channel or gas furnace blacks, acetylene black is very difficult to disperse in coking charge stocks. A final choice of charge stock for experimental delayed coker trials has not yet been made pending results of bench-scale dispersion trials. With vacuum residuum, lumpy, high-viscosity dispersions result even at low black concentrations. Low-viscosity materials of low coking value, such as kerosene, diesel oil and gas oils are being evaluated as diluents for vacuum residuum, atmospheric residuum, or other charge stocks to promote wetting of acetylene black and to reduce the viscosity of the dispersions. Bench-scale experiments are under way to determine whether seeded coke characteristics are altered by the use of diluents.

### 3.2.1.3.   Lewis Acids

The known effect of Lewis acids (electron acceptors) such as anhydrous ferric chloride, in the chlorination and subsequent polymerization of simple aromatic hydrocarbons led to an experiment in which a mixture of vacuum residuum and ferric chloride (3.1 w/o) was coked at atmospheric pressure. The graphitized extruded billets had an average with-grain thermal expansion (30 to 100°C) of $3.97 \times 10^{-6}/°C$. Other experiments with ferrous chloride and ferric chloride hydrate are being made to determine if the thermal expansion elevation is due to the catalytic effect or the physical effect of mechanical hindrance of orderly crystallite growth.

### 3.2.1.4.   Graphite and Coke as Seed Material

For applications where thermal shock resistance is considered important, such as rocket nozzle inserts and nose cones, it is desirable to use a material that not only is isotropic but also has low thermal expansion characteristics.

In an effort to produce a graphite meeting these requirements, vacuum residuum and thermal tar have been seeded with low thermal expansion cokes and graphites of various sizings. As shown in Table 31, the goal has not been accomplished. Although the with-grain thermal expansion levels in the extruded billets were increased slightly by seeding, the with-grain and across-grain thermal expansion values from molded billets do not indicate that isotropy has been approached. No further work is planned in this direction.

### 3.2.1.5.   Future Work

Plans for future work include bench-scale investigation of methods of dispersing acetylene black in coker charge stocks in preparation for experimental delayed coker trials. High thermal expansion cokes

117

Table 31. Graphitized Billet Data for Seeded and Control Coking Charges;
Seeding of Coker Charge Stocks with Coke and Graphite Materials

| Calculated Composition of Calcined Beaker Coke | Extruded Billet Thermal Expansion $10^{-6}/°C$ (30-100°C) | Molded Billet Thermal Expansion $10^{-6}/°C$ (30-100°C) | |
|---|---|---|---|
| | W. G. | W. G. | A. G. |
| 43.3 wt. % Vacuum Residuum 56.7 wt. % Graphite Milled to 74μ Maximum Particle Diameter | 2.04 | 2.62 | 3.41 |
| 66.0 wt. % Vacuum Residuum 34.0 wt. % Graphite Milled to 44μ Maximum Particle Diameter | 2.19 | 2.77 | 3.92 |
| 63.8 wt. % Vacuum Residuum 34.0 wt. % Coke Milled to 10μ Maximum Particle Diameter | 2.43 | 3.14 | 3.72 |
| 62.0 wt. % Thermal Tar 38.0 wt. % Graphite Milled to Approximately 150μ Average Diameter | 1.04 | 2.20 | 3.56 |
| 100.0 wt. % Vacuum Residuum | 1.31 | 2.06 | 3.60 |
| 100.0 wt. % Thermal Tar | 0.47 | - | - |

produced from these trials will be evaluated by bench-scale coke examination methods.

The high-temperature thermal expansion characteristics of acetylene black seeded materials produced from various charge stocks will be investigated.

Gilsonite materials seeded with acetylene black, in conjunction with various diluents, will be evaluated as possible sources for isotropic graphite materials having high thermal expansion.

3.2.2. Air Blowing of Coker Charge Stocks

It was previously reported that the thermal expansion of graphite stock fabricated from a coked air-blown vacuum residuum sample was greater than for an unblown vacuum residuum processed similarly. The thermal expansion (30 to 100°C) of the reported example increased from 1.3 to 4.3 x $10^{-6}/°C$.

Air blowing of coker charge stocks is thought to produce a reaction which proceeds by changing the oils to resins and the resins to asphaltenes, these reactions occurring simultaneously. If the reaction is allowed to continue, the asphaltenes convert to free carbon. The converted stocks yield space-condensed polymers which lead to highly disordered cokes upon thermal decomposition.

### 3.2.2.1. Laboratory Air-Blowing Experiments

The laboratory pitch still was modified for use in air-blowing experiments. A flowmeter in the air supply line provided accurate metering of the air which was directed into the kettle and up through the impeller blades. This permitted good surface contact of the air with the charge stock. A paramagnetic-type oxygen analyzer allowed continuous monitoring of the product gas and provided a guide to the degree of reaction. Whenever severe exothermic reactions occurred during the air-blowing process, cooling water was circulated around the kettle, and nitrogen replaced the air flow. At the end of the run, the system was flushed with nitrogen, allowed to cool to about the lowest temperature at which the product would still flow and the material drained into a receiving drum.

Experiments in air blowing vacuum residuum resulted in an apparent upper limit of thermal expansion (30 to 100°C) measured with the grain on graphitized extruded and molded billets of approximately 5.5 and 6.0 x $10^{-6}/°C$, respectively. The higher with-grain thermal expansion values are typical for molded as opposed to extruded stock.

A relationship (Figures 53 and 54) was noted between the asphaltene content (n-pentane insoluble) of the various coker charge stocks, and the resultant thermal expansion for the fabricated graphite article. However, as the asphaltenes of the air-blown vacuum residuum approached 50 weight per cent, the increase in the rate of thermal expansion diminished and at the 55 to 60 per cent level an actual decrease in thermal expansion had occurred. Other feed stock correlations were possible as illustrated by the melting point versus asphaltene content and standard penetration[45] for air-blown vacuum residuum coker charge stocks in Figure 55.

A comparison of two very high thermal expansion graphites is presented in Table 32. The low product yield in Experiment No. 60 was caused by the removal of the column packing in the still which provided an easier volatile path and by a higher blowing temperature. Although billets made from Experiment No. 60 had slight increases in thermal expansion over Experiment No. 49, bake-to-graphite volume shrinkage increased from 9.2 to 14.8 per cent, and flexural strength (across grain) decreased from 2780 to 2200 lbs./in.$^2$. The high-temperature thermal expansion characteristics of graphite billets produced from Experiments Nos. 49 and 60 are compared to those of niobium carbide in Figure 56. The graphite per cent thermal expansion for the complete temperature range of Experiment No. 60 and for most of the range of Experiment No. 49 is higher than niobium carbide. Therefore, both graphites may be suitable substrates for niobium carbide.

119
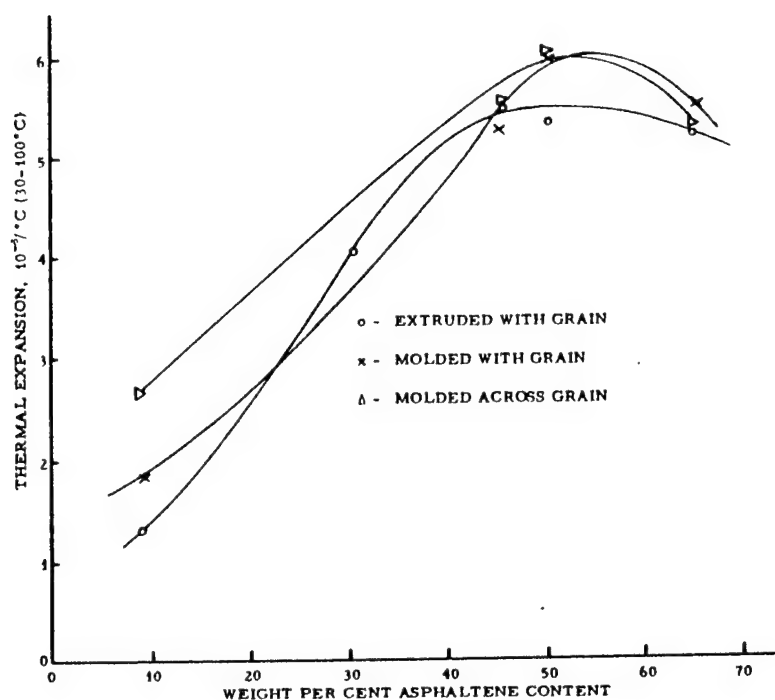
Figure 53. 30-100°C Thermal Expansion of Graphite Articles as a Function of Asphaltene Content in Vacuum Residuum Charge Stock
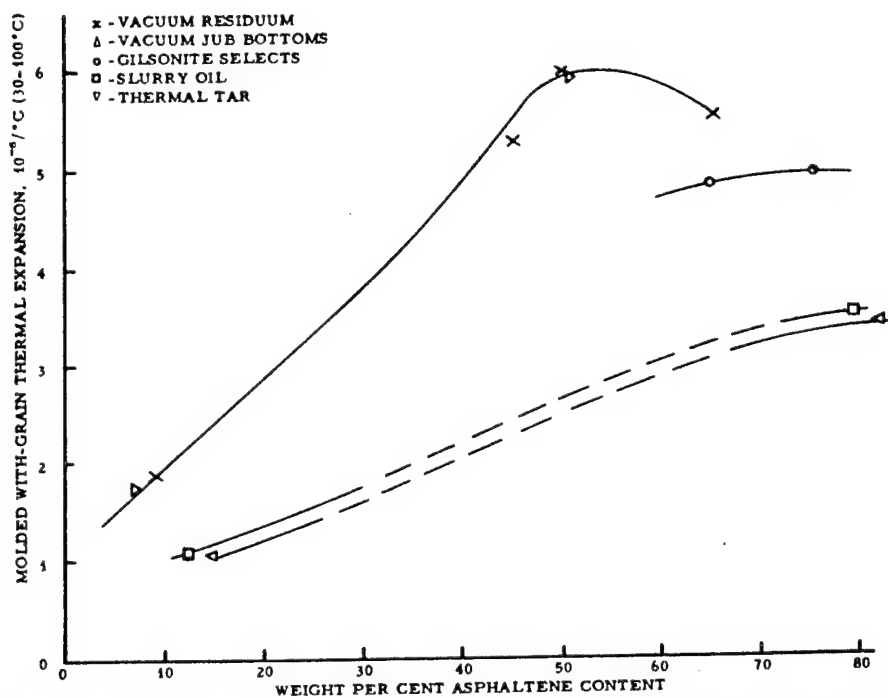


Figure 54. 30-100°C Thermal Expansion of Graphite Articles as a Function of Asphaltene Content in Various Coker Charge Stocks

120
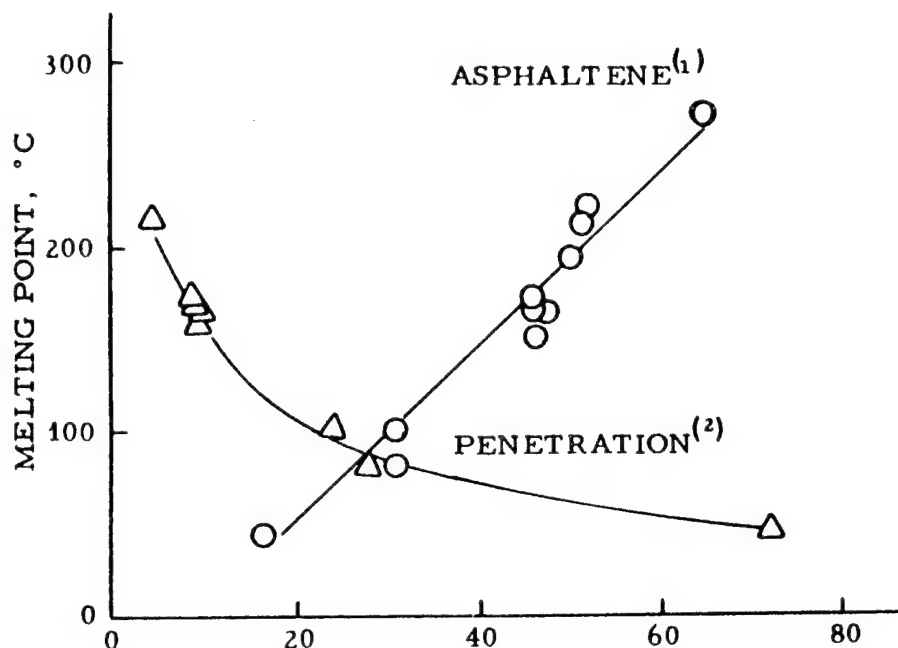
(1)   Asphaltene Content,(Weight Per Cent)
(2)   Penetration, (Comparative Units)[45] 77°F,
         100 g, 5 sec.                                        L-867

Figure 55.   Melting Point as a Function of Asphaltene Content
and Penetration (Air-Blown Vacuum Residuum)

Table 32.   Laboratory-Produced Air-Blown Asphalt Evaluated
as a Source for High Thermal Expansion Graphite

| Experiment No. | 49 | 60 |
|---|---|---|
| Air-Blowing Temperature, °C | 300 | 310 |
| Air-Blowing Yield, wt. % | 80.5 | 32.3 |
| Air-Blown Stock Melting Point, °C | 196 | 226 |
| Air-Blown Stock Asphaltene Content (n-Pentane Insoluble) | 50.1 | 51.5 |
| Thermal Expansion, $10^{-6}$/°C (30-100°C) | | |
| With Grain | 5.99 | 6.22 |
| Across Grain | 6.06 | 6.23 |
| Flexural Strength, lbs./in.$^2$ | | |
| With Grain | 3460 | - |
| Across Grain | 2780 | 2200 |

121
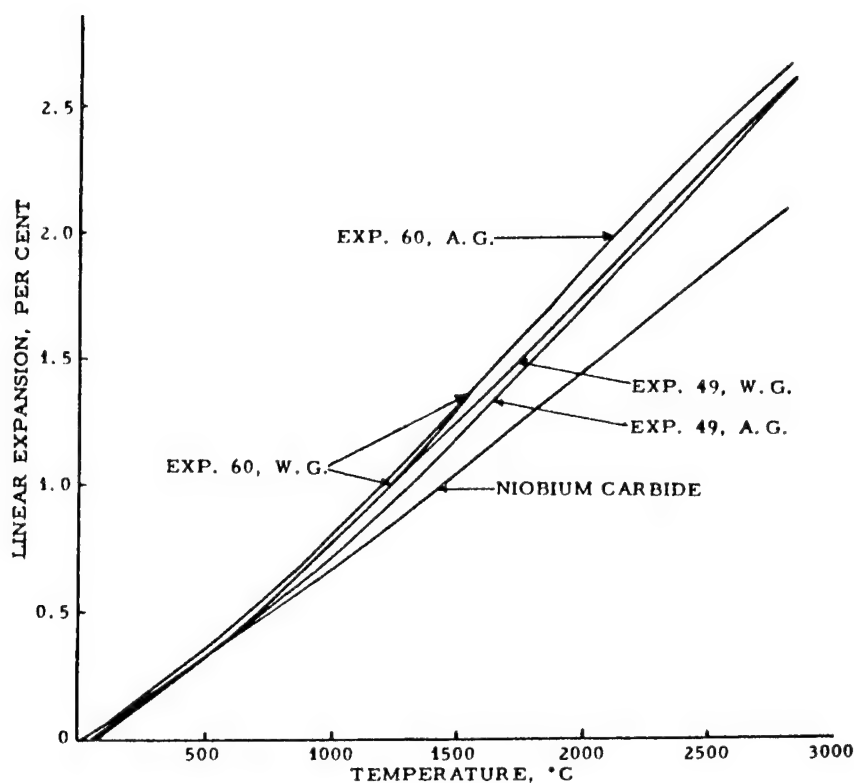
Figure 56.   High-Temperature Thermal Expansion for Graphites
from Two Different Air-Blown Vacuum Residuum
Experiments and Niobium Carbide

## 3.2.2.2.   Commercial Asphalts

Three air-blown asphalts from Trumbull Asphalt Company were
investigated as possible sources for large-scale production of high ther-
mal expansion graphite.   A high-sulfur-source, air-blown residue iden-
tified as A-112, and two low-sulfur-source, air-blown residues, labeled
A-113 and A-114, respectively, were coked as received and processed
into $\frac{5}{8}$-inch diameter graphite billets for thermal expansion (30 to 100°C)
determinations.   To check the feasibility of coking these asphalts in the
experimental coker, either gas oil or diesel oil was used as a diluent and
the product evaluated as above.   The diluents were used in blends to give
viscosities similar to or lower than vacuum residuum.   The results of
this evaluation are presented in Table 33.   With respect to melting point
and asphaltene content, the A-112 material is a poor source for high ther-
mal expansion graphite while A-113 and A-114 show promise.   A reduc-
tion of thermal expansion (30 to 100°C) from 5.08 to 4.57 for A-113 and
4.96 to 4.60 x $10^{-6}$/°C for A-114 resulted from the coking charge dilution
effect.   Other diluents will be evaluated for their effect on graphite ther-
mal expansion.

122

Table 33. Commercial Air-Blown Asphalts Evaluated as a
Source For High Thermal Expansion Graphite

| Code Number | A-112 | A-113 | A-114 |
|---|---|---|---|
| Asphalt Melting Point, °C | 165 | 100 | 128 |
| Asphalt-Asphaltene Content, wt. % | 52.6 | 44.2 | 40.6 |
| Extruded $\frac{5}{8}$-Inch Diameter Graphitized Billet Thermal Expansion, $10^{-6}/°C$ (30-100°C) | | | |
| With Grain | | | |
| Asphalt | 3.72 | 5.08 | 4.96 |
| 7 parts Gas Oil, 3 parts Asphalt | 3.25 | - | - |
| 5 parts Diesel Oil 5 parts Asphalt | - | - | 4.60 |
| 3 parts Diesel Oil, 7 parts Asphalt | - | 4.57 | - |

### 3.2.2.3. Future Work

Future bench-scale effort will study asphaltic crudes and conventional air-blown materials as possible source stocks for producing graphite with unique properties. Air-blowing experiments will evaluate differences in naphthenic and paraffinic virgin stocks and synthetic aromatic stocks for the base raw materials.

### 3.3. Pilot-Scale Coker Experiments

The major effort on raw materials research has centered around batch-scale coking experiments. However, these findings need to be applied to a commercial continuous flow operation in order to realize the separate effects of furnace and coke drum. The following experiments were conducted in $1/100$ scale pilot coker, located on the site of the Marathon Oil Company in Robinson, Illinois. The unit was designed to operate both as a coker (Figure 57) and a thermal cracking unit (Figure 58).

### 3.3.1. Low Thermal Expansion Coke

For applications where thermal shock resistance is necessary, a coke that yields a graphite of low thermal expansion characteristics is considered to be one of the requirements.
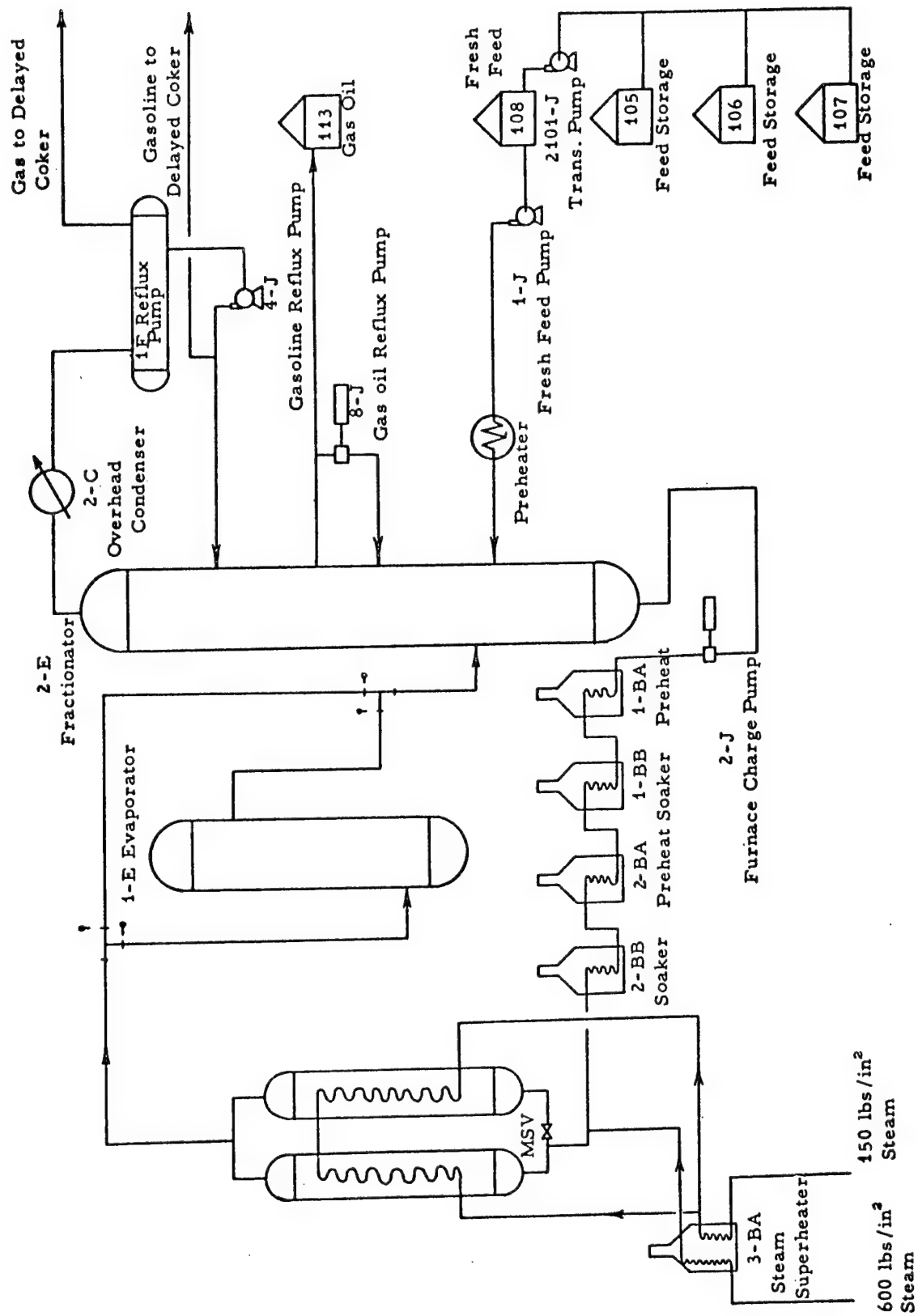
Figure 57. Schematic of Coking Operation, Pilot-Scale Coker

124

L-434
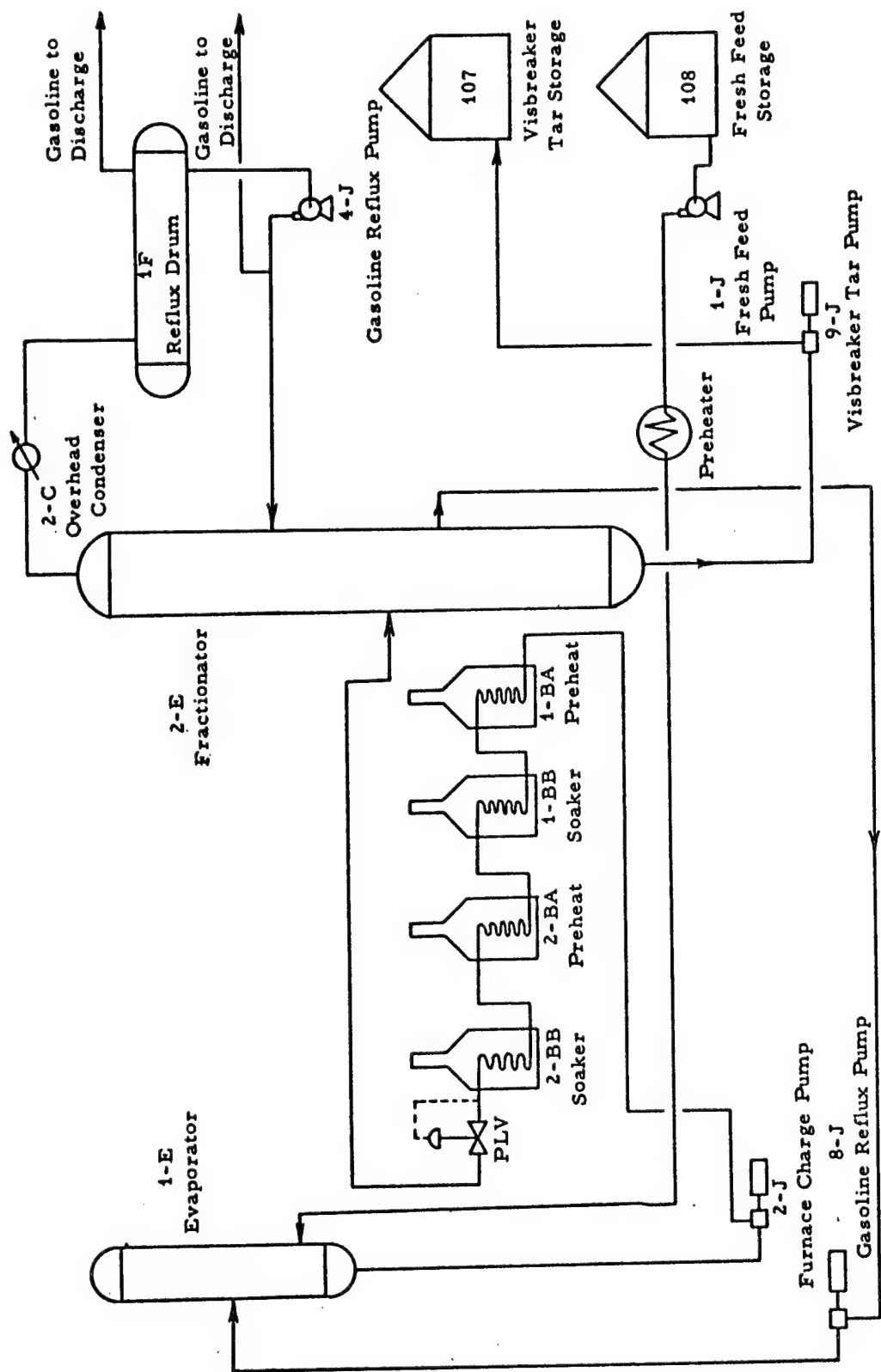
Figure 58. Schematic of Thermal Cracking Operation, Pilot-Scale Coker

L-435

125

Previous bench-scale efforts[43] have indicated that such stock may be prepared through coking of highly aromatic feed stocks or by controlling the time, temperature, and pressure parameters during the cracking and coking operations of a material known to yield a higher thermal expansion coke, e.g., a virgin vacuum residuum.

Pilot coker experiments of a vacuum residuum have indicated a thermal expansion (30 to 100°C) reduction of approximately 0.4 to 0.5 x $10^{-6}$/°C by increasing the coke drum pressure from 50 to 350 lbs./in.² gauge (Table 34). By increasing the residence time at temperature (increasing severity) in the furnace tubes prior to entering the coke drum, a reduction in thermal expansion (30 to 100°C) of 0.4 x $10^{-6}$/°C is realized (Table 34).

Table 34. Effect of Furnace Cracking Severity and Coke Drum Pressure on Thermal Expansion

| Cycle No. | Furnace Temperature, °F | | | | Recycle Ratio | Combined Feed bbls./day | S.V.[1] hr.$^{-1}$ | Drum Pressure lbs./in.² | Extruded Rod, Thermal Expansion $10^{-6}$/°C (30-100 °C) W.G. |
|---|---|---|---|---|---|---|---|---|---|
| | 1BA Outlet | 1BA Outlet | 2BA Outlet | 2BB Outlet | | | | | |
| 6N | 630 | 817 | 935 | 935 | 1.0 | 200 | 18 | 50 | 1.72 |
| 40S | 686 | 879 | 936 | 936 | 1.0 | 100 | 7 | 50 | 1.30 |
| 41S | 679 | 883 | 947 | 947 | 1.0 | 125 | 10 | 50 | 1.29 |
| 31S | 634 | 822 | 935 | 935 | 1.0 | 200 | 18 | 250 | 1.36 |
| 32S | 631 | 816 | 935 | 935 | 1.0 | 200 | 18 | 350 | 1.22 |

[1] Space velocity (indication of cracking severity in furnaces)

$$S.V. = \frac{\text{Combined Feed Rate } (\frac{\text{Volume}}{\text{Time}})}{\text{Furnace Volume above 750°C}} = \frac{1}{\text{Time}} \quad ; \quad \frac{1}{S.V.} = \text{Residence Time above 750°C}$$

Attempts were then made to determine the maximum severity that can be accomplished in the furnace coils with the resultant effect on thermal expansion of the coke. This was accomplished through by-passing the coke drum and operating the unit as a thermal cracker. The thermal tar was collected, characterized, and coked in beakers at atmospheric pressure. The results (Table 35) indicate about the same magnitude of thermal expansion reduction as was achieved by varying furnace schedules and drum pressure during the experimental coking phases.

The most recent work considered the extension of time in the coke drum in addition to longer times at lower temperatures in the furnace coils. The lower temperature necessitated a post-treatment period since there was not enough incipient heat to carry the liquid through the coking cycle. All three experiments (Table 36) had cycle times (before post-treatment) of 36 hours with the last (Cycle No. 51-N) having no post-treatment

126

Table 35. Thermal Cracking Experiments on Vacuum Residuum

| Experiment No. | Furnace Temperatures, °F 1BA Outlet | 1BB Outlet | 2BA Outlet | 2BB Outlet | Recycle Ratio | Combined Feed bbls./day | S.V.[1] hr.$^{-1}$ | Drum Pressure lbs./in.$^2$ | Product Thermal Tar Characterizations[2] Aromatics % | Nonaromatics % | Oxy % | Loss % | M.W.[3] | Beaker Coking[4] Raw Yield % | Extruded Rod, Thermal Expansion 10$^{-5}$/°C (30-100°C) W.G. |
|---|---|---|---|---|---|---|---|---|---|---|---|---|---|---|---|
| 41 | 635 | 707 | 817 | 935 | 0.34 | 150 | 13.2 | 150 | 58.2 | 33.2 | 5.4 | 3.2 | 652 | 28.9 | 1.64 |
| 44 | 725 | 850 | 850 | 850 | 1.00 | 102 | 3.2 | 50 | 42.5 | 53.3 | 3.5 | 1.0 | 656 | 27.5 | 1.68 |
| 45 | 750 | 875 | 875 | 873 | 0.90 | 97 | 3.1 | 50 | 55.5 | 37.8 | 5.0 | 1.9 | 625 | 29.5 | 1.24 |
| 46 | 775 | 900 | 900 | 900 | 0.71 | 87 | 2.9 | 50 | 65.0 | 17.9 | 14.2 | 2.9 | 548 | 36.4 | 1.12 |

[1] See Note on Table 34

[2] Silica Gel Chromatography

[3] Molecular Weight (Vapor Pressure Osmometer)

[4] Firing Schedule, Rush to 350°C, 60°C/hr. to 400°C - 14 hr. hold, 10°C/hr. to 470°C - 10 hr. hold.

Table 36. Effect of Post-Treatment in Coke Drum on Thermal Expansion of Cokes

| Cycle No. | Cycle Hrs. | Furnace Temperatures, °F 1AA Outlet | 1BB Outlet | 2AA Outlet | 2BB Outlet | Re-cycle Ratio | Combined Feed, bbls./day | Drum Pressure, lbs./in.$^2$ | Post-Treatment 1 Furnace Temperatures, °F 1BA Outlet | 1BB Outlet | 2BA Outlet | 2BB Outlet | Time, hrs. | Total Time, hrs. | Extruded Rod, Thermal Expansion With Grain 10$^{-5}$/°C (30-100°C) Top | Bottom | Average |
|---|---|---|---|---|---|---|---|---|---|---|---|---|---|---|---|---|---|
| 49N | 36 | 750 | 875 | 875 | 875 | 1.0 | 99 | 50 | 637 | 711 | 827 | 950 | 9 | 45 | 0.94 | 1.39 | 1.16 |
| 50N | 36 | 725 | 850 | 850 | 850 | 1.8 | 101 | 50 | 635 | 710 | 820 | 930 | 7 | 43 | - | - | 1.32 |
| 51N | 36 | 725 | 875 | 875 | 900 | 1.8 | 99 | 50 | None | None | None | None | 0 | 36 | 1.00 | 204 | 1.52 |

127

but a higher final temperature. The data again showed no reduction in thermal expansion beyond the point achieved by increasing furnace severity and coke drum pressure.

Since a virgin vacuum residuum does not lend itself to operating conditions that would result in a recycle ratio greater than 1:1, a series of experiments was designed using a virgin atmospheric residuum where more recycling is possible. The results (Tables 37 and 38) show a thermal expansion decrease in going from a vacuum residuum at low recycle ratio to an atmospheric residuum at a higher recycle ratio. The atmospheric residuum is also slightly more sensitive to cracking as severity increases (more time at temperature) than the vacuum residuum as measured by thermal expansion changes.

The atmospheric residuum yielded a more uniform raw coke with a higher bulk density than the vacuum residuum. The above data, while showing definite trends on the effect of increased recycle on thermal expansion reduction, have not shown the major effect that was anticipated from this series of experiments.

### 3.3.2. Future Work

The thermal expansion reduction of a virgin stock as shown in Section 3.3.1. does, however, justify further work to achieve an extremely low thermal expansion coke by applying the above experience (long times, low temperature and post-treatment) to the coking of an aromatic stock; e.g., slurry oil or thermal tar. These experiments will also utilize the higher drum pressure available on the pilot coker.

### 3.3.3. High Thermal Expansion Coke

It is intended to produce cokes with high thermal expansion isotropic characteristics. The cokes from carbon-seeded and air-blown stocks will yield graphites of similar thermal expansion properties. They will be made in ton quantities to gain experience in fabrication techniques and to allow the determination of all properties similar to the slurry oil and vacuum residuum coke program reported in the following section.

### 3.4. Graphite Fabrication

Graphite property variation and property adjustment through control of raw materials has been demonstrated by large-scale evaluation.

### 3.4.1. Materials and Processes

Two different batches of pressure-cured (R process) graphite have been fabricated using cokes from controlled raw materials. One batch was low thermal expansion (30 to 100°C) coke, and the other batch was a high thermal expansion coke. Comparative properties for the two cokes are listed in Table 39. These cokes were produced from the pilot-scale experimental coker at Robinson, Illinois and, at the time, represented cokes at extremes of the thermal expansion scale. The low thermal

128

Table 37. Summary of Operating Parameters and
Physical Property Data of Extruded Rods

| Cycle No. Hrs. | Drum Pressure lbs./in² | Recycle Ratio (1) | S.V. (2) hr⁻¹ | Raw Coke Yield(1) % | Raw Coke Bulk Density lbs./cu.ft. | Binder Level pph | Bulk Density - g/cc green | bake | grph | Specific Resistance, 10⁻⁴ Ω-cm Max. | Min. | Ave. | Drum Average | Run Average | Thermal Expansion, 10⁻⁷/°C (30-100°C), With Grain Max. | Min. | Ave. | Drum Average | Run Average |
|---|---|---|---|---|---|---|---|---|---|---|---|---|---|---|---|---|---|---|---|
| **Atmospheric Residuum** | | | | | | | | | | | | | | | | | | | |
| 46S-T 50‡ B | 55 | 2.3 | 17 | 21.8 | 63 / 66 | 36 / 36 | 1.54 / 1.59 | 1.50 / 1.50 | --- / 1.64 | 8.17 / 8.24 | 6.43 / 7.52 | 6.98 / 8.00 | 7.49 | 7.49 | 1.05 / 1.32 | 0.96 / 1.20 | 1.02 / 1.25 | 1.14 | 1.14 |
| 47N-T 61‡ B | 50 | 3.4 | 13 | 23.6 | 62 / 68 | 36 / 36 | 1.57 / 1.54 | 1.48 / 1.47 | 1.61 / 1.61 | 7.93 / 9.10 | 6.77 / 7.26 | 7.34 / 7.44 | 7.39 | 7.39 | 0.99 / 0.90 | 0.84 / 0.78 | 0.94 / 0.85 | 0.90 | 0.90 |
| 47S-T 60 B | 59 | 3.5 | 11 | 23.8 | 62 / 65 | 36 / 36 | 1.54 / 1.67 | 1.48 / 1.52 | 1.60 / 1.60 | 8.58 / 8.18 | 7.38 / 7.54 | 8.02 / 7.91 | 7.97 | 7.97 | 1.14 / 1.18 | 1.02 / 0.96 | 1.06 / 1.02 | 1.04 | 1.04 |
| **Vacuum Residuum** | | | | | | | | | | | | | | | | | | | |
| 6N (compl) 24 | 53 | 1.7 | 18 | 34.3 | 40 | 32 | 1.59 | 1.53 | 1.63 | 8.27 | 7.62 | 7.88 | 7.88 | 7.73 | 1.82 | 1.62 | 1.72 | 1.72 | 1.65 |
| 10S-T 24 B | 50 | 2.0 | 8 | 32.3 | 40 / 48 | 32 / 32 | 1.63 / 1.63 | 1.56 / 1.55 | 1.60 / 1.62 | 7.48 / 8.55 | 6.64 / 7.34 | 7.23 / 7.91 | 7.57 | | 1.04 / 2.17 | 0.98 / 1.99 | 1.03 / 2.11 | 1.57 | |
| 40S-T 24 B | 50 | 2.0 | 7 | 30.5 | 63 / 52 | 32 / 32 | 1.61 / 1.69 | 1.54 / 1.57 | 1.53 / 1.61 | 7.44 / 7.25 | 6.65 / 6.71 | 7.13 / 7.03 | 7.09 | 7.20 | 0.62 / 2.05 | 0.56 / 1.96 | 0.59 / 2.00 | 1.30 | 1.30 |
| 41S-T 24 B | 50 | 2.1 | 8 | 28.4 | 64 / 60 | 32 / 32 | 1.69 / 1.71 | 1.53 / 1.55 | 1.56 / 1.59 | 7.67 / 7.80 | 6.94 / 6.80 | 7.16 / 7.46 | 7.35 | | 0.86 / 1.84 | 0.77 / 1.67 | 0.81 / 2.76 | 1.30 | |

(1) Ratio recycle to fresh feed

(2) See note on Table 34

(3) Calculated by Coke Volume (cu.ft.) x sampled Bulk Density (lbs./cu.ft.) ÷ Fresh Feed (lbs.)

129

Table 38.  Summary of Physical Property Data on 3-Inch Molded Plugs

| Cycle No. | Binder Level pph | Bulk Density - g/cc green | bake | graph | Specific Resistance, $10^{-4}$ Ω-cm Max. | Min. | Ave. | Flexural Strength, lbs./in.$^2$ Max. | Min. | Ave. | Thermal Expansion, $10^{-5}$/°C (30-100°C) Max. | Min. | Ave. |
|---|---|---|---|---|---|---|---|---|---|---|---|---|---|
| **Atmospheric Residuum** | | | | | | | | | | | | | |
| 46S | 36 | 1.63 | 1.49 | 1.53 | w.g. 8.21 | 7.40 | 7.87 | 1730 | 1470 | 1600 | 1.93 | 1.69 | 1.81 |
|  |  |  |  |  | a.g. 11.90 | 7.98 | 10.68 | 1360 | 990 | 1150 | 2.97 | 2.70 | 2.83 |
| 47S | 36 | 1.55 | 1.47 | 1.48 | w.g. 8.62 | 7.64 | 7.96 | 1460 | 1270 | 1370 | 1.69 | 1.49 | 1.57 |
|  |  |  |  |  | a.g. 11.87 | 10.41 | 11.13 | 1160 | 750 | 960 | 2.96 | 2.56 | 2.73 |
| 47N | 36 | 1.55 | 1.51 | 1.51 | w.g. 8.31 | 7.70 | 7.91 | 1700 | 1350 | 1490 | 1.66 | 1.53 | 1.59 |
|  |  |  |  |  | a.g. 11.34 | 10.22 | 10.78 | 1190 | 830 | 1015 | 2.79 | 2.66 | 2.70 |
| **Vacuum Residuum** | | | | | | | | | | | | | |
| 6N | 32 | 1.63 | 1.54 | 1.57 | w.g. 11.98 | 8.04 | 9.82 | 1880 | 1840 | 1860 | 2.20 | 1.87 | 2.02 |
|  |  |  |  |  | a.g. 16.15 | 10.57 | 13.24 | 1730 | 1450 | 1560 | 3.21 | 2.81 | 3.00 |
| 40S & 41S | 32 | 1.58 | 1.54 | 1.57 | w.g. 18.72 | 8.46 | 8.60 | 1655 | 1120 | 1390 | 2.03 | 1.84 | 1.93 |
|  |  |  |  |  | a.g. 12.70 | 11.37 | 12.07 | 1200 | 870 | 1060 | 3.30 | 2.88 | 3.12 |

130

Table 39. Room-Temperature Extruded Rod Physical
With-Grain Properties of Vacuum Residuum
and Slurry Oil Cokes (1000°C Calcined Coke)

| Type Cycles | Bulk Density, g/cc | | | Specific Resistance, $10^{-4}\,\Omega$-cm | | | Thermal Expansion, $10^{-6}/°C$ (30-100°C) | | |
|---|---|---|---|---|---|---|---|---|---|
| | Green | Bake | Graph. | Max. | Min. | Avg. | Max. | Min. | Avg. |
| Vacuum Residuum (26S-28S) | 1.62 | 1.52 | 1.58 | 12.11 | 8.46 | 9.77 | 2.07 | 1.87 | 1.97 |
| Slurry Oil (23S-25S) | 1.62 | 1.49 | 1.52 | 8.07 | 7.41 | 7.94 | 0.33 | 0.30 | 0.31 |

expansion coke was made from slurry oil charge stock at high drum pressure (350 lbs./in. $^2$), and the high thermal expansion coke from vacuum residuum charge stock at low drum pressure (50 lbs./in. $^2$), with high steam injection into the hot-oil stream between furnace and coke drum. The cokes were then processed into graphite as outlined by the flow sheet' in Figure 59. The different lots of graphite are designated as RT-0033 from slurry oil stock, and RT-0034 from vacuum residuum stock. The coke used in grade RVA is made from charge stock combining a thermal tar with various other nonaromatic hydrocarbons in a routine commercial coker operation. Particle size distribution was comparable in all of the above grades.

3.4.2. Properties

After fabrication of 12 blocks of RT-0033 and 14 blocks of RT-0034, comparison of properties was made on samples cut from the individual blocks according to the sampling diagram in Figure 60. Table 40 lists the room-temperature properties of these blocks along with properties of the RVA.

Two points are evident from the data of Table 40:

1) The character of the coke used in forming is carried through to the finished graphite article;

2) Variability in bulk density and compressive strength has been substantially reduced in cokes from a controlled source.

131
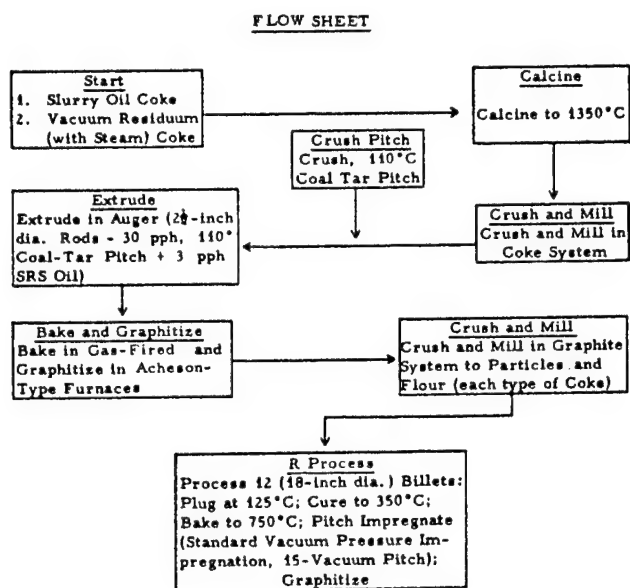
Figure 59. Evaluation of Robinson Coke

| SAMPLE DESIGNATION | | PROPERTIES TO BE MEASURED |
|---|---|---|
| A. | ACROSS GRAIN | SPECIFIC RESISTANCE<br>YOUNG'S MODULUS<br>FLEXURAL STRENGTH<br>BULK DENSITY |
| B. | WITH GRAIN | THERMAL EXPANSION |
| C. | WITH GRAIN | COMPRESSIVE STRENGTH |
| D. | WITH GRAIN | SPECIFIC RESISTANCE<br>YOUNG'S MODULUS<br>FLEXURAL STRENGTH<br>BULK DENSITY |
| E. | ACROSS GRAIN | THERMAL EXPANSION |
| F. | ACROSS GRAIN | COMPRESSIVE STRENGTH |
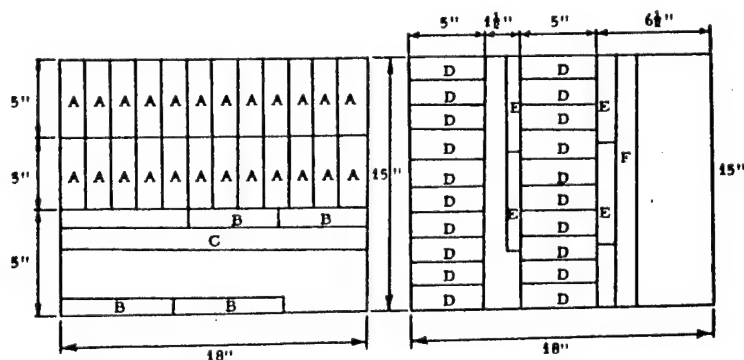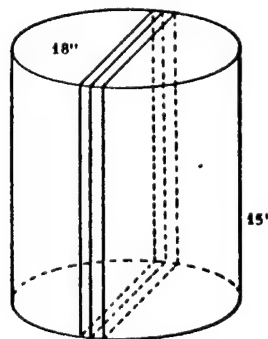


L- 164

Figure 60. Sampling Diagram of Graphite Blocks

132

Figure 62. Vacuum Residuum Coke, 1000°C Calcine (500 X)



Figure 61. Slurry Oil Coke, 1000°C Calcine (500 X)

133

Table 40. Room-Temperature Graphite Properties, RVA, RT-0033, and RT-0034

| | RVA* | | RT-0033** | | RT-0034*** | |
|---|---|---|---|---|---|---|
| **Bulk Density, g/cc** | | | | | | |
| X**** | 1.838 | | 1.868 | | 1.887 | |
| σ | 0.019 | | 0.011 | | 0.012 | |
| N | 312 | | 545 | | 614 | |
| | W.G. | A.G. | W.G. | A.G. | W.G. | A.G. |
| **Specific Resistance, $10^{-4}$ Ω-cm** | | | | | | |
| X | 12.21 | 15.73 | 9.50 | 15.36 | 10.90 | 12.98 |
| σ | 0.37 | 0.96 | 0.44 | 0.95 | 0.61 | 0.75 |
| N | 149 | 162 | 258 | 287 | 284 | 330 |
| **Young's Modulus, $10^6$ lbs./in.$^2$** | | | | | | |
| X | 1.837 | 1.301 | 1.775 | 0.944 | 1.727 | 1.372 |
| σ | 0.073 | 0.094 | 0.086 | 0.048 | 0.053 | 0.050 |
| N | 128 | 162 | 258 | 287 | 284 | 330 |
| **Flexural Strength, lbs./in.$^2$** | | | | | | |
| X | 3800 | 2995 | 3314 | 2111 | 3809 | 3123 |
| σ | 321 | 203 | 260 | 280 | 236 | 240 |
| N | 135 | 121 | 258 | 287 | 284 | 330 |
| **Compressive Strength,***** lbs./in.$^2$** | | | | | | |
| X | 9960 | 9000 | 6225 | 6377 | 11,995 | 11,999 |
| σ | 1308 | 2000 | 385 | 254 | 153 | 566 |
| N | 46 | 46 | 118 | 120 | 140 | 140 |
| **Thermal Expansion, $10^{-6}$/°C Mean 30-100°C** | | | | | | |
| X | 1.65 | 2.77 | 1.12 | 2.52 | 2.25 | 2.94 |
| σ | 0.09 | 0.07 | 0.09 | 0.10 | 0.07 | 0.09 |
| N | 12 | 12 | 24 | 24 | 28 | 28 |

\* Samples cut from 3 pieces, 33 inches in diameter by 42 inches in length.

\*\* Samples cut from 12 pieces, 18 inches in diameter by 15 inches in length.

\*\*\* Samples cut from 14 pieces, 18 inches in diameter by 15 inches in length.

\*\*\*\* X = Average; σ = Standard Deviation; N = Number of Samples.

\*\*\*\*\* One-inch cubes were used to test the RVA and RT-0033. One-inch diameter by one-inch long cylinders were used for the RT-0034 tests. The cylindrical specimen usually gives results ~ 10 per cent higher than the cube specimen and mere comparison of the data is not valid; however, the uniformity of the pieces is illustrated.

Comparison of properties on samples cut from the individual blocks of RT-0033 and RT-0034 RVA can be made from Tables 41 through 52.

3.4.3. Future Work

To complete the slurry oil-vacuum residuum coke comparison, the remaining portions of the blocks will be impregnated and rebaked. Testing will then be carried out in the same fashion as before to determine if reduction in property variation and control of properties can be extended through the further impregnation and rebaking processing steps.

Table 41.  Bulk Density, g/cc, Property Variation
for RT-0033

| Block Number | N* | X̄* | σ* |
|---|---|---|---|
| 230 | 44 | 1.874 | 0.095 |
| 231 | 46 | 1.871 | 0.094 |
| 232 | 46 | 1.870 | 0.0105 |
| 233 | 46 | 1.868 | 0.0116 |
| 234 | 46 | 1.871 | 0.0114 |
| 235 | 46 | 1.870 | 0.0084 |
| 236 | 44 | 1.867 | 0.0117 |
| 237 | 46 | 1.861 | 0.0109 |
| 238 | 45 | 1.869 | 0.0091 |
| 239 | 46 | 1.866 | 0.0091 |
| 240 | 44 | 1.866 | 0.0112 |
| 241 | 46 | 1.864 | 0.0116 |
| All Samples | 545 | 1.868 | 0.0109 |
| Piece-to-Piece Variation | 12 | 1.868 | 0.0035 |

Table 42.  Specific Resistance, $10^{-4}$ Ω-cm, Property
Variation for RT-0033

| Block Number | With Grain | | | Across Grain | | |
|---|---|---|---|---|---|---|
| | N | X̄ | σ | N | X̄ | σ |
| 230 | 20 | 9.07 | 0.286 | 24 | 15.01 | 1.019 |
| 231 | 22 | 9.85 | 0.595 | 24 | 15.23 | 0.892 |
| 232 | 22 | 9.59 | 0.385 | 24 | 14.92 | 1.093 |
| 233 | 22 | 9.63 | 0.386 | 24 | 15.66 | 0.932 |
| 234 | 22 | 9.93 | 0.312 | 24 | 15.69 | 1.035 |
| 235 | 22 | 9.49 | 0.439 | 24 | 14.65 | 0.729 |
| 236 | 20 | 9.71 | 0.414 | 24 | 15.94 | 0.775 |
| 237 | 22 | 9.60 | 0.298 | 24 | 15.57 | 0.718 |
| 238 | 22 | 9.35 | 0.307 | 23 | 14.89 | 0.719 |
| 239 | 22 | 9.16 | 0.276 | 24 | 15.50 | 0.729 |
| 240 | 20 | 9.40 | 0.215 | 24 | 15.39 | 0.869 |
| 241 | 22 | 9.19 | 0.353 | 24 | 15.85 | 0.871 |
| All Samples | 258 | 9.50 | 0.444 | 287 | 15.36 | 0.946 |
| Piece-to-Piece Variation | 12 | 9.50 | 0.272 | 12 | 15.36 | 0.415 |

* N = Number of Samples; X̄ = Average Value; σ = Standard Deviation.

135

Table 43.  Young's Modulus, $10^6$ lbs./in.$^2$, Property
Variation for RT-0033

| Block | With Grain | | | Across Grain | | |
|---|---|---|---|---|---|---|
| Number | N | $\overline{X}$ | $\sigma$ | N | $\overline{X}$ | $\sigma$ |
| 230 | 20 | 1.793 | 0.0713 | 24 | 0.948 | 0.0506 |
| 231 | 22 | 1.768 | 0.0732 | 24 | 0.948 | 0.0462 |
| 232 | 22 | 1.692 | 0.0884 | 24 | 0.981 | 0.0581 |
| 233 | 22 | 1.771 | 0.0840 | 24 | 0.941 | 0.0349 |
| 234 | 22 | 1.851 | 0.0818 | 24 | 0.976 | 0.0459 |
| 235 | 22 | 1.745 | 0.0822 | 24 | 0.940 | 0.0293 |
| 236 | 20 | 1.836 | 0.0581 | 24 | 0.959 | 0.0338 |
| 237 | 22 | 1.773 | 0.0442 | 24 | 0.932 | 0.0356 |
| 238 | 22 | 1.694 | 0.0790 | 23 | 0.913 | 0.0304 |
| 239 | 22 | 1.816 | 0.0610 | 24 | 0.957 | 0.0322 |
| 240 | 20 | 1.805 | 0.0584 | 24 | 0.951 | 0.0439 |
| 241 | 22 | 1.767 | 0.0788 | 24 | 0.879 | 0.0427 |
| All Samples | 258 | 1.775 | 0.0858 | 287 | 0.944 | 0.0482 |
| Piece-to-Piece Variation | 12 | 1.775 | 0.0494 | 12 | 0.944 | 0.0273 |

Table 44.  Flexural Strength, lbs./in.$^2$, Property
Variation for RT-0033

| Block | With Grain | | | Across Grain | | |
|---|---|---|---|---|---|---|
| Number | N | $\overline{X}$ | $\sigma$ | N | $\overline{X}$ | $\sigma$ |
| 230 | 20 | 3412 | 297 | 24 | 2123 | 205 |
| 231 | 22 | 3245 | 255 | 24 | 2184 | 136 |
| 232 | 22 | 3322 | 239 | 24 | 2323 | 147 |
| 233 | 22 | 3246 | 276 | 24 | 2187 | 248 |
| 234 | 22 | 3514 | 242 | 24 | 2145 | 350 |
| 235 | 22 | 3269 | 246 | 24 | 2112 | 180 |
| 236 | 20 | 3538 | 203 | 24 | 2148 | 364 |
| 237 | 22 | 3269 | 203 | 24 | 2004 | 337 |
| 238 | 22 | 3191 | 257 | 23 | 2042 | 226 |
| 239 | 22 | 3263 | 196 | 24 | 2177 | 187 |
| 240 | 20 | 3306 | 178 | 24 | 2101 | 295 |
| 241 | 22 | 3226 | 276 | 24 | 1784 | 253 |
| All Samples | 258 | 3314 | 260 | 287 | 2111 | 280 |
| Piece-to-Piece Variation | 12 | 3314 | 112 | 12 | 2111 | 130 |

Table 45. Compressive Strength, lbs./in.$^2$, Property Variation for RT-0033

| Block Number | With Grain | | | Across Grain | | |
|---|---|---|---|---|---|---|
| | N | $\overline{X}$ | $\sigma$ | N | $\overline{X}$ | $\sigma$ |
| 230 | 10 | 6152 | 214 | 10 | 6385 | 136 |
| 231 | 10 | 6027 | 216 | 10 | 6242 | 113 |
| 232 | 10 | 6394 | 292 | 10 | 6603 | 126 |
| 233 | 10 | 5995 | 436 | 10 | 6316 | 135 |
| 234 | 10 | 6334 | 302 | 10 | 6511 | 243 |
| 235 | 9 | 5915 | 272 | 10 | 6190 | 106 |
| 236 | 10 | 6704 | 247 | 10 | 6541 | 202 |
| 237 | 10 | 6390 | 231 | 10 | 6560 | 128 |
| 238 | 10 | 5884 | 268 | 10 | 6214 | 211 |
| 239 | 10 | 6599 | 265 | 10 | 6399 | 252 |
| 240 | 10 | 6362 | 195 | 10 | 6518 | 112 |
| 241 | 9 | 5879 | 251 | 10 | 6041 | 328 |
| All Samples | 118 | 6225 | 385 | 120 | 6377 | 254 |
| Piece-to-Piece Variation | 12 | 6225 | 284 | 12 | 6377 | 177 |

Table 46. Thermal Expansion, $10^{-6}/°C$, Property Variation for RT-0033

| Block Number | With Grain | | | Across Grain | | |
|---|---|---|---|---|---|---|
| | N | $\overline{X}$ | $\sigma$ | N | $\overline{X}$ | $\sigma$ |
| 230 | 2 | 1.15 | | 2 | 2.60 | |
| 231 | 2 | 1.06 | | 2 | 2.57 | |
| 232 | 2 | 1.20 | | 2 | 2.54 | |
| 233 | 2 | 1.08 | | 2 | 2.59 | |
| 234 | 2 | 1.15 | | 2 | 2.59 | |
| 235 | 2 | 1.08 | | 2 | 2.55 | |
| 236 | 2 | 1.25 | | 2 | 2.59 | |
| 237 | 2 | 1.10 | | 2 | 2.47 | |
| 238 | 2 | 1.18 | | 2 | 2.44 | |
| 239 | 2 | 1.22 | | 2 | 2.39 | |
| 240 | 2 | 1.02 | | 2 | 2.48 | |
| 241 | 2 | 0.99 | | 2 | 2.45 | |
| All Samples | 24 | 1.12 | 0.093 | 24 | 2.52 | 0.0100 |

Table 47.  Bulk Density, g/cc, Property Variation
for RT-0034

| Block Number | N | $\overline{X}$ | $\sigma$ |
|---|---|---|---|
| 270 | 44 | 1.882 | 0.011 |
| 271 | 46 | 1.879 | 0.009 |
| 272 | 46 | 1.882 | 0.012 |
| 273 | 40 | 1.887 | 0.011 |
| 274 | 42 | 1.889 | 0.010 |
| 275 | 44 | 1.892 | 0.010 |
| 276 | 44 | 1.886 | 0.009 |
| 277 | 46 | 1.891 | 0.011 |
| 278 | 46 | 1.880 | 0.010 |
| 279 | 42 | 1.890 | 0.010 |
| 280 | 44 | 1.882 | 0.010 |
| 281 | 42 | 1.900 | 0.012 |
| 282 | 44 | 1.891 | 0.066 |
| 283 | 44 | 1.895 | 0.011 |
|  |  |  | 0.008 |
| All Samples | 614 | 1.887 | 0.012 |
| Piece-to-Piece Variation | 14 | 1.887 | 0.0064 |

Table 48.  Specific Resistance, $10^{-4}\Omega$-cm, Property
Variation for RT-0034

| Block Number | With Grain | | | Across Grain | | |
|---|---|---|---|---|---|---|
|  | N | $\overline{X}$ | $\sigma$ | N | $\overline{X}$ | $\sigma$ |
| 270 | 20 | 10.65 | 0.43 | 24 | 12.97 | 0.38 |
| 271 | 22 | 10.87 | 0.31 | 24 | 13.27 | 0.51 |
| 272 | 22 | 11.11 | 0.39 | 24 | 13.11 | 0.49 |
| 273 | 18 | 11.15 | 0.50 | 22 | 13.00 | 0.44 |
| 274 | 18 | 10.89 | 0.32 | 24 | 12.42 | 0.64 |
| 275 | 20 | 10.72 | 0.36 | 24 | 12.54 | 0.68 |
| 276 | 20 | 10.88 | 0.43 | 24 | 12.70 | 0.46 |
| 277 | 22 | 10.87 | 0.25 | 24 | 12.93 | 0.41 |
| 278 | 22 | 9.96 | 1.04 | 24 | 12.43 | 1.03 |
| 279 | 20 | 11.28 | 0.49 | 22 | 13.99 | 0.83 |
| 280 | 20 | 10.71 | 0.56 | 24 | 12.61 | 1.02 |
| 281 | 20 | 10.75 | 0.47 | 22 | 13.10 | 0.52 |
| 282 | 20 | 11.20 | 0.30 | 24 | 13.52 | 0.44 |
| 283 | 20 | 11.62 | 0.51 | 24 | 13.25 | 0.52 |
| All Samples | 284 | 10.90 | 0.61 | 330 | 12.98 | 0.75 |
| Piece-to-Piece Variation | 14 | 10.90 | 0.38 | 14 | 12.98 | 0.44 |

Table 49. Young's Modulus, $10^6$ lbs./in.$^2$, Property Variation for RT-0034

| Block Number | With Grain | | | Across Grain | | |
|---|---|---|---|---|---|---|
| | N | $\overline{X}$ | σ | N | $\overline{X}$ | σ |
| 270 | 20 | 1.725 | 0.0372 | 24 | 1.350 | 0.0392 |
| 271 | 22 | 1.698 | 0.0281 | 24 | 1.328 | 0.0381 |
| 272 | 22 | 1.718 | 0.0396 | 24 | 1.343 | 0.0364 |
| 273 | 18 | 1.697 | 0.0372 | 22 | 1.346 | 0.0409 |
| 274 | 18 | 1.750 | 0.0404 | 24 | 1.399 | 0.0329 |
| 275 | 20 | 1.697 | 0.0306 | 24 | 1.342 | 0.0440 |
| 276 | 20 | 1.695 | 0.0288 | 24 | 1.363 | 0.0340 |
| 277 | 22 | 1.696 | 0.0411 | 24 | 1.351 | 0.0287 |
| 278 | 22 | 1.799 | 0.0511 | 24 | 1.442 | 0.0404 |
| 279 | 20 | 1.693 | 0.0384 | 22 | 1.347 | 0.0353 |
| 280 | 20 | 1.758 | 0.0246 | 24 | 1.397 | 0.0447 |
| 281 | 20 | 1.721 | 0.0501 | 22 | 1.382 | 0.0215 |
| 282 | 20 | 1.749 | 0.0391 | 24 | 1.356 | 0.0266 |
| 283 | 20 | 1.801 | 0.0380 | 24 | 1.450 | 0.0306 |
| All Samples | 284 | 1.727 | 0.0534 | 330 | 1.372 | 0.0498 |
| Piece-to-Piece Variation | 14 | 1.727 | 0.0392 | 14 | 1.372 | 0.0379 |

Table 50. Flexural Strength, lbs./in.$^2$, Property Variation for RT-0034

| Block Number | With Grain | | | Across Grain | | |
|---|---|---|---|---|---|---|
| | N | $\overline{X}$ | σ | N | $\overline{X}$ | σ |
| 270 | 20 | 3711 | 237 | 24 | 2975 | 218 |
| 271 | 20 | 3695 | 169 | 24 | 2982 | 217 |
| 272 | 22 | 3843 | 209 | 24 | 2970 | 246 |
| 273 | 18 | 3834 | 168 | 22 | 3146 | 160 |
| 274 | 18 | 3794 | 168 | 24 | 3216 | 204 |
| 275 | 20 | 3846 | 166 | 24 | 3189 | 164 |
| 276 | 20 | 3886 | 250 | 24 | 3209 | 181 |
| 277 | 22 | 3697 | 228 | 24 | 3065 | 270 |
| 278 | 22 | 3941 | 322 | 24 | 3322 | 243 |
| 279 | 20 | 3786 | 178 | 22 | 3130 | 212 |
| 280 | 20 | 4050 | 221 | 24 | 3235 | 244 |
| 281 | 20 | 3660 | 233 | 22 | 3058 | 245 |
| 282 | 20 | 3764 | 247 | 24 | 2972 | 157 |
| 283 | 20 | 3792 | 187 | 24 | 3253 | 190 |
| All Samples | 284 | 3809 | 236 | 330 | 3123 | 240 |
| Piece-to-Piece Variation | 14 | 3809 | 104 | 14 | 3123 | 119 |

Table 51. Compressive Strength, lbs./in.$^2$, Property Variation for RT-0034

| Block Number | With Grain | | | Across Grain | | |
|---|---|---|---|---|---|---|
| | N | X̄ | σ | N | X̄ | σ |
| 270 | 10 | 11865 | 203 | 10 | 11480 | 512 |
| 271 | 10 | 11585 | 274 | 10 | 11171 | 264 |
| 272 | 10 | 12294 | 359 | 10 | 11711 | 350 |
| 273 | 10 | 12013 | 197 | 10 | 12088 | 454 |
| 274 | 10 | 12105 | 331 | 10 | 12085 | 587 |
| 275 | 10 | 11546 | 163 | 10 | 11843 | 179 |
| 276 | 10 | 11684 | 273 | 10 | 11787 | 204 |
| 277 | 10 | 12074 | 349 | 10 | 11870 | 319 |
| 278 | 10 | 12826 | 265 | 10 | 12968 | 212 |
| 279 | 10 | 12102 | 377 | 10 | 12173 | 145 |
| 280 | 10 | 12492 | 240 | 10 | 12119 | 233 |
| 281 | 10 | 11594 | 221 | 10 | 11984 | 329 |
| 282 | 10 | 12244 | 572 | 10 | 11731 | 142 |
| 283 | 10 | 11511 | 375 | 10 | 12916 | 420 |
| All Samples | 140 | 11995 | 153 | 140 | 11995 | 566 |
| Piece-to-Piece Variation | 14 | 11995 | 392 | 14 | 11995 | 483 |

Table 52. Thermal Expansion, $10^{-6}$/°C, Property Variation for RT-0034

| Block Number | With Grain | | | Across Grain | | |
|---|---|---|---|---|---|---|
| | N | X̄ | σ | N | X̄ | σ |
| 270 | 2 | 2.27 | - | 2 | 2.93 | - |
| 2 271 | 2 | 2.34 | - | 2 | 3.09 | - |
| 272 | 2 | 2.25 | - | 2 | 3.06 | - |
| 273 | 2 | 2.27 | - | 2 | 2.93 | - |
| 274 | 2 | 2.37 | - | 2 | 2.77 | - |
| 275 | 2 | 2.27 | - | 2 | 3.01 | - |
| 276 | 2 | 2.18 | - | 2 | 2.95 | - |
| 277 | 2 | 2.20 | - | 2 | 2.86 | - |
| 278 | 2 | 2.23 | - | 2 | 3.04 | - |
| 279 | 2 | 2.26 | - | 2 | 2.97 | - |
| 280 | 2 | 2.23 | - | 2 | 2.84 | - |
| 281 | 2 | 2.24 | - | 2 | 2.93 | - |
| 282 | 2 | 2.12 | - | 2 | 2.83 | - |
| 283 | 2 | 2.27 | - | 2 | 2.95 | - |
| All Samples | 28 | 2.25 | 0.07 | 28 | 2.94 | 0.09 |

140

## 3.5. Pitch Binder Studies

A program is under way to evaluate various sulfur-free binder systems. A comparison of commercial grade coal tar pitches, laboratory-produced petroleum pitches, and commercial grade petroleum pitches will be made. After compiling sufficient data, a computer characterization will be attempted relating properties of pitches to properties of graphite billets which utilized the corresponding pitches as binders when originally formed.

# 4. REFERENCES

1.  Lewis, I.C., and T. Edstrom, "Thermal Reactivity of Aromatic Hydrocarbons," WADD Technical Report 61-72, Volume X.

2.  Lewis, I.C., and T. Edstrom, "Thermal Reactivity of Aromatic Hydrocarbons," WADD Technical Report 61-72, Supplement to Volume X.

3.  Lewis, I.C., and T. Edstrom, "Carbonization Studies of Aromatic Hydrocarbons," WADD Technical Report 61-72, Volume XXVII.

4.  Ferguson, G., and J. M. Robertson, "Advances in Physical Organic Chemistry," Academic Press, New York (1963), p. 203.

5.  Clar, E., "Aromatische Kohlenwasserstoffe," Springer-Verlag, Berlin (1952), p. 421.

6.  Grummitt, O., and A. Jenkins, J. Am. Chem. Soc. 68, 914 (1947).

7.  Nenitzescu, C. D., and E. Solomonica, Organic Syntheses, Col. Vol. 2, 496 (1955).

8.  Cava, M. P., R. L. Litle, and D. R. Napier, J. Am. Chem. Soc. 80, 2259 (1958).

9.  Cohen, S. G., F. Cohen, and C. Wang, J. Org. Chem. 28, 1479 (1963).

10. Bell, F., and D. H. Waring, J. Chem. Soc. 267 (1949).

11. Ritter, J. J., and G. M. Wiedeman, J. Am. Chem. Soc., 51, 3585 (1929).

12. Ingram, D.J.E., "Free Radicals as Studied by Electron Spin Resonance," Butterworths, London (1958), p. 207.

13. Singer, L. S., Proc. Fifth Carbon Conf., Pergamon Press, New York (1963), Vol. 2, p. 121.

14. Singer, L. S., and I.C. Lewis, "An Electron Spin Resonance Study of Thermal Decomposition Reactions of Organic Compounds," WADD Technical Report 61-72, Volume XVI.

15. Stehling, F.C., and K. W. Bartz, J. Chem. Phys., 34, 1076 (1961).

16. Bennett, J.E., Proc. Chem. Soc. 144 (1961).

142

## 3.5. Pitch Binder Studies

A program is under way to evaluate various sulfur-free binder systems. A comparison of commercial grade coal tar pitches, laboratory-produced petroleum pitches, and commercial grade petroleum pitches will be made. After compiling sufficient data, a computer characterization will be attempted relating properties of pitches to properties of graphite billets which utilized the corresponding pitches as binders when originally formed.

# 4. REFERENCES

1. Lewis, I. C., and T. Edstrom, "Thermal Reactivity of Aromatic Hydrocarbons," WADD Technical Report 61-72, Volume X.

2. Lewis, I. C., and T. Edstrom, "Thermal Reactivity of Aromatic Hydrocarbons," WADD Technical Report 61-72, Supplement to Volume X.

3. Lewis, I. C., and T. Edstrom, "Carbonization Studies of Aromatic Hydrocarbons," WADD Technical Report 61-72, Volume XXVII.

4. Ferguson, G., and J. M. Robertson, "Advances in Physical Organic Chemistry," Academic Press, New York (1963), p. 203.

5. Clar, E., "Aromatische Kohlenwasserstoffe," Springer-Verlag, Berlin (1952), p. 421.

6. Grummitt, O., and A. Jenkins, J. Am. Chem. Soc. 68, 914 (1947).

7. Nenitzescu, C. D., and E. Solomonica, Organic Syntheses, Col. Vol. 2, 496 (1955).

8. Cava, M. P., R. L. Litle, and D. R. Napier, J. Am. Chem. Soc. 80, 2259 (1958).

9. Cohen, S. G., F. Cohen, and C. Wang, J. Org. Chem. 28, 1479 (1963).

10. Bell, F., and D. H. Waring, J. Chem. Soc. 267 (1949).

11. Ritter, J. J., and G. M. Wiedeman, J. Am. Chem. Soc., 51, 3585 (1929).

12. Ingram, D. J. E., "Free Radicals as Studied by Electron Spin Resonance," Butterworths, London (1958), p. 207.

13. Singer, L. S., Proc. Fifth Carbon Conf., Pergamon Press, New York (1963), Vol. 2, p. 121.

14. Singer, L. S., and I. C. Lewis, "An Electron Spin Resonance Study of Thermal Decomposition Reactions of Organic Compounds," WADD Technical Report 61-72, Volume XVI.

15. Stehling, F. C., and K. W. Bartz, J. Chem. Phys., 34, 1076 (1961).

16. Bennett, J. E., Proc. Chem. Soc. 144 (1961).

## REFERENCES (CONT'D)

17. Sogo, P. B., M. Nakazaki, and M. Calvin, J. Chem. Phys. <u>26</u>, 1343 (1957).

18. Lewis, I. C., and T. Edstrom, J. Org. Chem. <u>28</u>, 2050 (1963).

19. Singer, L. S., and I. C. Lewis, J. Carbon, to be published.

20. Singer, L. S., W. J. Spry, and W. H. Smith, Proc. Third Carbon Conf., Pergamon Press, New York (1959), p. 123.

21. "Summary Technical Report," WADD Technical Report 61-72, Volume XLII.

22. Lebedev, Ya. S., D. M. Chernikova, N. N. Tikhomirova, and V. V. Voevodskii, "Atlas of Electron Spin Resonance Spectra," Consultants Bureau, New York (1963), p. 62.

23. Dehl, R., and G. K. Fraenkel, J. Chem. Phys. <u>39</u>, 1793 (1963).

24. McConnell, H. M., J. Chem. Phys. <u>25</u>, 709 (1956).

25. Kivelson, D., J. Chem. Phys. <u>33</u>, 1094 (1960).

26. Kommandeur, J., Mol. Phys. <u>4</u>, 509 (1961).

27. Blois, M. S., H. W. Brown, and J. E. Maling, "Free Radicals in Biological Systems," Academic Press, New York (1961), p. 117.

28. Dearman, H. H., and H. M. McConnell, J. Chem. Phys. <u>33</u>, 1877 (1960).

29. McLachlan, A. D., Mol. Phys. <u>3</u>, 233 (1960).

30. Tolkachev, V. A., I. I. Chkheidze, and N. Ya. Buben, Dok. Akad. Nauk. <u>147</u>, 643 (1962); Translated in Proc. Acad. Sciences, Chemistry Section, <u>147</u>, 1036 (1962).

31. Pople, J. A., W. G. Schneider, and H. J. Bernstein, "High-Resolution Nuclear Magnetic Resonance," McGraw Hill Co., New York (1959).

32. Jonathan, N., S. Gordon, and B. P. Dailey, J. Chem. Phys. <u>36</u>, 2443 (1962).

33. Freyman, R., M. Dvolaitsky, and J. Jacques, Comp. Rend. <u>253</u>, 1436 (1961).

34. Chamberlain, N. F., Anal. Chem. <u>31</u>, 56 (1959).

## REFERENCES (CONT'D)

35. Bartz, K. W., T. Aezel, H. E. Lampkin, and F. C. Stehling, Anal. Chem. **34**, 1814 (1962).

36. Maclean, C., and E. L. Mackor, Mol. Phys. **4**, 241 (1961).

37. Durand, P., J. Parello, and N. P. Buu-Hoi, Bull. Soc. Chim. 2438 (1963).

38. Edstrom, T., I. C. Lewis, R. L. Racicot, and C. F. Stout, "Studies of Binder Systems for Graphite," WADD Technical Report 61-72, Volume **XXXII**.

39. Clar, E., "Aromatische Kohlenwasserstoffe," Springer-Verlag, Berlin (1952).

40. Aalbersberg, W.I., G. J. Hoijtink, E. L. Mackor, and W. P. Weijland, J. Chem. Soc. 3049 (1959).

41. Symons, M. C. R., "Advances in Physical Organic Chemistry," Academic Press, London (1963), p. 283.

42. Carrington, A., Quart. Rev. **17**, 67 (1963).

43. Stout, C. F., M. Janes, and J. A. Biehl, "Studies of the Quality of Petroleum Coke from a Pilot-Scale Delayed Coker, WADD Technical Report 61-72, Volume **XXXVI**.

44. Howard, R. A., and E. L. Piper, "Development of a Fine-Grain Isotropic Graphite Material for Structural and Substrate Applications," WADD Technical Report 61-72, Volume **XIII**.

45. "Penetration of Bituminous Materials," ASTM D5-61